



HAL
open science

Metasomatic Alteration of Type 3 Ordinary and Carbonaceous Chondrites

A N Krot, M I Petaev, L. Piani, Y. Marrocchi, W. Fujiya, O V Pravdivtseva,
E. Dobrică, L G Vacher, A J King, M. Lee, et al.

► **To cite this version:**

A N Krot, M I Petaev, L. Piani, Y. Marrocchi, W. Fujiya, et al.. Metasomatic Alteration of Type 3 Ordinary and Carbonaceous Chondrites. *Space Science Reviews*, 2025, 221 (1), pp.7. 10.1007/s11214-025-01135-z . hal-04960286

HAL Id: hal-04960286

<https://hal.science/hal-04960286v1>

Submitted on 21 Feb 2025

HAL is a multi-disciplinary open access archive for the deposit and dissemination of scientific research documents, whether they are published or not. The documents may come from teaching and research institutions in France or abroad, or from public or private research centers.

L'archive ouverte pluridisciplinaire **HAL**, est destinée au dépôt et à la diffusion de documents scientifiques de niveau recherche, publiés ou non, émanant des établissements d'enseignement et de recherche français ou étrangers, des laboratoires publics ou privés.



Distributed under a Creative Commons Attribution 4.0 International License



Metasomatic Alteration of Type 3 Ordinary and Carbonaceous Chondrites

A.N. Krot¹ · M.I. Petaev² · L. Piani³ · Y. Marrocchi³ · W. Fujiya⁴ · O.V. Pravdivtseva⁵ · E. Dobrică¹ · L.G. Vacher⁶ · A.J. King⁷ · M. Lee⁸ · E. Van Kooten⁹ · B. Jacobsen¹⁰ · C.M.O'D. Alexander¹¹ · A. Bischoff¹² · A.J. Brearley¹³ · C. Le Guillou¹⁴ · L. Remusat¹⁵ · J. Leitner^{16,17} · G.R. Huss¹

Received: 2 April 2024 / Accepted: 28 December 2024
© The Author(s) 2025

Abstract

Metasomatism refers to the process during which a pre-existing rock undergoes compositional and mineralogical transformations associated with chemical reactions triggered by the reaction of fluids which invade the protolith. It changes chemical compositions of minerals, promotes their dissolution and precipitation of new minerals. In this paper, we review metasomatic alteration of type 3 ordinary (H, L, LL) and carbonaceous (CV, CO, CK) chondrites, including (i) secondary mineralization, (ii) physicochemical conditions, (iii) chronology (^{53}Mn - ^{53}Cr , ^{26}Al - ^{26}Mg , ^{129}I - ^{129}Xe) of metasomatic alteration, (iv) records of metasomatic alteration in H, O, N, C, S, and Cl isotopic systematics, (v) effects of metasomatic alteration on O- and Al-Mg-isotope systematics of primary minerals in chondrules and refractory inclusions, and (vi) sources of water ices in metasomatically altered CV, CO, and ordinary chondrites, and outline future studies.

Keywords Carbonaceous chondrites · Ordinary chondrites · Metasomatic alteration · Water · Oxygen · Hydrogen · Nitrogen and sulfur isotopes · ^{53}Mn - ^{53}Cr chronology · ^{129}I - ^{129}Xe chronology

1 Introduction

There are several classes of chondritic meteorites comprising a number of groups: carbonaceous (CI, CM, CR, CO, CV, CK, CR, CH, CB, CY, CL), ordinary (H, L, LL), enstatite (EH, EL), Kakangari (K), and Rumuruti (R) (Krot et al. 2014a). Some chondrites cannot be classified into the existing groups and are named ungrouped or unique, e.g., Acfer 094 (Newton et al. 1995). CV chondrites are subdivided into three subgroups, oxidized Allende-like (CV_{oxA}), oxidized Bali-like (CV_{oxB}), and reduced (CV_{red}), which may or may not represent fragments of the same parent asteroid (Weisberg et al. 2006; Gattacceca et al. 2020). Virtually all chondrites experienced aqueous alteration and/or thermal metamorphism in their parent asteroids. Based on the degree of aqueous alteration and thermal metamorphism, chondrites are classified into petrologic types from 1 to <3 and from 3 to 6, respectively. Based on the distribution of chromium in chondrule ferroan olivines (Grossman and Brearley 2005), Raman parameters of matrix organic matter (Bonal et al. 2006, 2007), sulfur

Extended author information available on the last page of the article

abundance in matrix (Grossman and Brearley 2005), composition of FeNi-metal (Kimura et al. 2007), matrix modal mineralogy (Brearley 1993; Greshake 1997), and abundance of presolar grains and noble gas components (Huss and Lewis 1995; Nguyen et al. 2010; Leitner et al. 2016; Nittler et al. 2018), type 3 chondrites are further subdivided into subtypes from 3.0 to 3.9; even more detailed classification is used for type 3.0–3.1 chondrites. We note that this classification scheme is rather simplistic, because aqueous alteration and thermal metamorphism are closely related processes and virtually all thermally metamorphosed type 3 chondrites experienced aqueous alteration (Bonal et al. 2020). The least altered and the least thermally metamorphosed chondrites are type 3.00. There are only a few type 3.00 chondrites known, including Semarkona (LL), Northwest Africa (NWA) 8276 (L), Dominion Range (DOM) 08006 (CO), and Acfer 094 (C-ungrouped) (Fig. SM1; Newton et al. 1995; Grossman and Brearley 2005; Alexander et al. 2018a; Davidson et al. 2019; Zanetta et al. 2022; Krämer Ruggiu et al. 2022; Barosch et al. 2022).

Here we review metasomatic alteration of type 3 ordinary (H, L, LL) and carbonaceous (CV, CO, CK) chondrites, including (i) secondary mineralization, (ii) physicochemical conditions and (iii) chronology (^{53}Mn – ^{53}Cr , ^{26}Al – ^{26}Mg , ^{129}I – ^{129}Xe) of metasomatic alteration; (iv) records of metasomatic alteration in H, O, N, C, S, and Cl isotope systematics; (v) effects of metasomatic alteration on O- and Al-Mg-isotope systematics of primary minerals in chondrules and refractory inclusions; (vi) sources of water ices in metasomatically altered CV, CO, and ordinary chondrites, and outline future studies.

2 Primary and Secondary Mineralization in Type 3 Chondrites

2.1 Primary Mineralogy of Chondritic Components in Primitive Chondrites

Chondrites are composed of several major components, including refractory inclusions [Ca,Al-rich inclusions (CAIs) and amoeboid olivine aggregates (AOAs) – aggregates of CAIs and forsterite+FeNi-metal condensates], chondrules, matrix, FeNi-metal, Fe±Ni-sulfides, and organic matter. Refractory inclusions consist of minerals that formed by gas-solid condensation above ~ 1300 K or by melting of gas-solid condensates in a gas of approximately solar chemical composition, i.e., highly reduced: $\text{H}_2\text{O}/\text{H}_2$ ratio of $\sim 6.6 \times 10^{-4}$ corresponding to ~ 7 log units below the iron-wüstite (IW) buffer (e.g., Krot 2019). As a result, primary oxide and silicate minerals in CAIs and AOAs from type 3.00 chondrites are Fe- and Na-free (Table SM1). Pristine refractory inclusions contain no oxidized and low-temperature secondary minerals, such as magnetite, nepheline, sodalite, etc.

Pristine chondrules consist of minerals (Table SM2) formed by melting of solid precursors during transient heating events at ~ 1600 – 2000 K in a gas much more oxidized than solar, IW–3 to IW–1, and contain no secondary minerals such as magnetite, phyllosilicates, nepheline, etc. Chondrules experienced gas-melt interaction before and during crystallization resulting in re-condensation and zoned distribution of moderately volatile elements, such as Si, Mn, Cr, Na, and K (Libourel et al. 2006). Because these elements are also mobile during aqueous/metasomatic alteration (Grossman and Brearley 2005), this may complicate distinguishing nebular and asteroidal records in chondrules.

Pristine matrices are composed predominantly of amorphous ferromagnesian silicates, sub-micron forsterite and enstatite grains, FeNi-metal, Fe-sulfides, organics, presolar grains, and have abundant porosity (Table SM2; Greshake 1997; Grossman and Brearley 2005; Davidson et al. 2019). Because crystalline silicates are common in pristine matrices but virtually absent in interstellar medium (ISM), some fraction of matrix materials must have

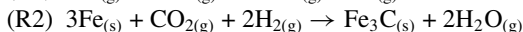
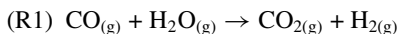
experienced thermal processing in the protoplanetary disk (PPD), most likely during formation of refractory inclusions and chondrules. We note that thermal processing of amorphous silicates in the PPD (*i*) below 1100 K that resulted in formation of crystalline silicates and/or (*ii*) below 900 K that may have modified their primordial oxygen-isotope composition without formation of crystalline silicates are also possible (Ishizaki et al. 2023; Sakurai et al. 2023; Yamamoto et al. 2024). The abundance of primordial, molecular cloud material in pristine chondrite matrices that avoided thermal processing in the PPD remains controversial (Alexander et al. 2017). Due to its extremely fine-grained nature and high porosity, matrix can be easily altered; e.g., amorphous material even in the most primitive carbonaceous chondrite Acfer 094 experienced hydration (Matsumoto et al. 2019).

Refractory inclusions, chondrules, and matrices having different mineralogies, textures, chemistry, and grain-sizes responded differently to metasomatic alteration.

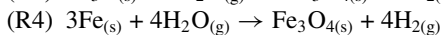
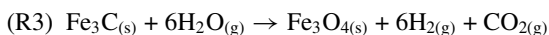
2.2 Initial Stages of Alteration of Chondritic Components in Type 3.0–3.1 Chondrites

The initial stages of metasomatic alteration are largely recorded by matrices and chondrules in ordinary, CV, and CO chondrites of petrologic types 3.0–3.1. The petrographic and chemical effects of metasomatic alteration include (*i*) dissolution of chondrule mesostasis and plagioclase, (*ii*) zoning of Na and Ca in chondrule mesostasis and plagioclase, (*iii*) replacement of chondrule mesostasis by phyllosilicates, and (*iv*) redistribution of matrix nanosulfides (Grossman et al. 2000; Grossman and Brearley 2005; Lewis and Jones 2019). Typical secondary minerals formed during the initial stages of metasomatic alteration of type 3 chondrites are listed in Table SM3; their textural occurrences are shown in Figures SM2–SM7.

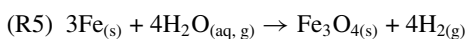
FeNi-metal experienced carburization to form FeNi-carbides (Figs. SM2a,b; Hutchison et al. 1987; Alexander et al. 1989; Taylor et al. 1981; Shibita 1996; Krot et al. 1997; Keller 1998; Krot and Todd 1998; Davidson et al. 2019):



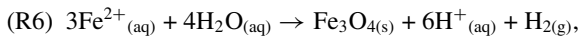
FeNi-metal and carbides were subsequently oxidized to form magnetite (Fig. SM2):



Note that reactions R1–4 do not require aqueous fluid and may have occurred either in the solar nebula or the chondrite parent bodies. For example, FeNi-carbides described in anhydrous interplanetary dust particles (IDPs) could be by-products of Fischer-Tropsch synthesis in the solar nebula (Christoffersen and Buseck 1983; Bradley et al. 1984; Bradley 1994). Oxidation of metal to magnetite is thermodynamically possible in the canonical solar nebula below < 400 K (Fegley and Prinn 1989) and was experimentally studied by Hong and Fegley (1998) (see Sect. 5.1). There are, however, mineralogical evidence suggesting formation of FeNi-carbides and magnetite in the chondrite parent asteroids (Krot et al. 1997). (*i*) FeNi-carbides replace metal nodules in chondrules and form veins crosscutting their fine-grained rims (Figs. SM2c–f). (*ii*) Two types of magnetite can be distinguished: (*a*) “dirty”, Cr-bearing magnetite that formed by *in situ* oxidation of Cr-bearing FeNi-metal nodules (Figs. SM2c, 4b):



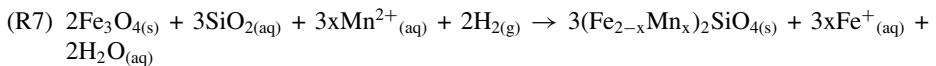
and (b) “clean”, Cr-free magnetite overgrowing oxidized nodules (Figs. SM2c, 4b) and crosscutting fine-grained rims around chondrules (Figs. SM2c–f, 5b,e). This magnetite formed by precipitation of Fe dissolved in aqueous solution:



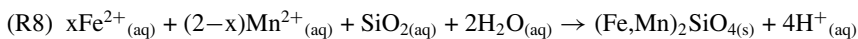
Marrocchi et al. (2016) interpreted clean Cr-free magnetite overgrowing opaque nodules in chondrules from the oxidized Bali-like CV3.1 chondrite Kaba as igneous, i.e., as a result of crystallization FeSO melts. Formation of FeSO melt requires drastic oxidizing conditions, too oxidizing even for chondrule formation, IW+1 to IW+2 (see Sect. 2.1). The lack of magnetite-bearing chondrules in the reduced CV3 chondrites and the differences in O-isotope compositions between Cr-free magnetite and chondrule phenocrysts in Kaba chondrules (Marrocchi et al. 2016; Krot et al. 2022a) contradict this interpretation (see Sect. 7.1.2).

In addition, framboidal magnetite occasionally observed in matrix of the oxidized CV3.1 chondrites Kaba and Mokoia also formed by direct precipitation from aqueous fluid (Keller and Buseck 1990; Tomeoka and Buseck 1990). The existence of aqueous solution during alteration of type 3.0–3.1 chondrites is supported by hydration and replacement of amorphous silicates by phyllosilicates and ferroan olivine (Fig. SM3).

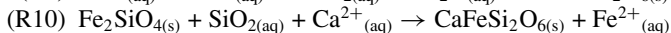
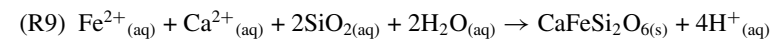
Subsequently, the Cr-free magnetite is preferentially replaced by Mn-bearing fayalite (Fig. SM4):



Isolated fayalite grains in matrices and pore space of AOA and fine-grained CAIs, as well as fayalite grains overgrowing chondrule olivines and fine-grained matrix-like rims (Figs. SM5–6) apparently formed by direct precipitation from aqueous solutions:

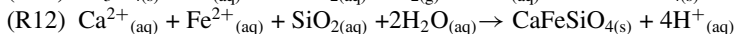
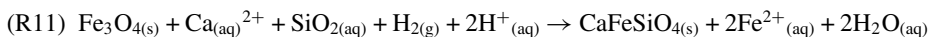


In Kaba and MacAlpine Hills (MAC) 88107 (CO3.1-like), fayalite often associates with hedenbergite (Fig. SM5) that may have formed by direct precipitation from aqueous fluid and by replacement of fayalite:

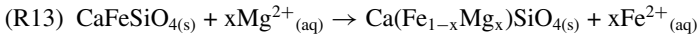


Manganese-bearing fayalite is critical for ^{53}Mn - ^{53}Cr dating of metasomatic alteration of UOCs, COs, and CVs (see Sect. 6.1). It is also important for constraining O-isotope composition of aqueous fluid, and, potentially, temperature of metasomatic alteration (see Sect. 7.1). We note, however, that reactional relationships between fayalite and magnetite (Fig. SM4) suggest these minerals may not have been in isotopic equilibrium with the same fluid. Therefore, temperature estimates based on O-isotope compositions of fayalite and magnetite must be taken with caution.

In the reduced CV3s (Efremovka, Leoville, Vigarano) and MAC 88107, magnetite, fayalite, and hedenbergite associate with kirschsteinite (Fig. SM7) (Krot et al. 2000; Ganino and Libourel 2017; MacPherson et al. 2017) that may have formed by replacement of magnetite and by direct precipitation from aqueous solution:

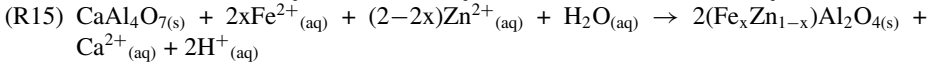
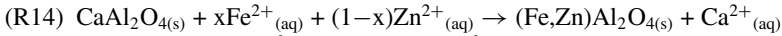


Kirschsteinite (kirschsteinite-monticellite solid solution) grains in CVs are often chemically-zoned (Fig. SM7b) suggesting evolution of chemical composition of aqueous fluid:



Kirschsteinite is a critical mineral for ^{53}Mn - ^{53}Cr chronology of metasomatic alteration of the reduced CVs (see Sect. 6.2), and potentially important for constraining O-isotope composition of aqueous fluid in their parent body. However, no SIMS (secondary ion mass spectrometry) standards for kirschsteinite are currently available.

In contrast to matrices and chondrules, most primary minerals in refractory inclusions from 3.0–3.1 chondrites show little evidence for metasomatic alteration. The only exception are Ca-aluminates, grossite and krotite, which can be replaced by hercynite that is commonly Zn-bearing (Fig. SM8; Krot et al. 2019b; Ebert et al. 2024; Han et al. 2024):



2.3 Advanced Stages of Alteration in Type 3 Chondrites of Higher Petrologic Subtypes

Studies of secondary mineralization in type 3 carbonaceous chondrites as a function of their petrologic subtypes are largely focused on the formation of nepheline in refractory inclusions and chondrules in CO3.0–3.8 s, where it formed by replacement of melilite, plagioclase, and chondrule mesostasis (Kojima et al. 1995; Tomeoka and Itoh 2004; Itoh et al. 2004; Brearley and Krot 2012; Wick and Jones 2012). There is a correlation between the amounts of nepheline in the CO chondritic components and the degree of thermal metamorphism of their host meteorites (Kojima et al. 1995; Itoh and Tomeoka 1998; Russell et al. 1998; Tomeoka and Itoh 2004), suggesting the nephelization resulted from fluid-assisted thermal metamorphism. Mineralogical changes during metasomatic alteration of CV3 and CK3 chondrites are poorly known, because (i) well established metamorphic sequence among CV3s is currently absent (Bonal et al. 2006) and (ii) CKs of petrologic type <3.7 are not known.

Bridges et al. (1997) and Lewis et al. (2022) showed that evidence of metasomatism is present throughout the metamorphic sequence in OCs, and thus was a ubiquitous process in the OC parent bodies. In types 3.0–3.8, chondrule glassy mesostasis experienced dissolution and replacement by phyllosilicates, which survived only in type 3.0–3.1. Oxidation of phosphorous exsolved from FeNi-metal resulted in formation of merrillite and apatite; apatite typically replaces merrillite. Primary calcic plagioclase in chondrules was altered to various degrees by sodalite, scapolite, and nepheline in petrologic types 3.2–3.9, and to albite in types 3.6–5 (see also Bischoff and Keil 1983, 1984, 2012). Plagioclase also developed alteration features such as Ca-Na zoning (Grossman et al. 2000), micropores, and alteration lamellae in types 3–4. Sodic plagioclase is present in minor amounts as a primary phase, but also formed from the crystallization of chondrule mesostasis glass (types 3.2–3.9), and predominantly through albitization reactions in calcic plagioclase (types 3.6–5). K-feldspar occurs in albite in types 3.6–6 as fine-scale exsolution lamellae and as larger patches. Not all K-feldspar in OCs is secondary: e.g., coarse-grained K-feldspar (Or_{95}) occurs in achondritic clasts of unknown origin in Adzhi-Bogdo (LL3–6) breccia (Bischoff et al. 1993). In type 4–6 Ls and LLs, mesostasis glass crystallized into secondary plagioclase of diverse composition ($\text{An}_{<85}$). Equilibration of plagioclase is observed through type 5 and by type 6, plagioclase is chemically equilibrated at $\sim\text{An}_{11}$. Apatite evolves to Cl-apatite with a minor F and no OH. There are, however, exceptions: e.g., apatite in Renchen (L5–6) contains 3.4 wt% F and only 0.47 wt% Cl (Bischoff et al. 2019). Based on these observations, Lewis

et al. (2022) concluded that aqueous alteration during prograde metamorphism of OCs produced most of the alteration and equilibration features in their plagioclase. During retrograde metamorphism, high temperature, short duration infiltration of anhydrous, alkali- and halogen-bearing fluids caused incorporation of potassium into plagioclase that subsequently exsolved.

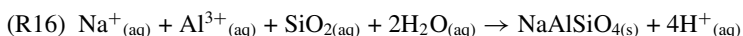
2.4 Metasomatic Alteration of Igneous CAIs in Allende ($CV_{\text{oxA}} > 3.6$)

Coarse-grained, cm-sized igneous CAIs are present exclusively in CV and CK chondrites. Several types of igneous CAIs are recognized: Compact Type A (CTA), Type B (B), Forsterite-bearing Type B (FoB), and Type C (C) (Fig. SM9). These types consist of similar primary minerals, but have different modal mineralogy and bulk chemical compositions (MacPherson 2014). Because of their large sizes, the common presence in a widely available CV3 chondrite fall Allende ($CV_{\text{oxA}} > 3.6$), and the importance for studying the early solar system chronology, the secondary mineralogy mainly of Allende igneous CAIs is characterized in detail (e.g., Krot et al. 2021).

Most of the secondary minerals in Allende igneous CAIs are Mg-rich and anhydrous (Table SM4). As a result, both nebular and asteroidal models have been proposed to explain their formation. According to the nebular models (Hashimoto and Grossman 1987; McGuire and Hashimoto 1989; Keller and Buseck 1991; Ushikubo et al. 2007a,b), secondary minerals formed during gas-solid reactions in the solar nebula. According to the asteroidal models (Brearley and Krot 2012; Krot et al. 2021), these minerals formed during aqueous fluid – rock interaction in the CV parent asteroid. Both nebular and asteroidal processes have been invoked to explain alteration of CV CAIs by Fagan et al. (2007).

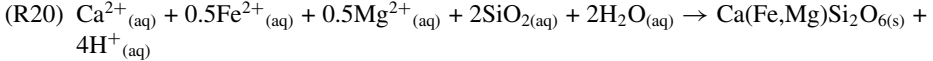
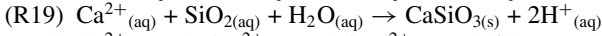
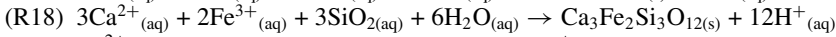
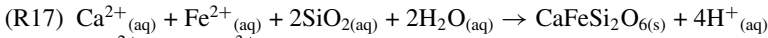
Secondary minerals providing clear evidence for involvement of the CO_2 - and H_2O -bearing fluid in their formation include clintonite, montmorillonite, margarite, biopyriboles, calcite, and tilleyite (Table SM4; Fig. SM10). Involvement of aqueous solutions is also indicated by the presence of veins of secondary minerals crosscutting primary anorthite and melilite, and by dissolution textures of anorthite and melilite with open space filled by secondary minerals (Fig. SM11).

Allende igneous CAIs are surrounded by Wark-Lovering (WL) rims that originated in the CAI-forming region (Wark and Lovering 1976), which are in turn surrounded by fine-grained matrix-like rims composed of secondary ferroan olivine and nepheline (Fig. SM9e), and by a layer of secondary CaFe-rich silicates (salite-hedenbergite pyroxenes, andradite, and wollastonite (Fig. SM9f). The altered regions of primary melilite are depleted in Ca and enriched in Si. There is a zoned distribution of secondary Na- and Cl-bearing minerals in the Allende CAIs: wadalite/adrianite is found almost exclusively in åkermanite-rich cores of Type B CAIs, whereas sodalite and nepheline are concentrated in their gehlenitic peripheries (Figs. SM9d,e). These observations provide clear evidence for an open-system behavior of several elements (Si, Na, Cl, Ca, and Al) during *in situ* metasomatic alteration of these CAIs: Si, Na, and Cl were added, whereas Ca and some Al were removed from the inclusions. The mobility of Al during the alteration is consistent with the presence of grossular, kushiroite, and Na-rich melilite in veins crosscutting primary anorthite grains inside the inclusions (Fig. SM11c). The outward transport of dissolved Al from CAIs and the influx of Na, K, and Si with an aqueous fluid equilibrated with the Allende matrix could explain the abundant nepheline grains in fine-grained rims around altered Allende CAIs (Fig. SM9e):

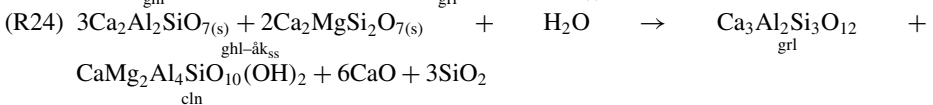
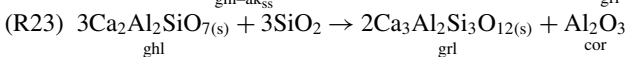
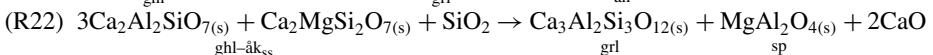
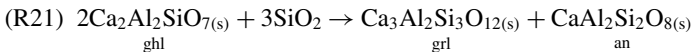


The zoned distribution of nepheline and sodalite in Allende CAIs and the lack of sodalite in fine-grained rims around these CAIs may indicate an earlier formation of nepheline than

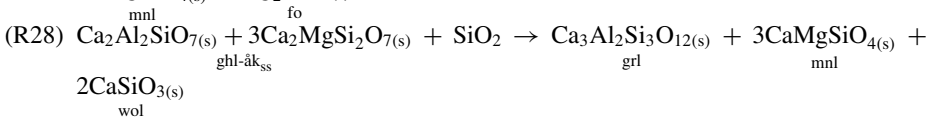
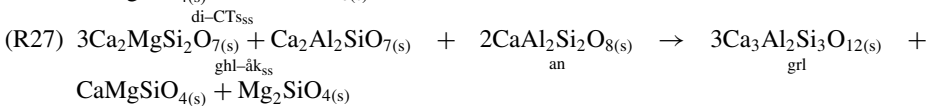
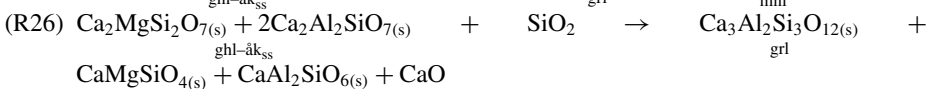
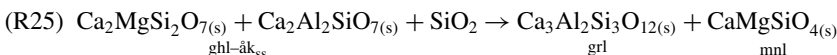
sodalite, consistent with observations of Che and Brearley (2021). Calcium released during alteration of melilite interacted with Fe-, Mg- and Si-enriched fluid that most likely was in equilibrium with the Allende fine-grained matrix (Krot et al. 2001; Ganino and Libourel 2017). This process resulted in precipitation of CaFe-rich silicates (hedenbergite, andradite, wollastonite, and salite-hedenbergite pyroxene) at the boundary between fine-grained rims and the Allende matrix:



Secondary mineral assemblages in Allende igneous CAIs are largely controlled by the elements mobilized by the fluid and chemical composition of melilite replaced, that ranges from nearly pure gehlenite ($\text{\AA}k_{<2}$) to $\text{\AA}k_{\sim 80}$. For example, gehlenitic melilite in CTA CAIs and in mantles of Type B1 CAIs is often crosscut by veins of grossular and anorthite with minor spinel and corundum (Figs. SM11a, 12). Mass-balance equations describing these reactions are:



\AA kermanite-rich melilite in cores of Type B1 CAIs and in Type C CAIs is replaced by coarse-grained grossular, monticellite, wollastonite, Al-diopside, and minor forsterite (Figs. SM13–14):

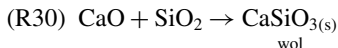


Because of large compositional variations of primary melilite in the Allende igneous CAIs, and, possibly, of local variations of fluid composition, different assemblages of secondary minerals can be observed even within a single inclusion (Fig. SM13).

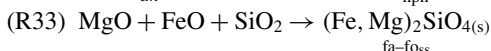
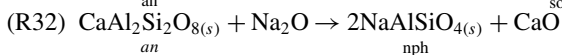
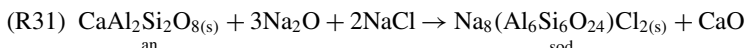
Secondary minerals in Allende igneous CAIs recorded multistage metasomatic alteration. For example, (i) melilite in a FoB CAI was replaced by grossular, monticellite, and wollastonite (Fig. SM14a). In the peripheral part of the same CAI, grossular and monticellite were subsequently replaced by Al-diopside (Fig. SM14b):



(ii) Secondary mineral assemblage of monticellite, Al-diopside, and wollastonite replacing åkermanitic melilite in a Type B2 CAI is crosscut by a monomineralic vein of wollastonite (Fig. SM14c):



(iii) Secondary anorthite in the peripheral portions of CAIs is often replaced by sodalite, nepheline, and ferroan olivine (Figs. 6c,d in Krot et al. 2021):



Secondary minerals also provide evidence for local variations in chemical composition of metasomatic fluid. These include (i) ferroan grossular overgrowing Fe-poor/free grossular (Fig. SM15a); (ii) ferroan monticellite overgrowing Fe-poor/free monticellite (Fig. SM15b), and (iii) hedenbergite and andradite overgrowing Fe-poor/free Al-diopside (Fig. SM15c). These late-formed Fe-bearing/rich secondary minerals are typically Ti-free. Only rare occurrences of Ti-rich garnet, hutchonite, overgrowing grossular have been described in the Allende Type B CAIs (Fig. SM15d). These observations suggest that mobility of titanium in the Allende aqueous fluid was very limited.

2.5 Metasomatic Alteration of Igneous CAIs in CK3.7–3.8 Chondrites

Coarse-grained igneous CAIs in CK3.7–3.8s have similar textures, primary mineralogies, and isotopic compositions to those from Allende (Chaumard et al. 2014; Shollenberger et al. 2018; Krot et al. 2024, 2023), but experienced higher degree of metasomatic alteration under much more oxidizing conditions, FMQ+2 to FMQ+4.5 *vs.* IW to ~FMQ, respectively (Righter and Neff 2007).

Only three igneous CAIs (CTA, B, FoB) have been studied in detail in CK3s so far (Fig. SM16; Krot et al. 2024). Secondary minerals identified in these CAIs are listed in Table SM5. In contrast to the commonly observed secondary monticellite, Na-melilite, nepheline, sodalite, and wollastonite in Allende igneous CAIs, none of these minerals have been identified in the CK3 CAIs studied. In addition, secondary grossular, Al-diopside, spinel, and olivine in CK3 CAIs are enriched in FeO, and secondary plagioclase contains significant Na₂O content (up to 85 mol% Ab).

Melilite is almost completely replaced by Fe-bearing grossular, Fe-bearing Al-diopside, clintonite, CaNa-plagioclase, FeMg-spinel, FeMg-olivine, and wadalite; anorthite is less altered (Figs. SM17–19). Primary Ti-rich pyroxenes (grossmanite and fassaite) are corroded by FeAl-diopside, ilmenite, titanite, FeMg-spinel, Ti-bearing grossular, and clintonite (Figs. SM17f, 18c–e). Low-Ti Al-diopside in a FoB CAI shows little evidence for alteration (Fig. SM19). Primary spinel and forsterite experienced Fe-Mg interexchange to various degrees. Coarse secondary grossular and Al-diopside in the CAIs cores are often chemically-zoned: the grain edges are enriched in TiO₂ (up to 3 and 7 wt%, respectively) suggesting local mobilization of Ti during metasomatic alteration (Figs. SM17c,d). Some grossular grains are overgrown by ferroan grossular with a sharp compositional boundary between them suggesting multistage formation of this mineral (Figs. SM17e, 18f).

The CK igneous CAIs are crosscut by veins of FeMg-olivine, CaNa-plagioclase, FeAl-diopside, Ti-bearing grossular, and occasionally contain geodes composed of these minerals (Figs. SM18b,f). These CAIs are also surrounded by a Ca-rich layer composed of chemically-zoned FeAl-diopside, Fe-grossular, and andradite; edges of the grossular and Al-diopside grains contain significant TiO₂ contents (up to 0.7 wt%) suggesting removal of Al and Ti from the host inclusions.

2.6 Metasomatic Alteration of Dark Inclusions in Allende

Chondritic lithic fragments, commonly observed in CV3s and named dark inclusions (DIs), appear to have experienced much higher degree of the metasomatic alteration than the host meteorites suggesting their alteration predated final accretion of the CV parent asteroid. Although originally the origin of DIs was attributed to nebular processes – condensation, aggregation, and alteration – under highly-oxidized, non-solar conditions (Kurat et al. 1989; Johnson et al. 1990), it was subsequently shown that alteration of DIs resulted in extensive mobilization of Ca, Na, K, and S and could have occurred in the CV parent asteroid in zones of high fluid permeability (Krot et al. 2001; Brearley and Krot 2012) prior to local impact brecciation and mixing. In this section, we will touch on only one aspect of Allende DIs – redistribution of Ca and formation of Ca-rich rims around them.

Figure SM20 shows three completely altered Allende DIs, 4302 – 1, IV – 1, and 3b – 1, which consist entirely of secondary minerals – ferroan olivine, nepheline, and CaFe-pyroxenes, and contain chondrule pseudomorphs (Fig. SM20d). In addition, the inclusion 4301 – 2 is crosscut by numerous CaFe-pyroxene veins. The DIs are surrounded by a thick layer of hedenbergite+wollastonite+andradite. High abundance of CaFe-silicate objects is also observed in the Allende host outside the CaFe-rich rim of 4302 – 1. The thickness of the CaFe-silicate layer around DIs is inversely proportional to the abundance of CaFe-pyroxenes inside their host inclusions suggesting loss of Ca from the previously altered DIs and its precipitation along the boundary with the Allende meteorite. Therefore, the Allende rimmed DIs, like CaFe-silicate layers around Allende CAIs (Fig. SM9), provide an important evidence for *in situ* alteration of Allende.

3 Modification of Organic Matter During Metasomatic Alteration

Organic material occurs in ordinary and carbonaceous chondrites (Yang and Epstein 1983; Robert et al. 1987; Alexander et al. 1998, 2007, 2012; Aponte et al. 2017, 2019), and mainly consists of insoluble organic matter (IOM); the soluble fraction (SOM) is very low in abundance. The IOM is located within the matrix, and is finely distributed through the mineral phases. The elemental and isotopic composition of IOM evolves with increasing petrologic type (see also Sects. 7.2 & 7.3), as well as its structural organization.

3.1 Abundance, Elemental and Isotopic Compositions of Insoluble Organic Matter

In comparison to lower grade (type 2 and 1) chondrites (CIs, CMs, and CRs), the IOM contents of CO3s, CV3s and UOCs are lower, which is mainly due to lower proportions of matrix in them. When normalized to the matrix contents, the IOM carbon content of the least metamorphosed type 3 chondrites is roughly comparable to those of CMs and CIs at ~2 wt% (Grady et al. 1989; Alexander et al. 2007). However, the H/C, N/C and O/C ratios

of IOM decrease with increasing petrologic type, indicating progressive loss of these heteroatoms as the structure becomes more aromatic in response to thermal stress (Remusat et al. 2019). For terrestrial samples, such as kerogens in sedimentary rocks, this process is called carbonization (Vandenbroucke and Largeau 2007).

The carbon-isotope compositions of IOM become progressively heavier with heating intensity in the parent body (Alexander et al. 2007). This is consistent with the usual process of “cracking” that organic macromolecules experience under thermal stress (Sackett 1978) in which the residual IOM gets heavier with preferential loss of ^{12}C -bearing functional groups (the ^{13}C bonds are stronger than ^{12}C bonds).

The nitrogen-isotope compositions of IOM are more variable, but scatter around $\delta^{15}\text{N}$ of $\sim 0\text{‰}$ and do not clearly correlate with the petrologic type. Heating experiments performed on the IOM from CIs and CMs also do not show evolution of N-isotope composition (Remusat et al. 2019).

The hydrogen-isotope compositions of IOM in UOCs exhibit a dramatic increase in δD (up to $\sim 12,000\text{‰}$) with increasing of petrologic type (Alexander et al. 2007). Flash pyrolysis to 600 °C of the IOM from the L3.3 chondrite Grosvenor Mountains (GRO) 95502 resulted in a sharp increase in the δD of the residue (Remusat et al. 2016). This could be due to (i) the presence of minute amounts of extremely D-rich and thermally resistant organic moieties in the IOM of UOCs (Aléon 2010; Remusat et al. 2016) or (ii) the loss of thermally labile functional groups that are hydroscopic and/or easily exchange hydrogen isotopes (e.g., OH or acid groups) during IOM isolation (Alexander et al. 2017). Hydrogen-isotope fractionation associated with the progressive oxidation of Fe by H_2O and loss of H_2 are also proposed to explain the progressive D-enrichment of OC IOM (Alexander et al. 2010). Relative to IOM in UOCs, the δD values are much lower in the IOM of COs and CVs. In the reduced CVs, δD only slightly increases with petrologic type (Alexander et al. 2007). This would imply that the putative D-rich, thermally resistant component in the UOC IOM is not present in the IOM of the COs and CVs. It is also problematic for the Fe oxidation explanation for the D-enrichments in the UOC IOM since there is clear petrologic evidence for oxidation of Fe in the COs and CVs (see Sect. 2.2).

3.2 Structural Organization of IOM: A Sensitive Tool of the Peak Metamorphic Temperature

Raman spectroscopy has turned out to be the instrument of choice to evaluate the extent of thermal metamorphism in type 3 chondrites (Michel-Levy and Lautie 1981; Quirico et al. 2003, 2009, 2014; Bonal et al. 2006, 2007, 2016, 2020, 2007). As for terrestrial sample analogues, the chondritic IOM is described as a disordered macromolecule and the so-called Raman “defect” bands are sensitive to the structural organization degree and to the size of the polyaromatic units. As largely documented for terrestrial samples (see Buseck and Beyssac 2014 for a review), with increasing peak metamorphic temperature, the defects progressively diminish and the size of the aromatic domains increases. Raman spectroscopy thus allows for classification of the petrologic grade of chondrites independently of the mineralogy. However, a precise cross comparison among chondrite groups is possible only if the accreted precursors were comparable, and if the conditions during metamorphism (duration, T , P , $f\text{O}_2$, etc.) were similar (Beyssac et al. 2003; Quirico et al. 2009). Unfortunately, Raman spectroscopy cannot be used as a thermometer, since we have a limited knowledge on the nature of the accreted organic precursors, and that simulating long term evolution over geological timescales in the laboratory is highly challenging. An attempt has been made to

use Raman spectra to estimate peak metamorphic temperatures in chondrites by correlating them with independent temperature estimates for specific meteorites (Busemann et al. 2007), but Bonal et al. (2016) questioned this approach.

The structural evolution of IOM under temperature increase can also be documented by high resolution TEM (transmission electron microscopy), which reveals the size of the aromatic units and the spacing between aromatic layers in them as the IOM becomes increasingly carbonized (Rouzaud and Oberlin 1990). It has been shown that the typical size of the aromatic units increases in COs, CVs, and UOCs between type 3 and 3.6, from dimensions of ~ 1 nm to ~ 5 – 10 nm, and the mean interlayer spacing decreases to values that are close to those of graphite (Smith and Buseck 1981; Rietmeijer and MacKinnon 1985; Remusat et al. 2008; Le Guillou et al. 2012). Nuclear magnetic resonance (NMR) spectroscopy shows that it is the aliphatic functional groups that are lost first during metamorphism, while in carbon XANES (X-ray absorption near edge structure) spectra the increasing absorption intensity of an exciton is directly linked to the growth of aromatic units (Cody et al. 2008).

3.3 Soluble Organic Matter

In type 3 chondrites, the abundance of soluble organic compounds is much lower than in meteorites of lower petrologic types and much more restricted in their diversity (Schmitt-Kopplin et al. 2012). As a result, the SOM in type 3 chondrites has received much less attention compared to low petrologic type counterparts. A few amino acids were reported in COs and CVs, with concentrations around ppm level ($\sim 10\times$ lower than in CMs, $\sim 300\times$ lower than in CRs). The predominance of amine terminal amino acids in COs and CVs is interpreted as the result of metasomatism in their parent bodies (Burton et al. 2012). A few monocarboxylic acids ranging from C1 to C6 have been reported in Allende, whereas acetic acid only has been detected in investigated COs and CVs (Aponte et al. 2019). However, the C-isotope compositions of the monocarboxylic acids in Allende indicate that they are dominated by terrestrial contamination. Aliphatic amines are also much less abundant in CVs and COs compared to CIs, CMs and CRs, with concentrations being one to three orders of magnitude lower (Aponte et al. 2017). In both cases, a lower abundance is likely the result of metasomatism in the parent body. Free polycyclic aromatic hydrocarbons (PAHs) show a similar pattern of decreasing abundance with increasing petrologic type (Elsila et al. 2005). In both COs and CVs, the lower abundances of SOM are almost certainly the result of metasomatic alteration in their parent bodies.

An extensive series of Mg-metalorganic compounds has been identified in thermally altered type 3 chondrites, but are virtually absent in type 1 and 2 chondrites (Ruf et al. 2017). This class of compounds is believed to be thermally stable, and hence can be used as a fingerprint for metasomatism in the parent bodies.

3.4 Open Questions

There is a clear effect of thermal metamorphism on organics in type 3 chondrites, which evolve chemically, isotopically and structurally. This transformation is interpreted as the result of long-term peak metamorphic temperature, likely related to ^{26}Al radioactive decay. It serves as a signature of the petrologic type and is a precious tool to classify chondrites.

Some questions remain open:

(i) The evolution mechanism (loss of hetero-atoms and structural reorganization) is assessed from measurements obtained on the bulk IOM but has not so far been studied *in situ*. This could reveal the organic-inorganic association and the role of the former on the maturation using scanning transmission X-ray microscopy (STXM) and TEM. This is, however,

made difficult by the increasing scarcity of organic particles within the matrix of higher petrologic types.

(ii) The origin of the precursors of OM in different chondrite groups and whether CVs, COs, and UOCs accreted the same mix of organic precursors remain unclear.

(iii) Whereas the role of fluids during metamorphism has been documented in UOCs, CVs and COs for inorganic phases, it is difficult to tell whether or not such fluids played a role on the organic evolution, or if temperature alone is responsible for the observed transformation. Experimentally identifying specific reaction pathways related to the presence of oxidizing fluids at temperature above 300 °C could potentially offer a way to resolve this question.

4 Modification of Presolar Grains Abundances and Abundances of Isotopically Anomalous Noble Gas Components Associated with Them During Aqueous/Metasomatic Alteration

Presolar grains are stellar condensates that form in the outflows of evolved stars (red giants, asymptotic red giants) and in the ejecta of stellar explosions (novae, supernovae), were incorporated in the protosolar molecular cloud (PMC), and can be found in chondrites and IDPs (e.g., Lewis et al. 1987; Tang and Anders 1988; Choi et al. 1998a; Zinner et al. 2005; Zinner 2014; Floss and Haenecour 2016). Presolar grains are distinguished from solar system material by their highly anomalous isotopic compositions and have been identified *in situ* with ion imaging techniques using either a NanoSIMS or SIMS+SCAPS (stacked CMOS-type active pixel sensor) detector. They are typically ~100–600 nm in size and include SiC, graphite, spinel, corundum, hibonite, and silicates (e.g., Nagashima et al. 2004; Zinner 2014; Nittler and Ciesla 2016).

In chondrites, presolar grains occur exclusively in interchondrule matrix and fine-grained chondrule rims, with apparently no systematic differences in the abundances among these locations (Leitner et al. 2016; Floss and Haenecour 2016). There are, however, indications of different alteration paths for interchondrule matrix and fine-grained rims in CRs and COs, resulting in differing presolar silicate abundances in matrix and rims (Leitner et al. 2016; Floss and Haenecour 2016).

Investigation of the abundance and distribution of presolar grains in different chondrite groups and petrologic types can shed light on possible heterogeneities in the PMC and/or PPD, and effects of metasomatic alteration and thermal metamorphism in the chondrite parent asteroids. To compare the distribution of presolar grains identified by ion imaging in matrices of different chondrites, they are commonly reported as matrix-normalized abundances. Presolar nanodiamond, SiC, and graphite contain relatively high abundance of isotopically anomalous noble gas components. As a result, the abundance of these presolar grains can be also inferred from whole-rock noble gas measurements (Huss 1990; Huss and Lewis 1995; Huss et al. 2003). Alexander (2005) argued that the relative abundances of presolar grains and their matrix-normalized absolute abundances are roughly CI-like in all chondrites. However, presolar SiC grain abundance estimates based on noble gas contents are inconsistent with this: they are typically lower (Huss and Lewis 1995; Huss et al. 2003). Alexander et al. (1990) and Russell et al. (1997) hypothesized that the presence of oxidants and a fluid to enhance diffusion and reaction may make it possible to degas/destroy the SiC grains at relatively low temperatures. Later Riebe et al. (2016) found that SiC grains in samples of Tagish Lake (C2ung) that experienced aqueous alteration to different degrees have different releases of noble gases when subjected to HNO₃ during Closed System Step

Etching (CSSE), a commonly used technique for extracting noble gases. This finding is in agreement with studies by Wieler et al. (1992), Floss and Stadermann (2009a), and Davidson et al. (2014) who showed that in CR2s the concentration of SiC grains determined by NanoSIMS raster ion imaging is higher than SiC concentrations derived from noble gas concentrations. Davidson et al. (2014) suggested that aqueous alteration in the CR parent body might have affected and degassed the outermost gas-rich layers of SiC grains, resulting in the lower estimate of SiC abundance based on noble gas concentrations.

Presolar silicate grains (typically amorphous), the most abundant type of presolar grains, make up to percent levels (on average ~ 400 ppm) of anhydrous IDPs (Floss et al. 2006; Busemann et al. 2009; Davidson et al. 2012; Alexander et al. 2017) and have a factor of a few lower abundance in type 3 carbonaceous chondrites (Nittler et al. 2018). The highest abundance of presolar silicates reported are in Acfer 094 and Chwichiya 002 (C3.00; 150–200 ppm), CO3.00 chondrites Allan Hills (ALHA)77307 (190 ppm) and DOM 08006 (240 ppm), minimally altered CRs (160–220 ppm), and the CM chondrite A-12169 (~ 275 ppm) (Nguyen et al. 2007, 2010, 2009b, 2009, 2015, 2018; Nittler et al. 2018, 2021; Davidson et al. 2019; Smith et al. 2023). Recent studies of UOCs showed similarly high presolar silicate abundances, although their distribution appears to be more heterogeneous. Presolar silicate abundances in relatively pristine matrices Semarkona (LL3.00), MET 00526 (L/LL3.05) and Queen Alexandra Range (QUE) 97008 (L3.05) are 150, 55–275, and 145 ppm, (see Fig. SM21 and references therein).

A systematic study of the inferred abundances of presolar SiC, diamond, and graphite in meteorites of various class and petrologic type showed correlations between the abundance patterns within a meteorite group and the metamorphic history of the host meteorite (Huss and Lewis 1995). Alexander et al. (1990) confirmed for a set of OCs the presence of isotopically anomalous phases only for specimens of petrologic type 3.6 or below, with destruction during metamorphism being the most likely and straightforward explanation. Besides SiC, presolar refractory oxide grains have been identified in grain separates from Tieschitz (H/L3.6) (Nittler et al. 1997, 2008). When compared the fraction of presolar Al-oxides among the total number of analyzed Al-oxide grains for the Tieschitz separates, $0.27 \pm 0.04\%$ (Nittler et al. 1997) and $1.59^{+0.44}_{-0.35}\%$ (Nittler et al. 2008), respectively, with those for ordinary chondrites of lower petrologic types, e.g., Krymka (LL3.2) with $0.85 \pm 0.11\%$, no significant difference is evident: i.e., the occurrence of refractory presolar grains appears to be, on a first order estimate, unchanged up to a petrologic type of ~ 3.6 .

Presolar silicates are sensitive indicators of aqueous alteration and thermal metamorphism (e.g., Zinner 2014) leading to rapid decreases in their abundance, decreases in the ratio of presolar silicates to oxides, and increases in the FeO contents in presolar silicates. However, abundances of presolar grains, especially of silicates, in chondrites of petrologic types >3.0 are not as thoroughly studied as in carbonaceous chondrites of lower petrologic types. Most of the available data are from OCs with petrologic types ranging from 3.00 to 3.2 (Fig. SM21).

Generally, the study of presolar grain abundances has the potential to support the identification of more complex, and potentially small, alteration processes affecting the fine-grained fractions of chondritic meteorites. Statistically significant variations of presolar silicate abundances could, in combination with other micro- and nanoanalytical techniques, provide additional information on the alteration state of a given area of a meteorite. The presolar silicate-to-oxide ratio can also be of limited value. Typically, presolar oxide abundances are very low (a few ppm), resulting in low grain numbers, which in turn are responsible for large errors for the respective ratios. Thus, statistically significant silicate-to-oxide ratios are only available for very thoroughly studied meteorites, or if the specimen contains

unusually high abundances of oxides (e.g., Leitner et al. 2012). A better approach might therefore be to monitor the presolar SiC abundances simultaneously, which are typically in the range of a few tens of ppm (e.g., Davidson et al. 2014); however, this requires even more effort, since both O-anomalous and C-anomalous grain abundances have to be measured. Such investigations are rather time-intensive, even more so, if presolar grain abundances are low. In addition, investigation of presolar silicates and oxides by AES (Auger Electron Spectroscopy, e.g., Floss and Stadermann 2009b; Bose et al. 2010) and TEM-EELS (Transmission Electron Microscopy-based Electron Energy Loss Spectroscopy) can yield information on their Fe contents and the oxidation state of iron in these grains, and thus, allow inferences about the alteration state of their host materials.

5 Experimental Studies and Physicochemical Analysis of Metasomatic Alteration Reactions

There are experimental and theoretical approaches in understanding physicochemical conditions of metasomatic alteration that affected type 3 ordinary, CO, and CV chondrites. Both are discussed below.

5.1 Experiments

Experimental studies are largely focused on the origin of FeNi-carbides (Llorca and Casanova 1998), magnetite (Hong and Fegley 1998), fayalite (Dobrică et al. 2022), and phyllosilicates (Tomeoka and Kojima 1995; Kojima and Tomeoka 1999, 2000) commonly observed in chondrules and matrices of type 3.0–3.2 chondrites, and alteration of melilite, anorthite, and enstatite described in refractory inclusions and chondrules in type 3 chondrites of higher petrologic subtypes (Nomura and Miyamoto 1998; Ohnishi and Tomeoka 2007; Ichimura et al. 2017). There are only a few experimental studies focused on the effects of alteration on noble gases concentrations and isotopic compositions (Nakasyo et al. 2000). Various types of starting materials were used in the experiments: synthetic and natural (meteorite fragments) samples, powder and block reactants, single crystals or polymineralic samples.

Llorca and Casanova (1998) studied reaction between kamacite grains and H_2+CO gas mixture in a nebular-type environment ($H_2/CO = 250:1$; 5×10^{-4} atm total pressure (P), and temperature (T) of 473K). Carbon deposition, hydrocarbon production in the C_1-C_4 range, and the formation of an ϵ -carbide phase occurs when FeNi-metal particles are exposed to the gas mixture for 10^3 hours, suggesting that gas-solid reactions in the solar nebula during CO hydrogenation represent a plausible mechanism for the formation of FeNi-carbides and carbonaceous material in IDPs.

The calculated magnetite formation temperatures in the canonical solar nebula are 357–384K, depending on the distribution of C between CO and CH_4 , but formation of magnetite in the solar nebula may be kinetically inhibited (Fegley and Prinn 1989). Hong and Fegley (1998) studied oxidation of FeNi-metal from the Gibeon meteorite to magnetite via the net reaction $3Fe_{(s)} + 4H_2O_{(g)} \rightarrow Fe_3O_{4(s)} + 4H_{2(g)}$ at ambient atmospheric P , at $T = 364-715K$, and a gas mixture with H_2/H_2O molar ratios of $\sim 4-41$. The obtained data were used to model the reaction time of FeNi-metal grains in the solar nebula as a function of grain size and T . Although the calculated reaction times for $0.1-1 \mu m$ radius metal grains are within theoretical lifetimes of the solar nebula (0.1–10 Ma), these estimates may provide only the lower limits (Hong and Fegley 1998) suggesting that formation of magnetite under nebular conditions (lower T , P , and higher H_2/H_2O ratio) seems unlikely.

Dobrică et al. (2022) performed a hydrothermal experiment using a mixture of FeO-rich amorphous silicates, Fe-metal powder, and water as starting components that was heated at $T = 493\text{K}$ for 6 days. Multiple mineral phases were observed in the experimental products, including elongated porous crystals of pure fayalite, greenalite $[(\text{Fe}^{2+}, \text{Fe}_{3+})_{2-3}\text{Si}_2\text{O}_5(\text{OH})_4]$, Fe-rich amorphous silicate, and iron oxide. The experiment supports a hydrothermal growth of fayalite in metasomatically altered type 3 chondrites (Zolotov et al. 2006). The lack of Mg in starting amorphous silicates is unfortunate, because matrices of primitive chondrites are dominated by FeMg-amorphous silicates which are often replaced by fayalite (Figs. SM3c,d).

Ohnishi and Tomeoka (2007) performed hydrothermal alteration reactions of enstatite at variable pH (0–14), T (373–573K), and reaction times (24–336 h). Under acidic conditions, no significant alteration occurred, whereas under neutral and alkaline conditions serpentine and saponite formed in different proportions. The amounts of phyllosilicates tend to increase with increasing pH , T , and run duration. There is also a tendency for saponite to form at higher pH and T and under longer run durations compared to serpentine. Ohnishi and Tomeoka (2007) concluded that alteration of CVs occurred at higher T and more alkaline conditions than that of CIs.

Tomeoka and Kojima (1995) and Kojima and Tomeoka (1999, 2000) performed long-time (7 weeks) hydrothermal alteration experiments of Allende at 723K, 800 bars pressure, under acidic and neutral conditions. It was found that pH and precursor mineralogy are important factors controlling phyllosilicate mineralogy. (i) *Under acidic conditions*, phyllosilicates replacing low-Ca pyroxene are dominated by a chlorite-group phyllosilicate containing 2–10 wt% Al_2O_3 ; serpentine and talc are minor. Phyllosilicates replacing matrix olivine consist of chlorite and serpentine and contain 8–10 wt% Al_2O_3 . Phyllosilicates replacing chondrule mesostasis are dominated by a high-Al (12–20 wt% Al_2O_3) phyllosilicate. CaFe-rich pyroxenes in the matrix are extensively replaced by saponite. Matrix altered under acidic conditions is depleted in Ca, Na, K, and S compared to the Allende matrix. (ii) *Under neutral conditions*, phyllosilicates produced are mainly low-Al chlorite containing up to 2.5 wt% Na_2O ; high-Al phyllosilicates were not observed. Diopside in CAIs and CaFe-rich pyroxenes in the matrix remain largely unaltered. Melilite and anorthite in CAIs are replaced by Al-saponite. Most common phyllosilicates in naturally altered CV3 are Fe-rich saponite and intergrowths of Na-mica with serpentine or saponite; chlorite is minor. Matrix altered under neutral conditions shows no significant differences in bulk major element compositions compared to the Allende matrix. By comparing the mineralogy and chemical compositions of naturally and artificially altered CVs, Kojima and Tomeoka (1999, 2000) concluded that alteration of CVs took place under variable pH .

In the experiments by Nomura and Miyamoto (1998) and Ichimura et al. (2017), pure gehlenite, diopside, spinel, and CaNa-plagioclase mixed with SiO_2 , $\pm\text{Al}_2\text{O}_3$ were heated in alkaline and acid solutions at T of $\sim 473\text{--}673\text{K}$. Spinel and diopside showed no evidence for alteration. Gehlenite was replaced by hydrogrossular $[\text{Ca}_3\text{Al}_2(\text{SiO}_4)_{3-x}(\text{OH})_{4x}]$, hydrosodalite $[\text{Na}_8\text{Al}_6\text{Si}_6\text{O}_{24}(\text{OH})_2 \times 2\text{H}_2\text{O}]$, analcime $(\text{NaAlSi}_2\text{O}_6 \times \text{H}_2\text{O})$, tobermorite $(\text{Ca}_5\text{Si}_6\text{O}_{18}\text{H}_2 \times 4\text{H}_2\text{O})$ and nepheline hydrate $(\text{NaAlSiO}_4 \times 0.5\text{H}_2\text{O})$; CaNa-plagioclase was replaced by Na-zeolites and analcime. Upon heating above 673 K, these minerals were transformed into grossular, dmisteinbergite, nepheline, sodalite, and wollastonite. Although none of the intermediate hydrated secondary phases have been observed in Allende CAIs, their formation cannot be excluded (e.g., Enokido et al. 2023). Studies of CAIs from CVs less metamorphosed than Allende are required to test this hypothesis.

Hydrothermal experiments performed on Allende at T of 473 K and water/rock of 1/50 showed that the concentration of noble gases decreased (Nakasyo et al. 2000). The loss of

noble gases also affected the isotopic composition of xenon, apparently due to the preferential alteration of nanodiamond containing mineral phase/phases relative to the trapped xenon component carrier ones.

5.2 Physicochemical Analysis of Metasomatic Alteration Reactions in CV Chondrites

5.2.1 Transport of Elements in Aqueous Solution and Steam During Metasomatic Alteration

It is inferred that CVs experienced fluid-rock interaction during progressive metamorphism (Krot et al. 1995, 1998). The common presence of phyllosilicates in Kaba (CV_{OxB}3.1) and nearly complete absence of hydrous minerals in Allende (CV_{OxA}>3.6) suggest the aqueous alteration in the CV parent asteroid occurred at progressively increasing temperatures and was followed by thermal metamorphism resulting in loss of aqueous solutions and dehydration of phyllosilicates in the CV_{OxA} chondrites.

Thermodynamic modeling of metasomatic alteration in a multisystem compositionally similar to the CVs (Petaev and Mironenko 1997) shows that there are two distinct stages of the alteration process. At low water/rock ratio, <0.1–0.3, no aqueous solution is present in the system, because all water is consumed by the oxidation and hydration reactions. Hydrogen released by these reactions forms large volumes of gaseous phase that contains trace amounts of volatile anionic elements (H, O, S, Cl, and C). At this stage, an aqueous alteration could proceed as an isochemical process without appreciable redistribution of cationic elements. At higher water/rock ratio, an aqueous solution coexists with the altered rock and is capable of redistributing cationic elements such as Na, Ca, Mg, Fe, Si, and Al among CV chondrite components.

The source of water in chondrite parent bodies was probably water ice. Upon heating, ice sublimates, melts and evaporates to form liquid water and steam, if the temperature exceeds boiling point (Fig. SM22). Liquid water and steam react with minerals and amorphous phases and leach some elements. Initially pure water is transformed into aqueous solution with SiO₂, Fe²⁺, Mn²⁺, Mg²⁺, Ca²⁺, Cl⁻, Na⁺, HCO₃⁻ etc. dissolved in it. Aqueous solution can transport dissolved elements at all temperatures. The ability of steam to transport elements depends on *P* and *T*. Supercritical fluid can efficiently transport elements, but measured Allende tensile strength values implies that at $P_{\text{gas}} > 100$ bars the rock would break and gas would be released (Grimm and McSween 1989). Therefore, the presence of supercritical fluid in the CV asteroid seems unlikely. Low density subcritical “wet” steam ($P_{\text{H}_2\text{O}} = P_{\text{H}_2\text{O, equil}}$, $T < 647$ K) or superheated “dry” steam ($P_{\text{H}_2\text{O}} < P_{\text{H}_2\text{O, equil}}$, $T > 647$ K) can transport some elements dissolved in the solution.

The concentration of a solute in steam depends on its *T*, *P*, and density. The distribution coefficients of solutes between the “parental” aqueous solution and the steam are low (Fig. SM23). Steam condensation would produce a “secondary” solution nearly free of solutes which cannot be efficiently transported by the steam. Solubility of iron in water under oxidizing conditions is low; therefore, equilibrium concentration of iron in the steam is close to 0. Calcium concentration in the steam is expected to be also low because of low distribution coefficients of CaCl₂ and CaSO₄ between steam and aqueous solution. Therefore, neither Fe nor Ca can be transported by steam. Note that rapid mobilization of Ca in aqueous solution in Allende at temperature < 473 K was experimentally demonstrated (Jones and Brearley 2006).

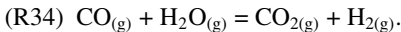
Metasomatic alteration was a non-equilibrium, multistage process with many reactions observed not going to a completion (see Sects. 2.2–2.6). Therefore, we used equilibrium approach in evaluating intensive parameters of the observed reactions assuming they reached

steady state. The calculated values of fugacities and activities of gaseous and aqueous species for each reaction are compared with each other and with independent estimates of these parameters when available. Gaseous and solid solutions were treated as ideal. For aqueous species, at any T , total pressure (P_{tot}) \approx pressure of saturated water vapor ($P_{\text{sat H}_2\text{O vapor}}$); i.e., gaseous phase involved in alteration reactions is nearly pure H_2O steam equilibrated with an aqueous solution.

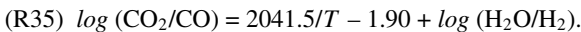
5.2.2 Fe-C-O-H System: Oxidation and Carburization of FeNi-Metal and Formation of FeNi-Carbides and Magnetite

Oxidation and carburization of FeNi-metal could have taken place by a gaseous phase only, without aqueous solutions (see Sect. 2.2). The gas-phase in the Fe-C-O-H system may contain up to three major C-bearing species (CO , CO_2 , and CH_4), depending on its chemical composition and P - T conditions. Carbon monoxide, CO , is dominant at high T , while methane, CH_4 , is the most thermodynamically stable C-bearing species at low T and moderate P characteristic of asteroidal alteration of type 3 chondrites as well as at low T and low P characteristic of the solar nebula. Therefore, if chemical equilibrium among gaseous species is reached in H-dominated nebular or asteroidal gases, then essentially all C will form CH_4 . However, in the cooling solar nebula the conversion of CO to CH_4 is kinetically inhibited (Fegley and Prinn 1989), thus CO remains the most abundant C-bearing species even at low T . Studies of hydrothermal gases in the H_2O - H_2 - CO_2 - CO - CH_4 system suggest that in hydrothermal natural systems formation of CH_4 is also kinetically inhibited (Chiodini and Marini 1998). Therefore, in the analysis of solid-gas equilibria, CH_4 can be neglected.

The partitioning of C between gaseous CO and CO_2 is governed by the redox reaction:

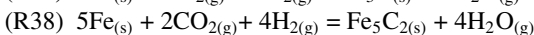
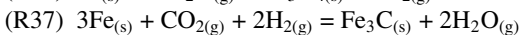
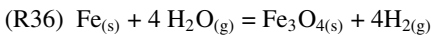


Concentration of either gaseous species can be used as an intensive parameter along with the T and P_{tot} of the system. Under oxidizing conditions necessary to stabilize magnetite, the CO_2/CO ratio in the gaseous phase is ~ 1 at high T ; below $\sim 900\text{K}$, it is rapidly increasing with falling T . Here we choose the $\text{H}_2\text{O}/\text{H}_2$ ratio and the concentration of CO_2 (X_{CO_2}) as intensive parameters. Then the CO_2/CO ratio in the gaseous phase can be calculated using the equation:



There are four Fe-carbides – orthorhombic Fe_2C (η -carbide), hexagonal Fe_7C_3 (ϵ -carbide), monoclinic Fe_5C_2 (χ -carbide or Hägg-carbide), and orthorhombic Fe_3C (θ -carbide or cementite, Ni-free analogue of meteoritic cohenite); their thermodynamic properties are poorly known (see *Gibbs free energies of Fe carbides in Supplementary Material to Sect. 5.2.2*).

The observed replacement of metal by magnetite and carbides in the Fe-C-O-H system can be described by the following chemical reactions:

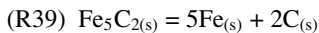


Similar reactions can be written for mutual replacements of metal, magnetite, cohenite, Hägg-carbide, wüstite ($\text{Fe}_{0.947}\text{O}$), and siderite (FeCO_3) (see *Fe-C-O-H system: Oxidation and carburization of FeNi-metal and formation of FeNi-carbides and magnetite in Supplementary Material to Sect. 5.2.2*).

Phase relations in the Fe-C-O-H system at different partial pressure of CO₂ (P_{CO_2}) as a function of T and H₂O/H₂ ratio are shown in Figure SM24. Low- and mid- T portions of the diagrams have the same topology at all P_{CO_2} : large stability fields of magnetite and Hägg-carbide are terminated by siderite at low T . As P_{CO_2} increases, the stability fields of siderite and Hägg-carbide increase at the expense of metal and magnetite; the Hägg-carbide–siderite–magnetite invariant point moves toward higher T and more oxidizing conditions (higher H₂O/H₂ ratios).

The topology of the high- T portions of the diagrams is P_{CO_2} -dependent. At $p_{\text{CO}_2} = 0.05$, the Hägg-carbide, unaltered (low-Ni) metal, magnetite, and wüstite are stable at $T = 812\text{K}$, H₂O/H₂ = 0.30, and CO₂/CO = 1.21. At lower P_{CO_2} values (Figs. SM24a,b), the invariant assemblage consists of metal, Hägg-carbide, and magnetite; the T and H₂O/H₂ ratio of the invariant point are decreasing as the P_{CO_2} decreases. If P_{CO_2} exceeds 0.05 bar, the invariant assemblage of metal, Hägg-carbide, and magnetite becomes unstable; metal and Hägg-carbide coexist with wüstite instead (Fig. SM24c). A decrease in X_{Fe} has the opposite effect on the phase boundaries due to enlargement of the metal stability field; e.g., altered metal is in equilibrium with magnetite and metastable Hägg-carbide even at $P_{\text{CO}_2} = 0.05$ (Fig. SM24d). A decrease in X_{mgt} would increase the magnetite stability field, but the amount of impurities in magnetite is so small, that the X_{mgt} never drops below ~ 0.98 ; this would result in a negligible shift (0.008 log unit) of the magnetite phase boundaries.

High- T portions of all diagrams include metastable fields of cohenite and/or Hägg-carbide (Fig. SM24). Cohenite is metastable at all T . Hägg carbide becomes metastable relative to unaltered metal ($X_{\text{Fe}} = 0.95$) and carbon above $\sim 700\text{K}$ according to reaction:



The assemblage of altered metal ($X_{\text{Fe}} = 0.5$) and Hägg-carbide is metastable above $\sim 650\text{K}$.

The lack of wüstite in FeNi-metal-carbide-magnetite assemblages places upper limits on the T (812K), P_{CO_2} (0.05 bar), and H₂O/H₂ ratio (0.30) of the initial stage of alteration of type 3 chondrites. However, at such conditions the Hägg-carbide would be metastable. To form a stable mineral assemblage of unaltered metal, magnetite, and Hägg-carbide, the T should be below 700K and P_{CO_2} in the gaseous phase less than ~ 0.002 bar (Fig. SM24a). No cohenite will be formed at this stage of alteration. Because both the T and H₂O/H₂ ratio of the invariant assemblage of metal, magnetite, and Hägg-carbide are decreasing with decreasing P_{CO_2} values, this assemblage can be formed either in a nebular (low P_{CO_2} values) or asteroidal (higher P_{CO_2} values) environment.

5.2.3 Ca-Fe-Mg-Si-O-H System: Formation of Pure Magnetite, Fayalite, Hedenbergite, Andradite, and Kirschsteinite

The formation conditions of these minerals have been first evaluated by Krot et al. (1998). Due to space limitation, an updated discussion of the reactions involved and their physicochemical parameters is presented in the *Supplementary Material to Sect. 5.2.3*. Overall, fayalite is stable in equilibrium with relatively reducing gaseous phase and Fe²⁺-rich aqueous solution. An increase of Ca²⁺ concentration in aqueous solution will result in formation of either hedenbergite or kirschsteinite at high or low SiO₂ concentrations in aqueous solution, respectively. Magnetite requires oxidizing gaseous phase and Fe²⁺-rich aqueous solution. Andradite would be the only mineral equilibrated with oxidizing gaseous phase and Ca²⁺-rich aqueous solution.

Thermochemical equilibria in closed gas-solution-rock system (Zolotov et al. 2006; Jogo et al. 2009) suggest that fayalite content in olivine is a function of T , P , water/rock ratio,

and ratios of activities of Mg and Fe in aqueous solution (Fig. SM26). Pure fayalite is stable at lower T and $\text{Fe}^{2+}/\text{Mg}^{2+}$ ratio in aqueous solution, and higher water/rock ratio and P than FeMg-olivine. In equilibrium, fayalite, magnetite, CaFe-pyroxenes, FeNi-carbides, and phyllosilicates coexist.

5.2.4 Ca-Fe-Mg-Si-O-H System: Formation of Ca-Rich Rims Around Allende Dark Inclusions

Petrographic observations (see Sect. 2.6) indicate that Ca-rich rims around Allende DIs grew *in situ*, at the interface between the DIs and the host Allende after the breccia formation of Allende. Because the growth of the Ca-rich rims requires significant transport (re-mobilization) of Ca, Fe, Si, and Mg, aqueous solutions must have played an important role in this process.

Physicochemical conditions of Ca-rich rim formation have been first evaluated by Krot et al. (2001) and are reviewed in some detail in the *Supplementary Material to Sect. 5.2.4*. The analysis of observed mineral-solution reactions revealed that the aqueous solutions locally equilibrated either with DIs or Allende matrix should have had $\text{Fe}^{2+}/\text{Ca}^{2+}$ ratios different by a factor of ~ 1.2 . This difference will result in diffusional fluxes of Ca^{2+} ions from the DIs towards the host Allende and Fe^{2+} ions in opposite direction, which will drive the reactive system toward equilibrium. Such compositional gradients and diffusional exchange of Ca and Fe between the solutions could exist only if the solutions are stagnant in pores of the host Allende and Allende DIs. Mixing of such solutions at the Allende–DI interface will increase concentrations of both Ca^{2+} and Fe^{2+} ions above the solubility limit of a CaFe-rich phase, which will precipitate in the cavities along the interface as a rim.

The rim formation will continue until matrix olivines in the DI and Allende become equilibrated, or the Ca-rich objects in the DI are exhausted, or when an aqueous solution dries out. Petrographic observations indicate that neither complete exhaustion of the DIs in Ca, nor complete equilibrium between the DIs and Allende have been achieved. As a result, the growth of the Ca-rich rims was probably terminated by disappearance of the aqueous solution.

5.2.5 Ca-Fe-Mg-Zn-H-O System: Formation of Zn-Bearing Hercynite and Ilmenite

Substitution of Ca by $\text{Fe}\pm\text{Zn}$ in krotite, grossite, and perovskite in CAIs indicates arrival Fe- and Zn-bearing aqueous solution from the matrix, perhaps, before the formation of CaFe-rich silicate rims around CAIs. As the $\text{Ca}^{2+}/\text{Fe}^{2+}$ ratio in the solution diminishes due to gradual removal of Ca^{2+} , krotite and grossite are altered first, followed by perovskite, well before the formation of Fe-bearing grossular (Figs. SM29a,b). An accompanying change of $\text{Mg}^{2+}/\text{Fe}^{2+}$ ratio should increase Fe content in spinel and olivine first, followed by formation monticellite-kirschsteinite solid solution (Fig. SM29c).

5.2.6 Alteration of Igneous CAIs in Allende

The altered patches and veins in mantles and cores of the Allende igneous CAIs are dominated by Ca,Al,Mg-rich phases which are enriched in SiO_2 and depleted in CaO compared to the primary phases (Tables SM1, 4). Such mineralogy requires an efficient addition of Si to and removal of Ca from CAIs. Most secondary FeMg-silicates in CAI interiors – forsterite, monticellite, grossular, and Al-diopside – are essentially Fe-free compared to the ferroan olivine, kirschsteinite, andradite, and salite–hedenbergite pyroxene in fine-grained rims and

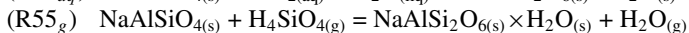
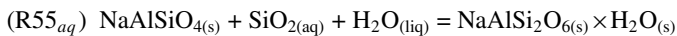
neighboring matrix. It appears that for some reason the Fe, abundant in an aqueous solution circulating through the Allende matrix (Krot et al. 1998; Ganino and Libourel 2017), has not been efficiently delivered to the interiors of the Allende igneous CAIs, which prior to the alteration were very compact. The same may be true for Na and Cl which are predicted to have high concentrations in an aqueous solution equilibrated with matrix (Petaev and Mironenko 1997), but in wadalite replacing åkermanitic melilite in Type B CAIs, these elements are decoupled from each other.

High concentrations of SiO₂, Na, and Cl are expected in both steam and aqueous solution. Therefore, these elements can be supplied to CAIs by steam equilibrated with aqueous solution without addition of Fe and Ca insoluble in steam. Reactions involving SiO₂, CO₂, Na, and Cl do not require aqueous solution. Reactions involving Ca, Fe, and Mg need aqueous solution for addition or removal of these elements. This may explain Fe-rich secondary minerals in matrix and FeO-poor secondary minerals in CAIs. Sodium and chlorine are not expected to be decoupled, unless steam formed at early stage of alteration contains only Cl-bearing species such as HCl and NH₄Cl which may be present in accreted ices (Zolotov and Mironenko 2007). This may explain formation of Na-free wadalite in CAI cores.

The inferences about the involvement of an aqueous solution or H₂O steam or both in the alteration process can be made based on a physicochemical analysis of the observed and/or possible alteration reactions and the textural relationships and mineral crystallization sequences in altered refractory inclusions. The textures and mineral chemistry of altered areas leave no doubt that an aqueous alteration was a non-equilibrium, multistage process, with many observed reactions not going to completion (see Sect. 2.4). Given the multitude of such non-equilibrium effects, considering them would make the problem intractable. Instead, an equilibrium approach in evaluating intensive parameters of the observed alteration reactions is employed here, assuming that they have reached a steady state. Then, in order to evaluate the plausibility of these reactions, the calculated values of fugacities and activities of different gaseous and aqueous species for each reaction are compared (for details see *Supplementary Material to Sect. 5.2.6.*). Since large number of cations and anions were involved in alteration reactions, the observed reactions can be split into several subsystems based on chemical elements added to and/or removed from primary mineral assemblages: (1) SiO₂, (2) CO₂, (3) SiO₂, CO₂, and Ca, and (4) Na±Cl and Ca±SiO₂. The results of modeling are shown in Figures SM30–33.

(1) The reactions involving addition of either gaseous H₄SiO₄ or aqueous SiO₂ (Fig. SM30), can proceed forward at any *T* and *P* because the required H₄SiO₄ fugacities in steam and activities of SiO₂ in aqueous solution are either much lower than or comparable with the solubility of SiO₂ in the steam or in the aqueous solution formed by its condensation.

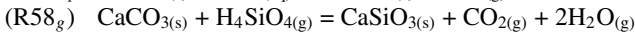
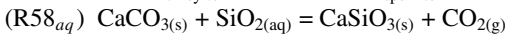
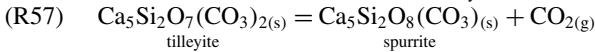
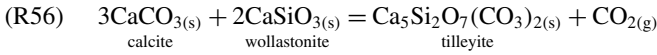
Of special value here are the reactions describing possible alteration of nepheline (NaAlSiO₄) to analcime (NaAlSi₂O_{6(s)} × H₂O):



Experimental studies at *T* – *P*_{H₂O} conditions identical to those considered here (Wilkin and Barnes 1998) showed that analcime is a stable phase, which can be dissolved or replaced by other phases if activities of SiO₂ and cations in the aqueous solution change. Therefore, the lack of analcime in the CV chondrites effectively places an upper limit on the H₄SiO₄ fugacity in the steam (Fig. SM30a) and *a*SiO₂ in aqueous solution (Fig. SM30b) implying that during CAIs' alteration, neither steam nor aqueous solution was SiO₂-saturated. Because the upper limit of aqueous *a*SiO₂ is 3–6 orders of magnitude higher than that in

the aqueous solution made by *in situ* condensation of steam (Fig. SM30b), a solution with a higher concentration of SiO₂, tentatively labeled as “external” aqueous solution, can be involved in CAI’s alteration. Such a solution must come to a CAI from outside (matrix?) as a liquid (Krot et al. 2001; Ganino and Libourel 2017). The lower limits on the H₄SiO₄ fugacity and α SiO₂ is set by reactions of melilite replacement by anorthite+grossular and by grossular+monticellite+wollastonite, respectively, which are widespread in the Allende igneous CAIs (Figs. SM12a, 14a).

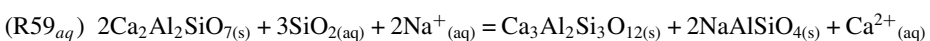
(2) The phase equilibria involving loss or gain of CO₂:

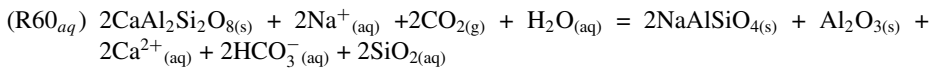


and the occurrence of tilleyite, wollastonite, and calcite within the same CAI (Fig. SM10a,c) allow to estimate of X_{CO_2} (P_{CO_2}) in steam as well as the activities of Ca²⁺ and HCO₃⁻ ions in aqueous solution (Fig. SM31). In Figure SM31, reactions involving melilite are shown for comparison; dashed lines denote metastable reactions. Relative stabilities of calcite and wollastonite are greatly dependent on the presence or lack of aqueous solution. If steam does not condense, stabilization of calcite requires high amounts of CO₂ (Fig. SM31a). If steam condenses, even very low (ppm) levels of CO₂ would result in precipitation of calcite. The general lack of calcite and common presence of wollastonite among melilite alteration products suggests that at the initial stages of melilite alteration silica was delivered as H₄SiO₄. Precipitation of calcite requires an aqueous solution with concentrations of [HCO₃⁻] $\approx 2 \times [\text{Ca}^{2+}]$ of $\sim 10^{-5} - 10^{-4}$ mol/kg_{H₂O} (Fig. SM31b) and rather low mole fraction of CO₂ in the steam (Fig. SM31), which seems to be reasonable for a C-bearing system such as carbonaceous chondrites. At such conditions, the observed replacement of melilite by grossular+monticellite+forsterite can readily proceed, providing the released CaO reacts with CO₂ to form calcite, regardless of whether an aqueous solution saturated in calcite is present or not.

(3) Many alteration reactions require addition of CO₂±SiO₂ accompanied by removal of Ca±SiO₂ (Fig. SM32). While both CO₂ and SiO₂ can be added or removed in either steam (Figs. SM32a,b) or aqueous solution (Figs. SM32c,d), the very low solubility of Ca in steam requires the presence of an aqueous solution, which would absorb the released Ca as either dissolved Ca bicarbonate, Ca²⁺ + 2HCO₃⁻ or calcite. If SiO₂ is delivered in the steam, the latter must condense to form an aqueous solution, initially Ca-free, before alteration reactions can proceed. In such a case, the amount of aqueous solution is expected to be rather small, with its Ca absorption capacity being limited. The calcium concentration in the aqueous solution will affect the sequence of alteration reactions, with the alteration of gehlenitic melilite to anorthite being the most sensitive to the Ca build up. If such aqueous solution was not effectively drained before becoming calcite saturated, one would expect to see widespread calcite associated with altered silicates. While calcite is present at least in some altered Allende CAIs, it tends to occur in nodules hinting for an effective removal of Ca²⁺ and HCO₃⁻ with drained solution, which can accumulate in cavities and fill them with calcite and other CO₂-bearing minerals upon evaporation of water to form nodules.

(4) The formation of nepheline and sodalite (Fig. SM33) requires an addition of Na and Cl and removal of Ca (reactions R31 and R32) and addition or removal SiO₂ (reactions R59_{aq} and R60_{aq}):





Sodium, chlorine, and SiO_2 can be transported by either steam or aqueous solution, but the necessity to remove Ca requires the presence of aqueous solution. As discussed above, the latter can be formed either by steam condensation or arrive from the matrix. The substitution of anorthite by sodalite at higher T requires a solution with rather low Na (and Cl) concentrations that can be formed by the steam condensation. At lower T , an ‘external’ aqueous solution with higher Na and Cl concentration is required. Other reactions can proceed only in the presence of ‘external’ aqueous solution with high concentrations of Na and Cl. It is interesting to note that the presence of widespread Cl-bearing and Na-free wadalite in many altered Type B CAIs (Fig. SM9d) points to the decoupling of Na and Cl during at least early stages of aqueous alteration. In this case, the Cl could be supplied by the steam containing HCl and NH_4Cl but neither NaCl nor NaOH.

6 Chronology of Metasomatic Alteration

The chronology of metasomatic alteration provides important constraints on the setting of alteration (nebular *vs.* asteroidal), the accretion time, and the thermal histories of chondrite parent asteroids.

6.1 ^{53}Mn - ^{53}Cr Chronology of Fayalite

Doyle et al. (2015) reported high precision SIMS analyses of nearly pure fayalite in EET 90161 (L3.05), A-881317 (CV_{oxB}3) and MAC 88107 (CO3.1-like). To ensure proper correction for relative sensitivities (RSF) between $^{55}\text{Mn}^+$ and $^{52}\text{Cr}^+$ ions, synthetic fayalite (Fa₉₉) doped with Mn and Cr was used as a standard. The excess of ^{53}Cr in fayalite from these meteorites correlates with the $^{55}\text{Mn}/^{52}\text{Cr}$ ratio, indicating *in situ* decay of ^{53}Mn . The inferred initial $^{53}\text{Mn}/^{55}\text{Mn}$ ratios [$^{53}\text{Mn}/^{55}\text{Mn}$]₀ in fayalite from EET 90161, A-881317 and MAC 88107 are $(4.35 \pm 1.23) \times 10^{-6}$, $(3.07 \pm 0.44) \times 10^{-6}$, and $(2.58 \pm 0.21) \times 10^{-6}$, respectively (Fig. SM34). Note that since RSF strongly depends on fayalite content in olivine (Fig. SM35), the reported ($^{53}\text{Mn}/^{55}\text{Mn}$)₀ in fayalite using San Carlos olivine (Fa₁₀) as a SIMS standard are incorrect (Table SM6).

^{53}Mn is a short-lived radionuclide, therefore a time anchor with a known $^{53}\text{Mn}/^{55}\text{Mn}$ ratio and U-corrected Pb-Pb absolute age is required to translate the inferred ($^{53}\text{Mn}/^{55}\text{Mn}$)₀ to absolute ages. The D’Orbigny angrite with the measured U-corrected Pb-Pb absolute age of 4563.37 ± 0.25 Ma (Brennecka and Wadhwa 2012) is often used as the time anchor. We note, however, that two different ($^{53}\text{Mn}/^{55}\text{Mn}$)₀ ratios have been reported for this meteorite, $(3.24 \pm 0.04) \times 10^{-6}$ (Glavin et al. 2004) and $(3.54 \pm 0.18) \times 10^{-6}$ (McKibbin et al. 2015). The former is based on whole-rock and mineral separates measurements using Thermal Ionization Mass Spectrometry (TIMS); the latter is based on *in situ* measurements of olivine and kirschsteinite using SIMS. When anchored to ($^{53}\text{Mn}/^{55}\text{Mn}$)₀ of D’Orbigny reported by Glavin et al. (2004), these ratios correspond to fayalite formation at $2.4^{+1.8}_{-1.3}$, $4.2^{+0.8}_{-0.7}$, and $5.1^{+0.5}_{-0.4}$ Ma after CV CAIs, respectively. If we use ($^{53}\text{Mn}/^{55}\text{Mn}$)₀ reported by McKibbin et al. (2015), these ages will be younger by ~ 0.5 Ma.

6.2 ^{53}Mn - ^{53}Cr Chronology of Kirschsteinite

MacPherson et al. (2017) reported high precision SIMS analyses of kirschsteinite (CaFeSiO_4) in the reduced CV3s Vigarano and Efremovka. To ensure proper correction for relative sensitivities between $^{55}\text{Mn}^+$ and $^{52}\text{Cr}^+$ ions, synthetic kirschsteinite doped with Mn and Cr was used as a standard. Well-resolved ^{53}Cr excesses correlate with $^{55}\text{Mn}/^{52}\text{Cr}$ indicative of *in situ* decay of ^{53}Mn ; the inferred initial ratio $(^{53}\text{Mn}/^{55}\text{Mn})_0$ is $(3.71 \pm 0.50) \times 10^{-6}$ (Fig. SM36). When anchored to ^{53}Mn - ^{53}Cr relative and U-corrected ^{207}Pb - ^{206}Pb absolute ages of the D'Orbigny angrite (Glavin et al. 2004; Brennecka and Wadhwa 2012), this ratio corresponds to kirschsteinite formation $3.2^{+0.8}_{-0.7}$ Ma after CV CAIs. If we use $(^{53}\text{Mn}/^{55}\text{Mn})_0$ reported by McKibbin et al. (2015) as an anchor, this age will be younger by ~ 0.5 Ma. The kirschsteinite data are consistent within error with the data for aqueously-formed fayalite from the CV_{oxB3} chondrite A-881317 as reported by Doyle et al. (2015), supporting the idea that CaFe-silicates in CV3s are cogenetic with fayalite and formed during metasomatic alteration in the CV parent asteroid(s).

6.3 ^{26}Al - ^{26}Mg Chronology of Secondary Minerals in CV3 Igneous CAIs

There are a number of secondary minerals in the Allende igneous CAIs with high $^{27}\text{Al}/^{24}\text{Mg}$ ratio, >20 , including anorthite, corundum, grossular, nepheline, and sodalite, and therefore suitable for search for a resolvable excess of radiogenic ^{26}Mg ($^{26}\text{Mg}^*$) using *in situ* SIMS measurements. Most analyses of these minerals showed no detectable $^{26}\text{Mg}^*$ [$(^{26}\text{Al}/^{27}\text{Al})_0 < 5 \times 10^{-6}$] suggesting formation > 3 Ma after primary CAI minerals (e.g., Hsu et al. 2006). This formation age is consistent with ^{53}Mn - ^{53}Cr ages of secondary fayalite and kirschsteinite in CV3s, and, thus suggesting metasomatic alteration of Allende CAIs occurred in an asteroidal setting. However, Fagan et al. (2007) reported resolvable $^{26}\text{Mg}^*$ in several grossular and plagioclase analyses of Type B and CTA CAIs in Allende which correspond to the inferred $(^{26}\text{Al}/^{27}\text{Al})_0$ of $\sim 4.5 \times 10^{-5}$ (see their Fig. 8). Fagan et al. (2007) concluded that Allende CAIs experienced a protracted, episodic alteration: some alteration occurred during the formation of CAIs; some continued in the CV parent asteroid. This interpretation was subsequently challenged by Krot et al. (2010) who demonstrated that $^{26}\text{Mg}^*$ in secondary grossular could have been inherited from primary gehlenitic melilite replaced by this grossular, and, thus has no chronological significance (Fig. SM37).

Ushikubo et al. (2007a,b) reported $^{26}\text{Mg}^*$ in anorthite of an Allende Type B CAI corresponding to $(^{26}\text{Al}/^{27}\text{Al})_0$ of $(1.2 \pm 0.5) \times 10^{-5}$ and interpreted this result as an evidence for a late-stage nebular episode of alteration. Krot et al. (2021) showed subsequently that anorthite measured by Ushikubo et al. (2007a,b) is in fact primary, igneous and its Al-Mg isotope systematics was probably disturbed during thermal metamorphism (see Sect. 6.4) and, therefore has no chronological significance.

To summarize, ^{26}Al - ^{26}Mg systematics of secondary minerals in Allende CAIs suggest that metasomatic alteration was a late-stage process, > 3 Ma after crystallization of primary minerals.

6.4 Modification of ^{26}Al - ^{26}Mg Systematics in Primary Minerals of CAIs and Chondrules from Metasomatically Altered Type 3 Chondrites

Metasomatic alteration could have disturbed Al-Mg isotope systematics in some primary phases in chondrules and refractory inclusions of type 3 chondrites. In type 3.0–3.1 UOCs, COs and CVs, most CAIs and AOs contain $^{26}\text{Mg}^*$ due to *in situ* decay of ^{26}Al and

define internal isochrons with the canonical $(^{26}\text{Al}/^{27}\text{Al})_0$ of $\sim 5 \times 10^{-5}$ (e.g., MacPherson et al. 1995; Ito and Messenger 2010; Ushikubo et al. 2017). These also include CAIs which experienced postcrystallization O-isotope exchange in melilite, anorthite, grossite, and krotite (e.g., Simon et al. 2019), suggesting that Mg self-diffusion in these minerals under $P - T - f_{\text{O}_2}$ conditions of metamorphic alteration of type 3.0–3.1 chondrites is much slower than O self-diffusion.

In CAIs from more metamorphosed chondrites such as Allende (CV>3.6), the $(^{26}\text{Al}/^{27}\text{Al})_0$ of anorthite show a wide spread, ranging from the canonical to ~ 0 , whereas other minerals in the same CAIs plot along the canonical isochron (e.g., Jacobsen et al. 2008). The observed spread in $(^{26}\text{Al}/^{27}\text{Al})_0$ in anorthite is most likely due to redistribution of Mg isotopes through Mg-self diffusion (Fig. SM38) during thermal metamorphism that resulted in homogenization of Mg isotopes and disturbance of its ^{26}Al - ^{26}Mg systematics (LaTourette and Wasserburg 1998; Ito and Messenger 2010). Although both melilite and anorthite in Allende igneous CAIs experienced postcrystallization O-isotope exchange (see Sect. 7.1.4.3), the ^{26}Al - ^{26}Mg systematics in melilite are undisturbed, suggesting its O self-diffusion in melilite is much faster than Mg self-diffusion under $P - T - f_{\text{O}_2}$ conditions of metamorphic alteration experienced by Allende.

In coarse-grained igneous CAIs from NWA 4964 (CK3.8) and NWA (CK3.7), fluid-assisted thermal metamorphism resulted in the disturbance of ^{26}Al - ^{26}Mg systematics to various degree in melilite, grossmanite, AlTi-diopside, and spinel (Fig. SM39; Krot et al. 2023).

In chondrules from type 3.0–3.1, ^{26}Al - ^{26}Mg systematics of chemically pristine plagioclase (having excess of Si and high Mg content; Tenner et al. 2019) appears to be undisturbed, even when plagioclase experienced extensive O-isotope exchange (Nagashima et al. 2017, 2018, 2018, 2021, 2022). In contrast, ^{26}Al - ^{26}Mg systematics of chondrule glassy mesostasis and plagioclase replaced by nepheline in weakly metamorphosed chondrites (3.05–3.1) can be reset resulting in younger crystallization ages (Van Orman et al. 2014; Nagashima et al. 2017; Piralla et al. 2023).

6.5 ^{36}Cl - ^{36}S Systematics of Sodalite and Wadalite in Allende and Ningqiang (C3-Ungrouped)

^{36}Cl is a short-lived radionuclide that decays to ^{36}Ar (98.1%, β^-) and ^{36}S (1.9%, ϵ and β^+) with a half-life of 0.3 Ma. Early ^{36}Cl studies of early solar system materials primarily focused on the search for ^{36}Ar excesses (Villa et al. 1981; Göbel et al. 1982; Murty et al. 1997; Rai et al. 2003) and provided no conclusive evidence for the presence of ^{36}Cl in the early solar system. Turner et al. (2013) first reported ^{36}Ar excesses produced by the decay of ^{36}Cl in sodalite from the Allende CAI *Pink Angel*. The initial $^{36}\text{Cl}/^{35}\text{Cl}$ ratio ($(^{36}\text{Cl}/^{35}\text{Cl})_0$) in sodalite that formed ~ 7 Ma after CAI formation (based on ^{129}I - ^{129}Xe chronology) is $(1.9 \pm 0.5) \times 10^{-8}$. No evidence for ^{26}Al , $(^{26}\text{Al}/^{27}\text{Al})_0 < 1.7 \times 10^{-6}$, was found in the *Pink Angel* sodalite (Hsu et al. 2006). Conversely, studies of the ^{36}Cl - ^{36}S systematics in sodalite and wadalite in CAIs and chondrules from Allende and Ningqiang showed clear excesses of ^{36}S correlated with $^{35}\text{Cl}/^{34}\text{S}$ ratios, indicative for *in situ* decay of ^{36}Cl (Lin et al. 2005; Hsu et al. 2006; Ushikubo et al. 2007a,b; Jacobsen et al. 2011). The inferred $(^{36}\text{Cl}/^{35}\text{Cl})_0$ in these minerals ranges from $(1.81 \pm 0.13) \times 10^{-5}$ to $(3.7 \pm 0.8) \times 10^{-6}$. The ^{26}Al - ^{26}Mg systematics in the same sodalite and grossular-wadalite mineral assemblage showed no resolvable excesses of ^{26}Al , with upper limits on $(^{26}\text{Al}/^{27}\text{Al})_0$ ranging between 0.4×10^{-6} and 7.0×10^{-6} . This corresponds to formation ages between 3 to 4 Ma after CAI formation, suggesting that sodalite and wadalite in the CV3 parent body formed after or close to the time ^{26}Al had gone extinct.

Large excesses of ^{36}S were reported in sodalite of a heavily metasomatically altered Allende CAI *Curious Marie*. These excesses do not correlate with the $^{35}\text{Cl}/^{34}\text{S}$ ratios, suggesting late closed-system homogenization of ^{36}S excesses after ^{36}Cl became extinct (Tang et al. 2017). The ^{26}Al - ^{26}Mg systematics of *Curious Marie* shows nearly flat, elevated $^{26}\text{Mg}^*$ ($\sim 40\%$) and extremely high bulk $^{27}\text{Al}/^{24}\text{Mg}$ ratio (~ 95). Assuming $\delta^{26}\text{Mg}_0 = 0$, the inferred model ($^{26}\text{Al}/^{27}\text{Al}$)₀ is $(6.2 \pm 0.9) \times 10^{-5}$. These observations suggest that either the secondary phases in *Curious Marie* formed early (< 0.15 Ma after CAI formation) when ^{26}Al was still at the canonical level, as favored by Tang et al. (2017), or the alteration took place after ^{26}Al had completely decayed away and $^{26}\text{Mg}^*$ had been homogenized.

No ^{36}S excesses were found in several CAIs and chondrules from CVs (Plagge et al. 2006; Nakashima et al. 2008) and in a halite from the Zag (H3-6) meteorite (Nakashima et al. 2010).

There is no agreement on the origin of the ^{36}Cl excesses. The proposed models include stellar nucleosynthesis (Lin et al. 2005; Tang et al. 2017) and irradiation by solar energetic particles (SEP) (Hsu et al. 2006; Jacobsen et al. 2011; Wasserburg et al. 2011; Leya et al. 2018). The initial abundance of ^{36}Cl and decoupling from ^{26}Al in same or co-existing minerals, as well as the “young” I-Xe ages in *Pink Angle* sodalite, indicate (i) the production of ^{36}Cl by late-stage SEP irradiation in the PPD, and (ii) the production of ^{36}Cl is unrelated to the origin of ^{26}Al (Jacobsen et al. 2011). Jacobsen et al. (2011) concluded that ^{36}Cl was largely produced by irradiation of a volatile-rich reservoir [$^{35}\text{Cl}(\text{n}, \gamma)^{36}\text{Cl}$], possibly HCl-bearing water ices (Zolotov and Mironenko 2007), in an optically thin region of the PPD adjacent to the region in which the CV chondrite parent asteroid accreted while the Sun was a weak T Tauri star. Subsequently, ^{36}Cl accreted into the Allende together with condensed water ices. Note that Leya et al. (2018) concluded that the correlation lines in the diagram $^{36}\text{S}/^{34}\text{S}$ and $^{35}\text{Cl}/^{34}\text{S}$ are not isochrons but mixing between water that contains chlorine (likely as ice) that has been irradiated either by galactic cosmic rays or SEP and sulfur (without any chlorine) with solar isotopic composition.

More work is needed to understand the origin of ^{36}Cl in the secondary metasomatic minerals in chondrites. For example, (i) wadalite is present in a CTA CAI from NWA 4964 (CK3.8) (Fig. SM17a) but has not been analyzed for its ^{36}Cl - ^{36}S systematics yet. (ii) Large excesses of ^{36}S correlating with $^{35}\text{Cl}/^{34}\text{S}$ ratios, with ($^{36}\text{Cl}/^{35}\text{Cl}$)₀ as high as $(9.4 \pm 0.8) \times 10^{-5}$, have been observed in lawrencite (FeCl_2) in an EL3 clast from the polymict ureilite Almahata Sitta (Feng et al. 2012). These preliminary results have not been published and need to be reinvestigated; they could have implication for the origin and distribution of ^{36}Cl in the early solar system as well as for gas dissipation in the PPD (Jacobsen and Desch 2023).

6.6 ^{129}I - ^{129}Xe Chronology of the CV, CO, and CK Chondritic Components

The ^{129}I - ^{129}Xe chronometer is based on the decay of now-extinct ^{129}I to ^{129}Xe with half-life of 16.14 Ma (García-Torano et al. 2018), where the ratio of the accumulated daughter ^{129}Xe to stable ^{127}I in the host mineral reflects the iodine isotopic ratio $^{129}\text{I}/^{127}\text{I}$ at closure to Xe loss. This ratio is measured as the ratio of radiogenic ^{129}Xe ($^{129}\text{Xe}^*$) present in the sample to $^{128}\text{Xe}^*$ produced by artificial neutron irradiation of ^{127}I . This relative chronometer can be tied to the absolute age through the Shallowater aubrite. The absolute age of Shallowater has not been measured directly due to the low U content; instead it is derived from the observed correlation between ^{129}I - ^{129}Xe and ^{207}Pb - ^{206}Pb ages in a number of samples. Currently, the re-evaluated absolute I-Xe age of Shallowater is 4562.4 ± 0.2 Ma (Pravdivtseva et al. 2017a).

I-Xe dating cannot be done *in situ*: separation of individual minerals or chondritic components is required. The separated polymineralic chondritic components could potentially

contain multiple I-carrier phases with different closure times. The I-Xe ages have been reported for single plagioclase and pyroxene grains (Pravdivtseva et al. 2009, 2013), phyllosilicate separates (Krot et al. 2006), and magnetite separates (Pravdivtseva et al. 2017b). All these minerals occur as secondary phases in metasomatically altered type 3 chondrites (Tables SM3–5). Such phases, when they are small, cannot be cleanly separated, which could make interpretation of I-Xe ages difficult. Nevertheless, the age information in such complex samples can be successfully resolved if, during step-wise heating, radiogenic Xe from different host phases is released at significantly different temperatures, resulting in multiple I-Xe isochrons.

I-Xe ages of magnetites separated from several CV3s, CO3s, and CK3–5 s and of Allende CAIs, chondrules, matrix, and DIs from several CVs relative to Shallowater are shown in Figure SM40 and listed in Tables SM7–8. It appears that formation of magnetite in CVs, COs, and CKs started nearly contemporaneously with the formation of magnetite in Orgueil (CI1; Pravdivtseva et al. 2017b) and Murchison (CM2; Pravdivtseva et al. 2013), ~ 0 –2 Ma prior to Shallowater.

I-Xe ages of the Allende matrix and most Allende DIs are within the range of the CV magnetite. These samples yielded high-precision I-Xe ages suggesting similar I-carrier phase. Two DIs, one from Allende and another from Efremovka have older I-Xe ages (5.7 ± 0.4 Ma and 4.92 ± 1.8 Ma prior to Shallowater, respectively), suggesting a different, more refractory, I-carrier phase that was apparently not affected by later metasomatic alteration.

The heavily-altered fine-grained CAIs from Allende, with the exception of the CAI *Curious Marie*, have nearly identical release profiles for radiogenic $^{129}\text{Xe}^*$ and $^{128}\text{Xe}^*$ suggesting the same I-carrier, most likely sodalite (Kirschbaum 1988; Pravdivtseva et al. 2003). The major release peak of $^{129}\text{Xe}^*$ in *Curious Marie* is also consistent with sodalite being the I-carrier phase. However, high-resolution step-wise pyrolysis of this CAI demonstrated that the I-Xe system survived intact in two different mineral phases, suggesting that metasomatic alteration affected them to different degrees. The fission composition in low- T extractions is consistent with Xe from ^{244}Pu while Xe from neutron-induced fission of ^{235}U resided in the high- T release peak, supporting two different I-carrier mineral phases.

I-Xe ages of the Allende fine-grained CAIs are ~ 3 Ma after Shallowater suggesting the I-carrier phase (sodalite) recorded later stage of metasomatic alteration compared to the Allende matrix and DIs. I-Xe ages of an altered chondrule, an altered coarse-grained CAI, and one of the I-carrier secondary phases in *Curious Marie* have intermediate ages, ~ 0 –1 Ma after Shallowater (Fig. SM40). Two DIs from the reduced CV3s Vigarano and Leoville have the youngest I-Xe ages, ~ 9 Ma after Shallowater. Overall, CV3 components recorded a prolonged duration of metasomatic alteration of the CV parent asteroid, ~ 11 Ma.

6.7 ^{129}I - ^{129}Xe Chronology of Chondrules from Type 3 Ordinary Chondrites

Among the 43 LL3 chondrules studied (Gilmour et al. 2006; Fig. SM41; Table SM9 and references therein), 10 have yielded two distinct isochrons, with higher temperature releases corresponding to the older apparent I-Xe ages, probably related to chondrule formation in the lower metamorphic grade chondrules. The I-Xe ages of the oldest OC chondrules cluster tightly at 2.6 ± 1.8 Ma after CV CAIs. Lower temperature I-Xe ages generally reflect post-formational alteration. Not only do LL chondrules tend to be younger with increasing metamorphic grade, but the spread between high- and low-temperature I-Xe ages increases also, suggesting longer or multiple alteration events for higher metamorphic grade LL meteorites. Within each OC group, the I-Xe ages of chondrules from the higher metamorphic

grades tend to be younger, indicating longer post-formational processing or multiple secondary alteration events (Caffee et al. 1982; Pravdivtseva et al. 2002, 2004).

6.8 Accretion Time and Thermal History of CV, CO, CK, and OC Parent Asteroids

The ^{129}I - ^{129}Xe ages of magnetites from CV3s, CO3s, and CK3–5 s indicate the accretion of their parent bodies no later than ~ 3 Ma after CV CAIs. Furthermore, the ^{129}I - ^{129}Xe ages of altered CAIs and DIs in CV3s suggest a prolonged duration of metasomatic alteration, longer than 11 Ma, although the carrier phases and corresponding closure temperatures of I-Xe isotopic systematics are not well-constrained. The latter requires a relatively large parent asteroid for CV chondrites.

Thermal evolution models of asteroids heated by ^{26}Al decay by Hevey and Sanders (2006) showed that asteroids as large as 50 km in radius can sustain high T close to peak T for longer than 10 Ma. Doyle et al. (2015) modelled the thermal evolution of the CV, CO, and L chondrite parent bodies heated by ^{26}Al decay. Peak T in asteroids with radius larger than 30 km are predominantly determined by their accretion time (the amount of ^{26}Al) but not by the parent body size. Thus, Doyle et al. (2015) determined the accretion time of these bodies, which are assumed to be >30 km in radius, to be 2.4–2.7 Ma, 2.1–2.4 Ma, and 1.6–1.8 Ma after CV CAIs for the CV, CO, and L chondrite parent bodies, respectively, so that the central T of these bodies reach the estimated peak metamorphic T (~ 600 °C, ~ 600 °C, and ~ 950 °C, respectively). They showed that fayalite can form ~ 0.6 Ma later than the accretion of the L chondrite parent body, or ~ 1.5 – 2.5 Ma later than the accretion of the CV and CO chondrite parent bodies in their outer regions where the peak T are no higher than 300 °C and suitable for fayalite formation without later Fe-Mg interdiffusion. These ages are consistent with the ^{53}Mn - ^{53}Cr ages of fayalite and kirschsteinite.

6.9 Future Studies

I-Xe ages of the Allende CV_{oxA} >3.6 components dominate the data set for CV3s (Fig. SM40), demonstrating a need for a broader I-Xe study of chondritic components from the reduced and oxidized CVs of different petrologic types. Although small single chondrules could yield high-precision I-Xe ages (Caffee et al. 1982), the I-Xe ages of CV, CO, and CK chondrules are virtually absent. Resonance ionization techniques, such as the RELAX instrument developed by the University of Manchester group (Gilmour et al. 2006; Crowther et al. 2008), yield greater sensitivity than conventional mass spectrometry and provide unique opportunities for small samples and single-mineral studies, which would be critical for identifying I-carrier phases in metasomatically altered chondritic components.

7 Records of Metasomatic Alteration in Oxygen, Hydrogen, Nitrogen, Carbon, Sulfur, and Chlorine Isotopic Systematics of Type 3 Chondrites and Their Components

7.1 Oxygen Isotopes

7.1.1 Introduction

Oxygen has three stable isotopes: ^{16}O , ^{17}O , and ^{18}O . Oxygen-isotope compositions of the solar system materials are typically expressed as permil deviations from the Vienna Standard

Mean Ocean Water (VSMOW) value, $\delta^{17}\text{O}$ and $\delta^{18}\text{O}$: $\delta^i\text{O} = ((i\text{O}/^{16}\text{O})_{\text{sample}}/(i\text{O}/^{16}\text{O})_{\text{VSMOW}} - 1) \times 1000$, where $i = 17, 18$. On a three-isotope oxygen diagram, $\delta^{17}\text{O}$ vs. $\delta^{18}\text{O}$, all terrestrial samples plot along a line with slope of ~ 0.52 , called the terrestrial fractionation (TF) line, whereas extraterrestrial materials deviate from this line; the deviation is expressed as $\Delta^{17}\text{O} = \delta^{17}\text{O} - 0.52 \times \delta^{18}\text{O}$. Bulk oxygen-isotope composition of chondrites is one of the most important parameters used for their classification (Clayton 2008; Yurimoto et al. 2008; Ireland et al. 2020).

Ultraviolet CO self-shielding either in the PMC and/or in the outer regions of the PPD (outside ~ 30 AU) resulting in formation of ^{16}O -rich CO and $^{17,18}\text{O}$ -enriched water followed by silicate dust – $\text{H}_2\text{O}_{\text{ice}} - \text{CO}_{\text{gas}}$ fractionation and evaporation is the currently favored mechanism invoked to explain the observed range of $\Delta^{17}\text{O}$ in the solar system (Clayton 2002; Yurimoto and Kuramoto 2004; Lyons and Young 2005; Krot et al. 2020).

Chondrules (phenocrysts and mesostasis) and fine-grained refractory inclusions in unmetamorphosed chondrites (petrologic type ≤ 3.0) have internally uniform $\Delta^{17}\text{O}$ and on a three-isotope oxygen diagram plot along \sim slope-1 line, named the primitive chondrule mineral (PCM) line (Fig. SM42; Ushikubo et al. 2012, 2017, 2018). Secondary minerals formed during metasomatic alteration of type 3 chondrites deviate from the slope-1 and are out of isotope equilibrium with the primary minerals (see Sects. 7.1.2 & 7.1.3). In addition, primary minerals chondrules and refractory inclusions in chondrites of petrologic type > 3.0 are often isotopically heterogeneous (see Sect. 7.1.4). The nature of this heterogeneity remains controversial. The proposed mechanisms include condensation from or gas-melt exchange with nebular gas of variable O-isotope composition, and isotope exchange with metasomatic fluids in the chondrites parent asteroids (e.g., Yurimoto et al. 2008; Kawasaki et al. 2018; Krot et al. 2022b).

In this section, we summarize O-isotope compositions of the aqueously/metasomatically-formed minerals in type 3 chondrites and discuss possible effects of metasomatic alteration on O-isotope compositions of the primary minerals in their chondrules and refractory inclusions.

7.1.2 Oxygen-Isotope Compositions of Magnetite and Fayalite in Type 3.0–3.1 Chondrites

Although Acfer 094 avoided metasomatic alteration in its parent asteroid, it contains intergrowths, named cosmic symplectites (COS) composed of magnetite, pentlandite, troilite, Na_2SO_4 , and elemental sulfur (Sakamoto et al. 2007; Matsumoto et al. 2022). Magnetite in COS is characterized by the anomalous O-isotope composition ($\delta^{17,18}\text{O} \sim +180\text{‰}$) and is interpreted to have recorded O-isotope composition of the primordial water in the PPD, and, hence, providing a strong argument supporting the CO self-shielding model (Yurimoto and Kuramoto 2004; Lyons and Young 2005; Sakamoto et al. 2007). The origin of COS, however, remains unclear: they may have formed by (i) oxidation and sulfidization of FeNi-metal in the PPD or in a pre-existing planetesimal (Sakamoto et al. 2007), (ii) high temperature interaction between FeNi-metal and O-Na-S-rich material (hot corrosion) (Matsumoto et al. 2022), and (iii) decomposition of amorphous ferric-hydroxysulfate-hydrate formed by interaction of sulfuric acid and ferric iron in a cryofluid environment on the Acfer 094 parent asteroid (Hashimoto and Nakano 2023).

Oxygen-isotope compositions of magnetite and fayalite formed during metasomatic alteration of type 3 UOCs, COs, CVs, and CKs are shown in Figures SM43–45. On the diagrams $\delta^{17}\text{O}$ vs. $\delta^{18}\text{O}$, magnetite in fayalite in type 3.0–3.2 UOCs plot along mass-dependent fractionation lines with $\Delta^{17}\text{O}$ of $\sim +4.3\text{‰}$ which correspond to $\Delta^{17}\text{O}$ of aqueous fluids in their parent asteroids. There are no resolvable differences in the inferred $\Delta^{17}\text{O}$

of aqueous fluids in H, L, and LL chondrites or among chondrites of different petrologic subtypes (Fig. SM43). Magnetite and fayalite in CO3.05–3.1 s and MAC 88107 (CO3.1-like) chondrites plot along mass-dependent fractionation lines with $\Delta^{17}\text{O}$ of $\sim -0.2\%$ and $\sim -1.8\%$, respectively (Figs. SM44). In contrast, magnetite and fayalite in the CV_{oxB} chondrites, Kaba (CV3.1), Mokoia (CV \sim 3.6), and Asuka (A)-881317 (CV3), show significant ranges in $\Delta^{17}\text{O}$, from ~ 0 to $\sim -4\%$ from $\sim +3.5$ to $\sim -2\%$, respectively (Figs. SM45a,b), suggesting either O-isotope evolution of aqueous fluid or heterogeneous O-isotope compositions of water ices that accreted into CV parent asteroid(s).

Oxygen-isotope compositions of magnetite in metamorphosed (petrologic types 3.6–3.8) CVs and CKs are shown in Figures SM45c,d. High precision data for magnetite in CKs have very limited ranges of $\delta^{18}\text{O}$ (from -2.5 to $+2.5\%$) and $\Delta^{17}\text{O}$ ($\sim -3\%$), possibly reflecting O-isotope equilibration with matrix silicates during thermal metamorphism. Data for magnetite from Allende and Ningqiang (C3-ungrouped) are less precise; within analytical uncertainty, their $\Delta^{17}\text{O}$ values are similar to those of CK magnetites; $\delta^{18}\text{O}$ values are more variable.

To summarize, there are differences in $\Delta^{17}\text{O}$ of fayalite and magnetite in UOCs, COs, CVs, and CKs suggesting different $\Delta^{17}\text{O}$ of aqueous fluids, and, possibly water ices, in their parent asteroids. In the CV_{oxB} chondrites, fayalite and magnetite show a range of $\Delta^{17}\text{O}$, possibly reflecting evolution of O-isotope composition of aqueous fluids. The inferred $\Delta^{17}\text{O}$ of aqueous fluids are very different from $\Delta^{17}\text{O}$ of COS that is hypothesized to represent O-isotope compositions of primordial water ices in the PPD.

7.1.3 Oxygen-Isotope Compositions of Secondary Minerals in Igneous CAIs from Allende and CK3.7–3.8 Chondrites

Oxygen-isotope compositions of the *in situ* SIMS measured secondary minerals in coarse-grained igneous CAIs from Allende (CV_{oxA}>3.6) and CK3.7–3.8 s are shown in Figures SM46a and SM46b, respectively. The data plot along mass-dependent fractionation lines with indistinguishable $\Delta^{17}\text{O}$ of $-3\pm 2\%$ (average \pm 2SD) and $-3.7\pm 1.9\%$, respectively. Although all minerals were measured with matrix-matched standards, there are some differences in chemical compositions of secondary minerals in CV and CK CAIs (see above) and the standards, which may explain some differences in their $\delta^{18}\text{O}$ values.

7.1.4 Oxygen-Isotope Heterogeneity of Refractory Inclusions and Chondrules in Metasomatically Altered Type 3 Chondrites

Fine-Grained CAIs and AOAs Amoeboid olivine aggregates and fine-grained CAIs in unmetamorphosed ordinary and carbonaceous chondrites (petrologic type ≤ 3.0) have internally uniform $\Delta^{17}\text{O}$, typically solar-like, $\sim -24\pm 2\%$ (Figs. SM42, 47–49) consistent with their formation in a gas of \sim solar oxygen-isotope composition. In contrast, AOAs and fine-grained CAIs in metamorphosed chondrites are isotopically heterogeneous: corundum, hibonite, spinel, forsterite, AlTi-diopside, and enstatite have ^{16}O -rich solar-like compositions, whereas Zr- and Sc-rich oxides and silicates, grossite, krotite, perovskite, melilite, anorthite, and perovskite are ^{16}O -depleted to various degrees (Figs. SM47–49). The $\Delta^{17}\text{O}$ values of the most ^{16}O -depleted primary minerals overlap with $\Delta^{17}\text{O}$ values of metasomatic fluids inferred from O-isotope compositions of secondary minerals (see Sects. 7.1.2 & 7.1.3). These observations and the fact that the O-isotope heterogeneity is inconsistent with a condensation sequence of minerals in refractory inclusions suggest that O-isotope heterogeneity in fine-grained CAIs and AOAs resulted from isotope exchange during aqueous fluid–rock interaction in the chondrite parent asteroids (Simon et al. 2019; Krot et al. 2019a,b,c; Ebert et al. 2020; Han et al. 2024).

Igneous Inclusions Coarse-grained igneous CAIs are found exclusively in CVs and CKs. Both groups experienced metasomatic alteration and thermal metamorphism and lack type 3.0 members. Like the fine-grained CAIs in metamorphosed ordinary and carbonaceous chondrites, the coarse-grained igneous CAIs in CV3.1–4 s and CK3.7–3.8 s have internally heterogeneous O-isotope compositions: hibonite, spinel, forsterite, and low-Ti Al-diopside have solar-like ^{16}O -rich ($\Delta^{17}\text{O} \sim -24 \pm 2\%$) compositions, whereas grossite, krotite, perovskite, melilite, anorthite, and Ti-rich pyroxenes (fassaite, grossmanite) are ^{16}O -depleted to various degrees (Fig. SM50). There is no agreement on the nature of this heterogeneity. It could have resulted from (1) O-isotope exchange during multistage, incomplete melting of CAIs in the nebular gas of variable $\Delta^{17}\text{O}$ (Yurimoto et al. 1998; Ito et al. 2004; Kawasaki et al. 2015, 2018; Aléon 2016, 2018) and/or (2) during aqueous fluid–rock interaction in the CV and CK parent asteroids (Yurimoto et al. 2008; Krot et al. 2022b, 2023).

(1) Igneous CAIs experienced melting in the solar nebula and thus could have experienced gas–melt O-isotope exchange. The early generation of gaseous reservoirs with variable $\Delta^{17}\text{O}$ has been advocated in several papers (Yurimoto et al. 1998; Itoh and Yurimoto 2003; Aléon et al. 2007; J. Simon et al. 2005, 2011, 2016; Kawasaki et al. 2012, 2018; Aléon 2016, 2018, 2018, 2020, 2020). If igneous CAIs experienced O-isotope exchange with the nebular gas of variable $\Delta^{17}\text{O}$, the distribution of oxygen isotopes in these CAIs must be consistent with igneous crystallization sequence studied experimentally (Stolper 1982). However, this is generally not the case. For example, in Type B CAIs eutectic melt regions composed of co-crystallized highly-åkermanitic melilite (Åk_{65-71}), anorthite, low-Ti ($\sim 2-5$ wt% TiO_2) fassaite, and spinel, the spinel and fassaite are similarly ^{16}O -rich ($\Delta^{17}\text{O} \sim -24\%$), whereas melilite and anorthite are ^{16}O -depleted to various degrees ($\Delta^{17}\text{O}$ up to $\sim -1\%$; see (see Figs. 11a,b in Krot et al. 2022b), suggesting post-crystallization O-isotope exchange.

The only mineral phase in igneous CAIs where igneous chemical zoning correlates with O-isotope zoning is AlTi-pyroxenes: Ti-rich pyroxene cores are ^{16}O -depleted to various degrees relative to Ti-poor pyroxene edges having solar-like $\Delta^{17}\text{O}$ (Kawasaki et al. 2018; MacPherson et al. 2022; Krot et al. 2022b). However, it remains unclear whether this O-isotope zoning was established during igneous crystallization or resulted from postcrystallization O-isotope exchange. Several observations may support the latter mechanism. (i) High-Ti pyroxene inclusions inside spinel grains were isolated from interaction with external O-isotope reservoir and preserved ^{16}O -rich compositions (Figs. SM50a,d, 51). (ii) O-isotope zoning is observed in igneously zoned Ti-rich pyroxenes in FUN (fractionation and unidentified nuclear effects) CAIs which experienced melting, evaporation and crystallization in nearly vacuum (Krot et al. 2014b; Mendybaev et al. 2013, 2017) and therefore must have avoided gas–melt isotope exchange. (iii) There is an apparent correlation of $\Delta^{17}\text{O}$ in pyroxenes and thermal history of the host meteorites: pyroxenes with similar chemical compositions are more ^{16}O -depleted in CAIs from more metamorphosed chondrites, CK3.7–3.8 and NWA 8418 (CV4) (Fig. SM51).

(2) Oxygen-isotope composition of aqueous fluid in Allende ($\text{CV}_{\text{oxA}} > 3.6$) and CK3.7–3.8 s is constrained by O-isotope compositions of their secondary minerals (see Sect. 7.1.3 and Fig. SM46). Postcrystallization O-isotope exchange of igneous CAIs with the fluid appears to be consistent with several observations: (i) $\Delta^{17}\text{O}$ of ^{16}O -depleted primary minerals (melilite, anorthite, high-Ti pyroxenes, grossite, krotite) approach $\Delta^{17}\text{O}$ of the fluid (Figs. SM47–49). (ii) On $\delta^{17}\text{O}$ vs. $\delta^{18}\text{O}$ plots (Fig. SM50), the ^{16}O -depleted primary minerals deviate to the right from a nebular slope-1 PCM line, i.e., towards the inferred compositions of aqueous fluids (Krot et al. 2022b). (iii) Oxygen self-diffusion in anorthite under wet conditions is several magnitudes higher than under dry conditions (Fig. SM52) and may explain its ^{16}O -poor composition.

To summarize, the coarse-grained igneous CAIs in CVs and CKs experienced post-crystallization O-isotope exchange to various degrees with an external ^{16}O -poor reservoir ($\Delta^{17}\text{O} \sim -3 \pm 2\text{‰}$), most likely aqueous fluid in the CV and CK chondrite parent asteroids. The isotope exchange appears to be mineralogically not petrologically controlled: i.e. variations in O-isotope compositions of minerals within individual CAIs are inconsistent with their inferred crystallization sequence. Oxygen-isotope compositions of melilite, anorthite, Ti-rich fassaite, perovskite, grossite, krotite, and davisite were affected by this process to various degrees. Hibonite, spinel, low-Ti fassaite, Al-diopside, and forsterite retained their original O-isotope compositions established during igneous crystallization of coarse-grained CAIs. This does not preclude O-isotope exchange in some igneous CAIs during melting in the solar nebula (e.g., some FoB and FUN CAIs having relatively ^{16}O -depleted compositions, $\Delta^{17}\text{O} > -20\text{‰}$, and CAIs melted during chondrule formation), but such inclusions appear to be rare (Kawasaki et al. 2012; Krot et al. 2005, 2014b).

Chondrules Chondrule phenocrysts and mesostasis in the least altered and the least metamorphosed carbonaceous chondrite Acfer 094 (C3.00) have internally uniform O-isotope compositions (Fig. SM42). Glassy mesostasis and plagioclase in chondrules from even weakly altered and metamorphosed ordinary and carbonaceous chondrites (Semarkona (LL3.00), Yamato (Y)-81020 (CO3.05), and Kaba (CV_{oxB}3.1) are ^{16}O -depleted relative to chondrule phenocrysts (Fig. SM53; see also Ebert et al. 2022). The $\Delta^{17}\text{O}$ values of mesostasis and plagioclase approach ^{17}O of aqueous fluid inferred from secondary magnetite and fayalite (see Sect. 7.1.2) suggesting they experienced O-isotope exchange with the fluid (Kita et al. 2010; Ebert et al. 2022; Fukuda et al. 2022; Krot et al. 2022a,b).

7.1.5 Future Studies

Oxygen-isotope compositions of aqueous fluid in the reduced CV3s is not known yet, but can be constrained by measuring secondary kirschsteinite. Development of the matrix-matched mineral standards, including kirschsteinite, for SIMS measurements is required to constrain the $\delta^{18}\text{O}$ values of aqueous fluids, and, potentially, crystallization temperature of secondary mineral parageneses.

To test the hypotheses of O-isotope exchange in igneous CAIs from CVs and CKs – gas-melt and fluid-rock – experimental data on oxygen self-diffusion in CAI minerals under proper physicochemical conditions ($P - T - f\text{O}_2$ –water/rock ratio) of metasomatic alteration of CVs and CKs are required.

7.2 Hydrogen Isotopes

7.2.1 Bulk Chondrite Hydrogen-Isotope Compositions

The first bulk H-isotope compositions measured in UOCs were obtained about 40 years ago (Robert et al. 1979; McNaughton et al. 1982; Yang and Epstein 1983) and shown to present high variabilities with δD relative to SMOW, from ~ -140 up to $+3000\text{‰}$. UOCs of petrologic type ≤ 3.2 generally contain the highest amounts of hydrogen (up to 0.1 wt% H) and are enriched in deuterium compared to UOCs of higher petrologic types (Alexander et al. 2012; Vacher et al. 2020; Grant et al. 2023; Table SM10, Fig. SM54a). The least metamorphosed LL3.00 Semarkona has the highest amount of hydrogen among non-weathered UOCs (average H content of 0.07 ± 0.04 wt%) and the highest and more variable δD value of $2000 \pm 745\text{‰}$ (Table SM10).

Metasomatized CVs, COs, and CKs are depleted in hydrogen compared to CIs, CMs, and CRs that experienced relatively low temperature aqueous alteration and present moderate δD variations with values ranging from -115 to $+240\text{‰}$, with the exception of one aliquot of Ormans (CO3.4) having a δD of $+2150\text{‰}$ (Kerridge 1985) (Table SM10 and references therein, Fig. SM54b).

7.2.2 Hydrogen-Isotope Compositions of Organics

As described in Sect. 3, the IOM is the major carrier of C, N and noble gases, and one of the two major carriers of hydrogen in type 3 chondrites. In the most primitive chondrites, the IOM is strongly enriched in δD compared to bulk rocks (Alexander et al. 2007, 2012, 2021) and shows heterogeneities with μm -sized areas both enriched and depleted in D compared to the average IOM value (Busemann et al. 2006; Remusat et al. 2006). With increasing temperatures during parent body alteration, the H/C ratio of the IOM decreases due to the re-organization of the organic matter structure, the loss of heteroatoms, and the development of large aromatic domains (see Sect. 3.1; Alexander et al. 2007, 2014, 2017, 2009). In carbonaceous chondrites, the hydrogen loss is associated with the destruction of μm -scale heterogeneities (Remusat et al. 2008) and likely to H-isotope fractionation (Alexander et al. 2010, 2014).

In CVs and COs, the IOM shows low-to-moderate D-enrichments relative to the bulk rocks compared to the more water-rich CIs, CMs, and CRs with δD ranging from $+60$ to $+1400\text{‰}$ and from $+130$ to $+700\text{‰}$, respectively (Alexander et al. 2007). Although there is only moderate D-increase for the CV IOM and no clear trend exists for the CO IOM δD compositions with petrological type or H contents (Alexander et al. 2007), the relatively low δD and H contents of these meteorites compared to those of CMs, CIs, and CRs could reflect the effects of parent body processes under increasing temperatures.

In UOCs, the IOM is enriched in δD (from $+3000$ to $12,000\text{‰}$) (Alexander et al. 2010) compared to those of other chondrites and to the UOC bulk compositions (Yang and Epstein 1983; Alexander et al. 2007, 2010, 2021). However, the IOM appears to be more homogeneous than in CCs showing only rare μm -sized D-rich anomalies (Remusat et al. 2016). The presence of a positive correlation between the IOM δD and its C/H ratio (Fig. SM55a) was initially proposed to result from isotopic exchanges between IOM and aqueous fluids following D enrichments of water through Rayleigh-type fractionations after metal oxidation during alteration processes in the parent asteroid (Alexander et al. 2010). However, this hypothesis is at odds with the absence of general D-enrichments in bulk UOCs with increasing the metamorphism degree (Fig. SM55a; Vacher et al. 2020; Marrocchi et al. 2020; Piani et al. 2021; Grant et al. 2023). Moreover, the IOM of ordinary chondrites seems to contain a D-rich thermally resistant component, whose proportions would be enhanced during heating due to the loss of more D-poor organic material (Figs. SM55b,c; Remusat et al. 2016). The presence of this D-rich component in UOCs that is unsampled by carbonaceous chondrites argues for a difference in the organic reservoirs of OC and CC IOMs.

7.2.3 Hydrogen-Isotope Compositions of Hydrated Silicates

Like for CMs, CIs and CRs (for details see Lee et al. this journal), the δD composition of water-bearing minerals in the oxidized Bali-like CVs (Kaba, Bali, and Grosnaja) was estimated by SIMS with an analytical protocol using Cs^+ primary ions and found to share a common δD composition of $\sim -80 \pm 100\text{‰}$ (Piani and Marrocchi 2018). The D-enrichment of the CV water-bearing minerals compared to those of CMs can be interpreted as the evidence that CVs accreted ices with a distinct hydrogen-isotope composition than those in

CMs or CRs. However, the additional presence of generally δD -depleted organic matter in CVs compared to that in CMs could also be seen as the result from isotopic exchanges between water and organics during parent body metasomatism (Piani and Marrocchi 2018). The exchange reactions could be favored in CVs compared to CMs by the higher T and/or different alteration mechanisms, possibly implying steam instead of, or in addition to, liquid fluids (see Sect. 5).

For COs, the δD of water-bearing minerals was measured only in DOM 08006 (CO3.00) and found to be $+306 \pm 135\text{‰}$ (Piani et al. 2021), a value slightly higher than for CVs. More measurements in this group of chondrites would be needed to determine if this unique value is representative for the water in all COs; only meteorites with low terrestrial weathering degrees should be selected for analyses to avoid terrestrial contamination (Alexander et al. 2018a).

Highly heterogeneous δD with extreme values up to $10,000\text{‰}$ have been measured in the H-bearing matrix of Semarkona (LL3.00) (Fig. SM56; Deloule and Robert 1995; Piani et al. 2015). The highest δD values in the matrix exceed by far the isotopic composition observed in primitive OC IOMs (Alexander et al. 2007; Remusat et al. 2016) and are not associated with C-rich areas indicating that their carrier is inorganic, likely hydrous silicates (Fig. SM56; Piani et al. 2015). The identification of the extreme δD variations associated with inorganic phases in Semarkona indicate that the parent body of LL-type ordinary chondrites have likely accreted some D-rich material derived from the molecular cloud and having escaped complete homogenization with hydrogen of the PPD (Aléon 2010; Piani et al. 2021). The nature of the D-rich inorganic carrier, possibly phyllosilicates or hydrated amorphous silicates (Dobrică and Brearley 2021), has yet to be characterized.

7.3 Carbon- and Nitrogen-Isotope Compositions of the Main C- and N-Bearing Phases

The carbon-isotope compositions of carbonates in UOCs, CVs, and COs ($\delta^{13}\text{C}$ range from -23 to $+5\text{‰}$) were determined from CO_2 released after phosphoric acid treatments of the whole rocks and found to be ^{13}C -depleted compared to carbonates in CIs, CMs, and CRs (Grady et al. 1988; Alexander et al. 2015). The limited quantities of carbon measured (e.g., 0.02 wt% C in Semarkona; Alexander et al. 2015) are consistent with the absence or scarcity of carbonates observed in these chondrites (e.g., Hutchison et al. 1987). The low $\delta^{13}\text{C}$ values of carbonates in CVs, COs and UOCs could be explained either by their formation at higher temperature and/or by more oxidized fluids (higher CO_2 fractions) than for the CIs, CMs, and CRs (Alexander et al. 2015).

In UOCs, the C-isotope compositions of organic matter were estimated using stepped heating combustion (Grady et al. 1989). Removing the terrestrial weathering contaminants that can constitute an important part of the low temperature released gases of chondrite finds, the $\delta^{13}\text{C}$ of the indigenous organic compounds were estimated to be of $\sim -28\text{‰}$ with no clear variation trend observed according to the chondrite petrographic type (Grady et al. 1989).

The carbon- and nitrogen-isotope compositions of CV and CO IOM range from -18 to -5‰ for $\delta^{13}\text{C}$ and from -65 to $+17\text{‰}$ for $\delta^{15}\text{N}$ (Alexander et al. 2007). Due to the high abundance of IOM among the known C-bearing components in CVs and COs, the bulk $\delta^{13}\text{C}$ and $\delta^{15}\text{N}$ values of CVs and COs appear to be dominated by the IOM (Greenwood and Franchi 2004; Alexander et al. 2015).

Although FeNi-carbides are commonly observed in the least metamorphosed COs, CVs, and UOCs (see Sect. 2.2), their C-isotope compositions are not known yet.

7.3.1 Future Studies

Trace amounts of carbonates appear to be present in CVs, COs and UOCs when measured in whole rocks (Grady et al. 1988), but no *in situ* measurement were ever reported for their carbon-isotope compositions. Such measurements should be possible with SIMS at least in Semarkona (LL3.00), in which 15 μm -sized calcites were observed (Hutchison et al. 1987) and would allow a better understanding of the conditions of secondary alteration. In addition, SIMS measurements of C-isotope compositions of FeNi-carbides in CVs, COs, and UOCs would be also important.

Although the organic matter (including both SOM and IOM) and carbonates are major carbonaceous constituents in chondrites, their reported abundances do not account for more than $\sim 60\%$ of the total carbon content of the rock (Smith and Kaplan 1970; Alexander et al. 2015). Investigations should aim to identify the exact nature and origin of the missing carbonaceous component, which possibly consists of some kind of organic compounds lost during the IOM isolation process (Alexander et al. 2015).

Finally, the nature of the inorganic H-bearing components at the origin of the D-rich signatures observed in UOCs and the amplitude of their modifications during parent body processes require thorough investigations that could be achieved by coupling high resolution mineralogical observations using TEM and isotope imaging using NanoSIMS.

7.4 Sulfur Isotopes

With four stable isotopes (^{32}S , ^{33}S , ^{34}S and ^{36}S), sulfur can be used as a probe of the astrophysical environment of mass-independent photochemistry (Thiemens 2006). The sulfur isotope ratios are usually expressed as $\delta^{33}\text{S}$, $\delta^{34}\text{S}$, and $\delta^{36}\text{S}$ ($\delta^n\text{S} = [({}^n\text{S}/{}^{32}\text{S})/({}^n\text{S}/{}^{32}\text{S}_{\text{V-CDT}}) - 1] \times 1000$; with n being the mass of the considered isotope and V-CDT: Vienna Canyon Diablo Troilite used as reference. Briefly, the extents of mass-independent anomalies for the different isotopes are thought to depend on the energy of the photons responsible for the photolysis of the major S-bearing phase in the gas of the solar nebula, H_2S (Chakraborty et al. 2013).

The highest mass-independent variations of sulfur reported so far in chondrites have been found to be associated with the ^{16}O -poor COS in Acfer 094 (weighted means of $\Delta^{33}\text{S} = +3.84 \pm 0.72\text{‰}$ and $\Delta^{36}\text{S} = -6.05 \pm 2.25\text{‰}$ with $\Delta^{33}\text{S} = \delta^{33}\text{S} + 1000 \times [(\delta^{33}\text{S}/1000 + 1)^{0.515} - 1]$ and $\Delta^{36}\text{S} = \delta^{36}\text{S} + 1000 \times [(\delta^{36}\text{S}/1000 + 1)^{1.9} - 1]$; Vacher et al. 2021). These values are inconsistent with the energy of ultraviolet-photons coming from the protosun and could imply the presence of massive O and B stars close to the solar system's parent molecular cloud (Vacher et al. 2021). Except in COS of Acfer 094, no significant mass-dependent or mass-independent isotopic variations were reported for type 3 chondrites so far (Tachibana and Huss 2005; Marrocchi et al. 2016; Alexander et al. 2022).

Large mass-dependent isotope fractionation effects ($\delta^{34}\text{S}$ from -8 to $+6\text{‰}$) have been described in aqueously formed sulfides from CIs, CMs, and volatile-rich clasts in polymict ureilites and HED meteorites (Visser et al. 2019). Aqueously formed magnetite and fayalite in chondrules and matrices of UOCs, CVs, and COs commonly associate with elongated sulfide (troilite or pyrrhotite?) grains, which may have formed by direct precipitation from aqueous fluid (Fig. SM57). Sulfur-isotope compositions of sulfides associated with Cr-free magnetite in Kaba chondrules and interpreted as igneous in origin (Marrocchi et al. 2016; but see Sect. 2.2 for an alternative explanation) show a small range of $\delta^{34}\text{S}$, from $-1 \pm 0.4\text{‰}$ to $+1.4 \pm 0.4\text{‰}$. Elongated sulfides associated with fayalite have yet to be analyzed.

7.5 Sources of Water in UOCs, COs, and CVs

The main process controlling the O-isotope composition of the CV and CO parent asteroids is related to isotopic exchange between ^{16}O -enriched anhydrous silicates and $^{17,18}\text{O}$ -enriched aqueous fluid (Fig. SM58; Marrocchi et al. 2018). The initial O-isotope composition of aqueous fluid and its abundance (water/rock ratio) in the CV and CO asteroids, however, are poorly constrained. It is commonly assumed that COS in Acfer 094 having anomalously $^{17,18}\text{O}$ -enriched compositions ($\delta^{17,18}\text{O} \sim +180\text{‰}$; $\Delta^{17}\text{O} \sim +85\text{‰}$; Sakamoto et al. 2007) and sulfur mass-independent isotope anomalies ($\Delta^{33}\text{S} \sim +4\text{‰}$ and $\Delta^{36}\text{S} \sim -6\text{‰}$; Vacher et al. 2021) recorded the primordial O-isotope composition of water ice in the PPD providing evidence for the CO self-shielding in the PMC and/or outer disk (Yurimoto and Kuramoto 2004; Lyons and Young 2005; Krot et al. 2020). The $^{17,18}\text{O}$ -depleted compositions of aqueously formed minerals in UOCs and CCs (see Sects. 7.1.2 & 7.1.3, and Lee et al. 2025, this collection) provide no evidence that such primordial water ice directly accreted into chondrite parent bodies, and suggest instead that prior to accretion into chondrite parent asteroids O-isotope composition of water ice evolved towards the Earth-like value ($\Delta^{17}\text{O} \sim 0\text{‰}$) through either partial evaporation and isotope exchange with ^{16}O -enriched silicates and CO gas or/and isotopic evolution of water with time during CO self-shielding in the outer disk (Yurimoto and Kuramoto 2004; Lyons and Young 2005; Lyons et al. 2009; Krot et al. 2015; Alexander et al. 2017; Marrocchi et al. 2018).

Once accreted and melted, the chondritic water evolved towards ^{16}O -rich composition by exchange with anhydrous minerals and amorphous phases (Marrocchi et al. 2018; see also Lee et al. 2025, this collection). The initial water ice that accreted into chondrite asteroids is thus expected to have had a $\Delta^{17}\text{O}$ value equivalent to or higher than any aqueously formed minerals present in chondrites (Krot et al. 2015; Fujiya 2018; Marrocchi et al. 2018; Alexander 2019a,b). In the case of weakly metamorphosed CO3.0–3.1 s and CV_{oxB}3.1 s, the highest $\Delta^{17}\text{O}$ values of aqueously formed minerals ranging from ~ -2 to $\sim +3.5\text{‰}$ (Figs. SM44–45) put the lower limits on the initial $\Delta^{17}\text{O}$ of water ice in COs and CVs. Alexander (2019b) suggested that (i) different carbonaceous chondrites, including CVs and COs, could have originated from a mixture of the same four components: (1) chondrule/chondrule precursor component that partially lost FeNi-metal and volatiles, (2) refractory inclusion component that has a refractory inclusion-like bulk composition, (3) anhydrous and reduced but otherwise CI-like matrix, and (4) water ice with relatively high $\Delta^{17}\text{O}$ ($+3.5\text{‰}$) and $\delta^{18}\text{O}$ ($18\text{--}21\text{‰}$). (ii) Variations in the amount of water ice accreted by different chondrite groups could be responsible for differences in their bulk O-isotope compositions and O-isotope compositions of aqueously formed minerals. For example, the ^{16}O -enriched bulk compositions of COs compared to CVs would result from lower amount of the water ice component accreted by COs (Alexander 2019b). Nonetheless, the observed differences in $\Delta^{17}\text{O}$ values of fayalite in Kaba (CV_{oxB}3.1) and Elephant Moraine (EET) 90043 (CO3.1), $\sim +3.5\text{‰}$ and -0.3‰ , respectively (Figs. SM45a, 44c), may suggest that CVs accreted a more $^{17,18}\text{O}$ -rich water ice than COs (Marrocchi et al. 2018). Using the estimated O-isotope composition of the CV_{oxB} aqueous fluids during precipitation of pure fayalite and the inferred water/rock ratio modeled for its formation (0.1–0.2; Zolotov et al. 2006), Marrocchi et al. (2018) calculated the initial O-isotope composition of the CV_{oxB} aqueous fluid ($\delta^{18}\text{O} \geq +60\text{‰}$, $\Delta^{17}\text{O} > 15\text{‰}$) suggesting a potential contribution of water ice from the outer solar system.

Hydrogen-isotope compositions estimated for hydrated minerals in CVs could also be the results of the parent body evolution from an initially D-poor CM-like water toward D-richer values through isotope exchanges with D-rich organics that would be favored by the high alteration temperatures of CV parent body (Piani and Marrocchi 2018). Alternatively,

the moderate δD values measured for both water and IOM in CVs and COs could have resulted from their early accretion in the disk at temperatures allowing a more efficient re-equilibration with the D-poor solar gas than for CIs, CMs, and CRs that accreted later or at higher heliocentric distances (Piani et al. 2021). Further isotopic measurements on natural samples and experimental constraints on isotope exchange reactions are needed to better differentiate primary isotopic signatures from secondary isotope modifications taking place in the parent bodies during metasomatic alteration.

As for weakly metamorphosed CVs and COs, the $\Delta^{17}\text{O}$ of ices accreted in the UOC parent bodies should be equal or higher than the highest value inferred from the alteration fluids at the origin of the secondary minerals, fayalite and magnetite (i.e., $\Delta^{17}\text{O} \sim +5\text{‰}$; Fig. SM43). However, the ranges of $\delta^{18}\text{O}$ and $\Delta^{17}\text{O}$ measured in bulk UOCs cannot be reconciled with a similar water ice O-isotope composition as those suggested for CCs, and $\Delta^{17}\text{O}$ values as high as $\sim 16\text{‰}$ were proposed for the OC initial water ice (Alexander 2019a). Additionally, the presence of D-rich IOM, including a D-rich thermally resistant component (Sect. 7.2.2), and the D-rich and isotopically heterogeneous hydrated silicates measured in Semarkona (Sect. 7.2.3) support the interpretation that OCs inherited a higher fraction of the primordial (i.e., molecular cloud) water ice and/or organics compared to CCs (Deloule and Robert 1995; Aléon 2010; Piani et al. 2015; Remusat et al. 2016). The inferred $\Delta^{17}\text{O}$ and δD values of water ice and δD composition of IOM seem to indicate that OCs have recorded lower degrees of re-equilibration between the primordial molecular cloud molecules and protosolar H_2 than most CCs, which might be at odds with their supposed formation locations in the inner and outer solar system, respectively (Warren 2011; Kruijer et al. 2017). However, the temperatures regulating the efficiency of re-equilibration between the primordial molecules and protosolar H_2 are not only dependent on the formation distance of the chondritic parent body but also on the thermal evolution of the disk with time and the nature of interactions with the parent molecular cloud. Strong differences exist in models trying to infer the H-isotope evolution of the disk water (see the discussion in Krot et al. 2015 and references therein); with no systematic dependences on the heliocentric distance (Yang et al. 2013; Jacquet and Robert 2013). Nonetheless, although the re-equilibration timescale could be different for oxygen and hydrogen isotopes (Lyons and Young 2005; Yang et al. 2013), no model allows a comprehensive description of the O- and H-isotope distribution for water throughout the disk evolution, nor does it explain the isotopic differences between OCs and CCs. Further attempts should be made in the future (*i*) to bring reliable constraints on isotope distribution in planetary materials, notably by deconvoluting the isotopic contribution of parent body processes from the hydrogen- and oxygen-isotope signatures of the primary ice in chondrites, and (*ii*) to estimate the spatial/temporal evolution of water hydrogen and oxygen-isotope compositions in the context of the recent disk dynamical evolution models.

8 Conclusions

1. Type 3 ordinary and CV, CO, and CK carbonaceous chondrites experienced aqueous fluid – rock interaction at $\sim 100\text{--}300\text{ °C}$ during progressive thermal metamorphism followed by loss of the fluid and nearly dry metamorphism. Both aqueous solution and steam played an important role in mobilization of rock-forming elements and resulted in metasomatic alteration of these meteorites. The alteration was multistage and produced different minerals and mineral assemblages in chondrite matrices, chondrules, and refractory inclusions reflecting differences in primary mineralogy, textures, and chemical compositions of these chondritic

components as well as temporal and local variations in fluid chemical composition. Detailed mineralogical studies of the secondary minerals and mineral assemblages in type 3 chondrites of different petrologic subtypes using FE SEM and focused ion beam (FIB) + TEM combined with physicochemical analysis and thermodynamic calculations could potentially constrain conditions during metasomatic alteration ($P - T - fO_2$ -water/rock ratio- $aSiO_2 - aCa - aFe \dots$).

2. Experimental syntheses of secondary minerals (grossular, wollastonite, nepheline, sodalite, dmisteinbergite) observed in metasomatically altered CAIs in Allende ($CV_{oxA} > 3.6$) resulted in formation of intermediate hydrated phases (e.g., hydrogrossular, hydrosodalite, analcime, nepheline hydrate) not observed in Allende. Studies of CAIs from less metamorphosed CVs are required to understand how relevant these experiments are. Although a hydrothermal experiment with Fe-metal, amorphous ferroan silicates and water did produce pure fayalite commonly observed in UOCs, CVs and COs of petrologic type 3.0–3.2, an experimental synthesis of FeMg-olivine from amorphous FeMg-silicates commonly observed in matrix of primitive chondrites is needed to understand a broad range of matrix olivine compositions ($Fa_{\sim 40-100}$) in these meteorites.

3. The origin of the precursors of organic matter in different chondrite groups and whether CVs, COs, and UOCs accreted the same mix of organic precursors remain unclear. Although IOM, SOM, and carbonates are the major carbon-bearing constituents in chondrites, their reported abundances do not account for more than ~60% of the chondrites total carbon content. Identification of the exact nature and the origin of the missing carbonaceous component is urgently needed. The role of metasomatic fluids in the evolution of organic matter in UOCs, COs, and CVs is not known. *In situ* studies of IOM using STXM and TEM and experimentally identifying specific reaction pathways related to the presence of oxidizing fluids at temperature above 300 °C could potentially offer a way to shed some light on this problem.

4. The ^{53}Mn - ^{53}Cr chronology of fayalite and kirschsteinite in UOCs, CVs, and COs measured with SIMS using matrix-matched standards suggests metasomatic alteration in their parent asteroids occurred ~2–5 Ma after formation of CAIs. However, the obtained data are very limited and do not allow the duration of metasomatic alteration in the UOC, CO, and CV parent asteroids to be constrained. The ^{129}I - ^{129}Xe ages of magnetites separated from CV3s, CO3s, and CK3–5 s are similar to those from CMs and CIs, ~3–5 Ma after CAIs, suggesting nearly contemporaneous aqueous activity in the carbonaceous chondrites parent asteroids. The ^{129}I - ^{129}Xe ages of polymineralic samples (matrix, chondrules, CAIs, dark inclusions) from CV chondrites (mostly from Allende) recorded prolonged duration of their metasomatic alteration, > 11 Ma. However, the ^{129}I -carrier phases and corresponding closure temperatures of I-Xe isotope systematics of these samples are not well-constrained yet. The ^{53}Mn - ^{53}Cr and ^{129}I - ^{129}Xe chronologies of metasomatic alteration and thermal evolution models of asteroids heated by ^{26}Al decay suggest that the CV, CO, and ordinary chondrite parent bodies accreted 2.4–2.7 Ma, 2.1–2.4 Ma, and 1.6–1.8 Ma after CV CAIs, respectively.

5. The ^{26}Al - ^{26}Mg systematics of secondary minerals having high Al/Mg ratio (anorthite, grossular, nepheline, sodalite) places only lower limits on their formation ages (> 3 Ma after formation of CAIs). The reported large excesses of radiogenic ^{26}Mg in some secondary minerals were probably inherited from the primary minerals after nearly complete decay of ^{26}Al and, thus, provide no chronological information. High precision Al-Mg isotope measurements of cogenetic secondary minerals (mineral parageneses) showing a large range of Al/Mg ratio (e.g., grossular, anorthite, monticellite, forsterite, corundum) can be used to construct internal Al-Mg isochrons and potentially date their formation.

6. The ^{26}Al - ^{26}Mg systematics of chondrule glasses can be disturbed in metasomatically altered chondrites even of low petrologic type (3.0–3.2) diminishing their chronological significance. Although chemically primitive chondrule plagioclase in some type 3.0–3.1 chondrites experienced aqueous/metasomatic alteration resulting in formation of phyllosilicates, there is no clear evidence that this process affected its ^{26}Al - ^{26}Mg systematics. Therefore, the observed ranges of $(^{26}\text{Al}/^{27}\text{Al})_0$ in plagioclase-bearing chondrules from type 3.0–3.1 chondrites are probably chronologically meaningful (but see Piralla et al. 2023). In chondrites of higher petrologic type, the ^{26}Al - ^{26}Mg systematics of plagioclase in chondrules and refractory inclusions, and even of melilite in CAIs can be disturbed and should be considered with caution in chronological interpretations.

7. The $\Delta^{17}\text{O}$ values of metasomatically formed minerals in UOCs, COs, CVs and CKs range from $\sim +5$ to $\sim -4\text{‰}$ suggesting differences in $\Delta^{17}\text{O}$ of aqueous fluids and, possibly, water ices that accreted into their parent asteroids. Development of the matrix-matched mineral standards for SIMS measurements is required to constrain the $\delta^{18}\text{O}$ values of aqueous fluids, and, potentially, crystallization temperature of secondary mineral parageneses. The fact that the inferred $\Delta^{17}\text{O}$ values of aqueous fluids in the UOCs, COs, CVs, and CKs parent asteroids are distinctly different from the hypothesized $\Delta^{17}\text{O}$ of primordial water ices recorded by cosmic symplectites in Acfer 094 ($\sim +80\text{‰}$) suggests either extensive thermal processing of water ices in the PPD accompanying by isotopic exchange with ^{16}O -enriched CO and anhydrous silicates or/and isotopic evolution of water with time during CO self-shielding in the outer disk.

8. Chondrule phenocrysts and plagioclase or glassy mesostasis as well as refractory inclusions in the least metamorphosed (type 3.00) chondrites have internally uniform $\Delta^{17}\text{O}$ values. Chondrules and refractory inclusions in UOCs, COs, CVs, and CKs of higher petrologic type (> 3.0) have internally heterogeneous $\Delta^{17}\text{O}$: glassy mesostasis, plagioclase, melilite, grossite, krotite, Ti-rich pyroxenes, perovskite and Sc- and Zr-rich oxides and silicates are ^{16}O -depleted relative to olivine, low-Ca pyroxene, hibonite, spinel, and low-Ti pyroxenes which retained their initial O-isotope compositions. The $\Delta^{17}\text{O}$ values of the ^{16}O -depleted phases approach the inferred $\Delta^{17}\text{O}$ values of aqueous fluid suggesting that the observed O-isotope heterogeneity most likely have resulted from isotopic exchange with aqueous fluids during metasomatic alteration. Most of the ^{16}O -depleted minerals show no evidence for disturbance of their Al-Mg isotope systematics, suggesting that Mg self-diffusion coefficients in these minerals under $P - T - f_{\text{O}_2}$ conditions of metasomatic alteration is much slower than oxygen self-diffusion. Therefore, CAIs with the canonical $(^{26}\text{Al}/^{27}\text{Al})_0$ and internally heterogeneous O-isotope compositions do not necessarily provide evidence for significant fluctuations in O-isotope composition of nebular gas in the CAI-forming region. At the same time, isotopic exchange with nebular gas of variable O-isotope composition cannot be excluded. Experimentally defined oxygen self-diffusion in CAI- and chondrule-like minerals under the inferred $P - T - f_{\text{O}_2}$ -water/rock ratio conditions during metasomatic alteration are required to test both hypotheses.

9. Carbon-isotope compositions of carbonates and FeNi-carbides in UOCs, CVs, and COs can potentially provide constraints on the origin of water ices in their parent asteroids, but are not known yet. These phases can be analyzed *in situ* by SIMS.

10. The main process controlling the O-isotope composition of the CV and CO parent asteroids is related to isotopic exchange between ^{16}O -enriched anhydrous silicates and $^{17,18}\text{O}$ -enriched aqueous fluid. The initial O-isotope of water ice and its abundance in the CV and CO chondrite parent asteroids are poorly constrained: its $\Delta^{17}\text{O}$ value must have been equal or higher than the highest $\Delta^{17}\text{O}$ of aqueously formed minerals in CV and CO chondrites, i.e., $> +3.2\text{‰}$ and $> -0.3\text{‰}$, respectively. The calculated water/rock ratios in

CV and CO asteroids are 0.1–0.2 and 0.01–0.1 (Marrocchi et al. 2018); these calculations, however, are highly model-dependent.

Parent asteroids of ordinary chondrites appear to have accreted low abundance of water ice, possibly, because of Jupiter blocking the inward flow of ice (Morbidelli et al. 2016), but with higher $\Delta^{17}\text{O}$ value than that in CVs and COs, $\geq +5\%$. These observations and the presence of D-rich IOM, including a D-rich thermally resistant component, and the D-rich and isotopically heterogeneous hydrated silicates measured in Semarkona (LL3.00) may indicate that (i) UOCs inherited a higher fraction of the primordial (molecular cloud) water ice and/or organics compared to CCs, and (ii) UOCs recorded lower degrees of re-equilibration between the primordial molecular cloud molecules and protosolar H_2 than most CCs. This interpretation appears to contradict the assumed formation locations of OCs and CCs in the inner and outer solar system (Warren 2011; Kruijer et al. 2017). Further attempts should be made to deconvolute the isotopic contribution of parent body processes from the hydrogen and oxygen isotopic signatures of the primary ice in chondrites, and to estimate the spatial/temporal evolution of water hydrogen- and oxygen-isotope compositions in the context of the recent disk dynamical evolution models (Desch et al. 2018; Burkhardt et al. 2019; Jacquet et al. 2019; Kleine et al. 2020).

Supplementary Information The online version contains supplementary material available at <https://doi.org/10.1007/s11214-025-01135-z>.

Funding Open Access funding enabled and organized by Projekt DEAL.

Declarations

Competing Interests The authors declare that they have no conflict of interest.

Open Access This article is licensed under a Creative Commons Attribution 4.0 International License, which permits use, sharing, adaptation, distribution and reproduction in any medium or format, as long as you give appropriate credit to the original author(s) and the source, provide a link to the Creative Commons licence, and indicate if changes were made. The images or other third party material in this article are included in the article's Creative Commons licence, unless indicated otherwise in a credit line to the material. If material is not included in the article's Creative Commons licence and your intended use is not permitted by statutory regulation or exceeds the permitted use, you will need to obtain permission directly from the copyright holder. To view a copy of this licence, visit <http://creativecommons.org/licenses/by/4.0/>.

References

- Aléon J (2010) Multiple origins of nitrogen isotopic anomalies in meteorites and comets. *Astrophys J* 722:1342–1351
- Aléon J (2016) Oxygen isotopes in the early protoplanetary disk inferred from pyroxene in a classical type B CAI. *Earth Planet Sci Lett* 440:62–70
- Aléon J (2018) Closed system oxygen isotope redistribution in igneous CAIs upon spinel dissolution. *Earth Planet Sci Lett* 482:324–333
- Aléon J, El Goresy A, Zinner E (2007) Oxygen isotope heterogeneities in the earliest protosolar gas recorded in a meteoritic calcium–aluminium-rich inclusion. *Earth Planet Sci Lett* 263:114–127
- Alexander CMO (1995) Trace element contents of chondrule rims and interchondrule matrix in ordinary chondrites. *Geochim Cosmochim Acta* 59:3247–3266
- Alexander CMO (2005) Re-examining the role of chondrules in producing the elemental fractionations in chondrites. *Meteorit Planet Sci* 40:943–965
- Alexander CMO (2019a) Quantitative models for the elemental and isotopic fractionations in the chondrites: the non-carbonaceous chondrites. *Geochim Cosmochim Acta* 254:246–276
- Alexander CMO (2019b) Quantitative models for the elemental and isotopic fractionations in chondrites: the carbonaceous chondrites. *Geochim Cosmochim Acta* 254:277–309

- Alexander CMO, Barber DJ, Hutchison R (1989) The microstructure of Semarkona and Bishunpur. *Geochim Cosmochim Acta* 53:3045–3057
- Alexander CMO, Arden JW, Ash RD, Pillinger CT (1990) Presolar components in the ordinary chondrites. *Earth Planet Sci Lett* 99:220–229
- Alexander CMO, Russell SS, Arden JW, Ash RD, Grady MM, Pillinger CT (1998) The origin of chondritic macromolecular organic matter: a carbon and nitrogen isotope study. *Meteorit Planet Sci* 33:603–622
- Alexander CMO, Fogel ML, Yabuta H, Cody GD (2007) The origin and evolution of chondrites recorded in the elemental and isotopic compositions of their macromolecular organic matter. *Geochim Cosmochim Acta* 71:4380–4403
- Alexander CMO, Newsome SD, Fogel ML, Nittler LR, Busemann H, Cody GD (2010) Deuterium enrichments in chondritic macromolecular material-implications for the origin and evolution of organics, water and asteroids. *Geochim Cosmochim Acta* 74:4417–4437
- Alexander CMO, Fogel ML, Howard KT, Herd CDK, Nittler LR (2012) The provenances of asteroids, and their contributions to the volatile inventories of the terrestrial planets. *Science* 337:721–723
- Alexander CMO, Cody GD, Kebukawa Y, Bowden R, Fogel ML, Kilcoyne ALD, Nittler LR, Herd CDK (2014) Elemental, isotopic, and structural changes in Tagish Lake insoluble organic matter produced by parent body processes. *Meteorit Planet Sci* 49:503–525
- Alexander CMO, Bowden R, Fogel ML, Howard KT (2015) Carbonate abundances and isotopic compositions in chondrites. *Meteorit Planet Sci* 50:810–833
- Alexander CMO, Nittler LR, Davidson J, Ciesla FJ (2017) Measuring the level of interstellar inheritance in the solar protoplanetary disk. *Meteorit Planet Sci* 52:1797–1821
- Alexander CMO, Greenwood RC, Bowden R, Gibson JM, Howard KT, Franchi IA (2018a) A multi-technique search for the most primitive CO chondrites. *Geochim Cosmochim Acta* 221:406–420
- Alexander CMO, McKeegan KD, Altwegg K (2018b) Water reservoirs in small planetary bodies: meteorites, asteroids, and comets. *Space Sci Rev* 214:36
- Alexander CMO, Wynn JC, Bowden R, Scott E (2022) Sulfur abundances and isotopic compositions in bulk carbonaceous chondrites and insoluble organic material: Clues to elemental and isotopic fractionations of volatile chalcophiles. *Meteorit Planet Sci* 57:334–351
- Aponte JC, Abreu NM, Glavin DP, Dworkin JP, Elsila JE (2017) Distribution of aliphatic amines in CO, CV, and CK carbonaceous chondrites and relation to mineralogy and processing history. *Meteorit Planet Sci* 52:2632–2646
- Aponte JC, Woodward HK, Abreu NM, Elsila JE, Dworkin JP (2019) Molecular distribution, ^{13}C -isotope, and enantiomeric compositions of carbonaceous chondrite monocarboxylic acids. *Meteorit Planet Sci* 54:415–430
- Barosch J, Nittler LR, Wang J, Dobrică E, Brearley AJ, Hezel DC, Alexander CMO (2022) Presolar O- and C-anomalous grains in unequilibrated ordinary chondrite matrices. *Geochim Cosmochim Acta* 335:169–182
- Beyssac O, Goffé B, Petit JP, Froigneux E, Moreau M, Rouzaud JN (2003) On the characterization of disordered and heterogeneous carbonaceous materials by Raman spectroscopy. *Spectrochim Acta, Part A, Mol Biomol Spectrosc* 59:2267–2276
- Bischoff A, Keil K (1983) Catalog of Al-rich chondrules, inclusions and fragments in ordinary chondrites. Special Publication No. 22, UNM, Institute of Meteoritics, Albuquerque, 1–33
- Bischoff A, Keil K (1984) Al-rich objects in ordinary chondrites: related origin of carbonaceous and ordinary chondrites and their constituents. *Geochim Cosmochim Acta* 48:693–709
- Bischoff A, Geiger T, Palme H, Spettel B, Schultz L, Scherer P, Schlüter J, Lkhamsuren J (1993) Mineralogy, chemistry, and noble gas contents of Adzhi-Bogdo – an LL3-6 chondritic breccia with L-chondritic and granitoidal clasts. *Meteoritics* 28:570–578
- Bischoff A, Barrat J-A, Berndt J, Borovicka J, Burkhardt C, Busemann H, Hakenmüller J, Heinlein D, Hertzog J, Kaiser J, Maden C, Meier MMM, Morino P, Pack A, Patzek M, Reitze MP, Rüfenacht M, Schmitt-Kopplin P, Schönbächler M, Spurny P, Weber I, Wimmer K, Zirkmund T (2019) The Renchen L5-6 chondrite breccia – the first confirmed meteorite fall from Baden-Württemberg (Germany). *Geochem Chem Erde* 79:125525
- Boata G (1954) The isotopic composition of hydrogen and carbon in the carbonaceous chondrites. *Geochim Cosmochim Acta* 6:209–220
- Bodénan J-D, Starkey NA, Russell SS, Wright IP, Franchi IA (2020) One of the earliest refractory inclusions and its implications for Solar System history. *Geochim Cosmochim Acta* 286:214–226
- Bonal L, Quirico E, Bourot-Denise M, Montagnac G (2006) Determination of the petrologic type of CV3 chondrites by Raman spectroscopy of included organic matter. *Geochim Cosmochim Acta* 70:1849–1863
- Bonal L, Bourot-Denise M, Quirico E, Montagnac G, Lewin E (2007) Organic matter and metamorphic history of CO chondrites. *Geochim Cosmochim Acta* 71:1605–1623

- Bonal L, Quirico E, Flandinet L, Montagnac G (2016) Thermal history of type 3 chondrites from the Antarctic meteorite collection determined by Raman spectroscopy of their polyaromatic carbonaceous matter. *Geochim Cosmochim Acta* 189:312–337
- Bonal L, Gattacceca J, Gerenne A, Eschrig J, Rochette P, Rügü L (2020) Water and heat: new constraints on the evolution of the CV chondrite parent body. *Geochim Cosmochim Acta* 276:363–383
- Bose M, Floss C, Stadermann FJ (2010) An investigation into the origin of Fe-rich presolar silicates in Acfer 094. *Astrophys J* 714:1624–1636
- Bose M, Zega TJ, Williams P (2014) Assessment of alteration processes on circumstellar and interstellar grains in Queen Alexandra Range 97416. *Earth Planet Sci Lett* 399:128–138
- Bradley JP (1994) Nanometer-scale mineralogy and petrography of fine-grained aggregates in anhydrous interplanetary dust particles. *Geochim Cosmochim Acta* 58:2123–2134
- Bradley JP, Brownlee DE, Fraundorf P (1984) Carbon components in interplanetary dust: evidence for formation by heterogeneous catalysis. *Science* 223:56–58
- Brearely AJ (1993) Matrix and fine-grained rims in the unequilibrated CO3 chondrite, ALHA77307: origins and evidence for diverse, primitive nebular dust components. *Geochim Cosmochim Acta* 57:1521–1550
- Brearely AJ, Krot AN (2012) Metasomatism in the early Solar System: the record from chondritic meteorites. In: *Metasomatism and the chemical transformation of rock. Lecture notes in Earth system sciences*, pp 659–789
- Brennecka GA, Wadhwa M (2012) Uranium isotope compositions of the basaltic angrite meteorites and the chronological implications for the early Solar System. *Proc Natl Acad Sci USA* 109:9299–9303
- Bridges JC, Alexander CMO, Hutchison R, Franchi IA, Pillinger CT (1997) Sodium-, chlorine-rich mesostases in Chainpur (LL3) and Parnallee (LL3) chondrules. *Meteorit Planet Sci* 32:555–565
- Burkhardt C, Dauphas N, Ulrik H, Bourdon B, Thorsten K (2019) Elemental and isotopic variability in Solar System materials by mixing and processing of primordial disk reservoirs. *Geochim Cosmochim Acta* 261:145–170
- Burton AS, Elsila JE, Callahan MP, Martin MG, Glavin DP, Johnson NM, Dworkin JP (2012) A propensity for n-u-amino acids in thermally altered Antarctic meteorites. *Meteorit Planet Sci* 47:374–386
- Buseck PR, Beyssac O (2014) From organic matter to graphite: graphitization. *Elements* 10:421–426
- Busemann H, Young AF, Alexander CMO, Hoppe P, Mukhopadhyay S, Nittler LR (2006) Interstellar chemistry recorded in organic matter from primitive meteorites. *Science* 312:727–730
- Busemann H, Alexander CMO, Nittler LR (2007) Characterization of insoluble organic matter in primitive meteorites by microRaman spectroscopy. *Meteorit Planet Sci* 42:1387–1416
- Busemann H, Nguyen AN, Cody GD, Hoppe P, Kilcoyne ALD, Stroud RM, Zega TJ, Nittler LR (2009) Ultra-primitive interplanetary dust particles from the comet 26P/Grigg-Skjellerup dust stream collection. *Earth Planet Sci Lett* 288:44–57
- Caffee MW, Hohenberg CM, Swindle TD, Hudson B (1982) I-Xe ages of individual Bjurböle chondrules. *J Geophys Res, Solid Earth* 87:A307–A317
- Chakraborty S, Jackson TL, Ahmed M, Thiemens MH (2013) Sulfur isotopic fractionation in vacuum UV photodissociation of hydrogen sulfide and its potential relevance to meteorite analysis. *Proc Natl Acad Sci USA* 110:17650–17655
- Chaumard N, Devouard B, Bouvier A, Wadhwa M (2014) Metamorphosed calcium-aluminum-rich inclusions in CK carbonaceous chondrites. *Meteorit Planet Sci* 49:419–452
- Che S, Brearely AJ (2021) The formation and alteration history of a forsterite-bearing Type C CAI from Allende: evidence for a Type B CAI precursor, and implications for fluid-assisted metasomatism on the CV chondrite parent body. *Geochim Cosmochim Acta* 293:277–307
- Chiodini G, Marini L (1998) Hydrothermal gas equilibria: the H₂O-H₂-CO₂-CO-CH₄ system. *Geochim Cosmochim Acta* 62:2673–2687
- Choi B-G, Huss GR, Wasserburg GJ, Gallino R (1998a) Presolar corundum and spinel in ordinary chondrites: origins from AGB stars and a supernova. *Science* 282:1284
- Choi B-G, McKeegan KD, Krot AN, Wasson JT (1998b) Extreme oxygen isotope compositions in magnetite from unequilibrated ordinary chondrites. *Nature* 392:577–579
- Christoffersen R, Buseck PR (1983) Epsilon carbide: a low-temperature component of interplanetary dust particles. *Science* 222:1327–1329
- Clayton RN (2002) Solar System: self-shielding in the solar nebula. *Nature* 415:860–861
- Clayton RN (2008) Oxygen isotopes in the early Solar System – a historical perspective. In: MacPherson GJ (ed) *Oxygen in the Solar System. Rev. Mineral. Geochem.*, vol 68, pp 5–14
- Clayton RN, Onuma N, Grossman L, Mayeda TK (1977) Distribution of the presolar component in Allende and other carbonaceous chondrites. *Earth Planet Sci Lett* 34:209–224
- Cody GD, Alexander CMO, Yabuta H, Kilcoyne ALD, Araki T, Ade H, Dera P, Fogel M, Mysen BO (2008) Organic thermometry for chondritic parent bodies. *Earth Planet Sci Lett* 272:446–455

- Costa F, Chakraborty S (2008) The effect of water on Si and O diffusion rates in olivine and implications for transport properties and processes in the upper mantle. *Phys Earth Planet Inter* 166:11–29
- Crowther SA, Mohapatra RK, Turner G, Blagburn DJ, Kehm K, Gilmour JD (2008) Characteristics and applications of RELAX, an ultrasensitive resonance ionization mass spectrometer for xenon. *J Anal At Spectrom* 23:938–947
- Davidson J, Busemann H, Franchi IA (2012) A NanoSIMS and Raman spectroscopic comparison of interplanetary dust particles from comet Grigg-Skjellerup and non-Grigg Skjellerup collections. *Meteorit Planet Sci* 47:1748–1771
- Davidson J, Busemann H, Nittler LR, Alexander CMO, Orthous-Daunay F-R, Franchi IA, Hoppe P (2014) Abundances of presolar silicon carbide grains in primitive meteorites determined by NanoSIMS. *Geochim Cosmochim Acta* 139:248–266
- Davidson J, Alexander CMO, Stroud RM, Busemann H, Nittler LR (2019) Mineralogy and petrology of dominion range 08006: a very primitive CO₃ carbonaceous chondrite. *Geochim Cosmochim Acta* 265:259–278
- Deloule E, Robert F (1995) Interstellar water in meteorites? *Geochim Cosmochim Acta* 59:4695–4706
- Desch SJ, Kalyaan A, Alexander CMO (2018) The effect of Jupiter's formation on the distribution of refractory elements and inclusions in meteorites. *Astrophys J* 238:11
- Dobrică E, Brearley AJ (2011) Earliest stages of metamorphism and aqueous alteration observed in the fine-grained materials of two unequilibrated ordinary chondrites. *Lunar Planet Sci* 42:2092
- Dobrică E, Brearley AJ (2020) Amorphous silicates in the matrix of Semarkona: the first evidence for the localized preservation of pristine matrix materials in the most unequilibrated ordinary chondrites. *Meteorit Planet Sci* 54:1973–1989
- Dobrică E, Brearley AJ (2021) Iron-rich olivine in the unequilibrated ordinary chondrite, MET 00526: earliest stages of formation. *Meteorit Planet Sci* 55:2652–2669
- Dobrică E, Nuth JA, Brearley AJ (2022) Fayalite formation through hydrothermal experiments: insights into early fluid-assisted aqueous alteration processes on asteroids. *Meteorit Planet Sci* 57:381–391
- Doyle PM, Jogo K, Nagashima K, Krot AN, Wakita S, Ciesla FJ, Hutcheon ID (2015) Early aqueous activity on the carbonaceous and ordinary chondrite parent asteroids recorded by secondary fayalite. *Nat Commun* 6:1–10
- Doyle PM, Jogo K, Nagashima K, Huss GR, Krot AN (2016) Mn-Cr relative sensitivity factor in ferromagnesian olivines defined for Sims measurements with a Cameca ims-1280 ion microprobe: implications for dating secondary fayalite. *Geochim Cosmochim Acta* 174:102–121
- Dyl KA, Bischoff A, Ziegler K, Young ED, Wimmer K, Bland PA (2012) Early Solar System hydrothermal activity in chondritic asteroids on 1-10-year timescales. *Proc Natl Acad Sci* 109:18306–18311
- Ebert S, Nagashima K, Krot AN, Bischoff A (2020) Oxygen-isotope heterogeneity in the northwest Africa 3358 (H3.1) refractory inclusions – fluid-assisted isotopic exchange on the H-chondrite parent body. *Geochim Cosmochim Acta* 282:98–112
- Ebert S, Nagashima K, Bischoff A, Berndt J, Krot AN (2022) Mineralogy, petrology, and oxygen isotopic compositions of aluminum-rich chondrules from unequilibrated ordinary and the Dar al Gani 083 (CO_{3.1}) chondrite. *Geochim Cosmochim Acta* 336:448–468
- Ebert S, Nagashima K, Krot AN, Patzek M, Bischoff A (2024) Oxygen isotopic variation in the CAI-forming region recorded by a single refractory inclusion from the CO_{3.1} carbonaceous chondrite Dar Al Gani 083. *Astrophys J* 966:10
- Enokido Y, Nakamura T, Matsumoto M, Miyake A, Shibuya T, Park C, Zolensky M (2023) Mineralogical alteration of a type A CAI from Allende CV3 chondrite: formation of secondary dmsteinbergite and its phase transition to anorthite. *Meteorit Planet Sci* 58:405–420
- Fagan TJ, Guan Y, MacPherson GJ (2007) Al-Mg isotopic evidence for episodic alteration of Ca-Al-rich inclusions from Allende. *Meteorit Planet Sci* 42:1221–1240
- Farver JR (1989) Oxygen self-diffusion in diopside with applications to cooling rate determination. *Earth Planet Sci Lett* 92:322–330
- Fayolle EC, Öberg KI, Cuppen HM, Visser R, Linnartz H (2012) Laboratory H₂O:CO₂ ice desorption: entrapment and its parameterization with an extended three-phase model. *EAS Publ Ser* 58:327–331
- Fegley B Jr, Prinn RG (1989) Solar nebula chemistry: implications for volatiles in the Solar System. In: Weaver H, Danly L (eds) *The formation and evolution of planetary systems*. Cambridge University Press, Cambridge, pp 171–211
- Feng L, El Goresy A, Zhang J, Hao J, Boyet M, Lin Y (2012) Excess ³⁶S in lawrencite and nitrogen isotopic compositions of sinoite from Almahata Sitta MS-17 EL3 chondrite fragment. *Lunar Planet Sci* 43:1766
- Floss C, Haenecour P (2016) Presolar silicate grains: abundances, isotopic and elemental compositions, and the effects of secondary processing. *Geochem J* 50:3–15
- Floss C, Stadermann FJ (2009a) High abundances of circumstellar and interstellar C-anomalous phases in the primitive CR3 chondrites QUE 99177 and MET 00426. *Astrophys J* 697:1242–1255

- Floss C, Stadermann FJ (2009b) Auger Nanoprobe analysis of presolar ferromagnesian silicate grains from primitive CR chondrites QUE 99177 and MET 00426. *Geochim Cosmochim Acta* 73:2415–2440
- Floss C, Stadermann FJ, Bradley JP, Dai ZR, Bajt S, Graham G, Lea AS (2006) Identification of isotopically primitive interplanetary dust particles: a NanoSIMS isotopic imaging study. *Geochim Cosmochim Acta* 70:2371–2399
- Foustoukos DI, Alexander CMO, Cody GD (2021) H and N systematics in thermally altered chondritic insoluble organic matter: an experimental study. *Geochim Cosmochim Acta* 300:44–64
- Fujiya W (2018) Oxygen isotopic ratios of primordial water in carbonaceous chondrites. *Earth Planet Sci Lett* 481:264–272
- Fukuda K, Tenner TJ, Kimura M, Tomioka N, Siron G, Ushikubo T, Chaumard N, Hertwig AT, Kita NT (2022) A temporal shift of chondrule generation from the inner to outer Solar System inferred from oxygen isotopes and Al-Mg chronology of chondrules from primitive CM and CO chondrites. *Geochim Cosmochim Acta* 322:194–226
- Ganino C, Libourel G (2017) Reduced and unstratified crust in CV chondrites parent body. *Nat Commun* 8:1–10
- García-Torano E, Altzitzoglou T, Auerbach P, Bé M-M, Bobin C, Cassette P, Chartier F, Dersch R, Fernández M, Isnard H, Kossert K, Lourenço V, Nähle O, Nonell A, Peyrés V, Pommé S, Rozkov A, Sánchez-Cabezudo A, Sochorová J (2018) The half-life of ^{129}I . *Appl Radiat Isot* 140:157–162
- Gattacceca J, Bonal L, Sonzogni C, Longerey J (2020) CV chondrites: more than one parent body. *Earth Planet Sci Lett* 547:116467
- Giletti BJ, Semet MP, Yund RA (1978) Studies in diffusion – III. Oxygen in feldspars: an ion microprobe determination. *Geochim Cosmochim Acta* 42:45–57
- Gilmour JD, Ash RD, Hutchison R, Bridges RC, Lyon IC, Turner G (1995) Iodine-xenon studies of Bjurböle and Parnallee using RELAX. *Meteorit Planet Sci* 30:405–411
- Gilmour JD, Crowther SA, Blagburn DJ, Turner G (2006) Recent and future developments of the RELAX mass spectrometer. *Geochim Cosmochim Acta* 70:A204
- Gilmour JD, Whitby JA, Turner G, Bridges JC, Hutchison R (2010) The iodine-xenon system in clasts and chondrules from ordinary chondrites: implications for early Solar System chronology. *Meteorit Planet Sci* 35:445–455
- Glavin DP, Kubny A, Jagoutz E, Lugmair GW (2004) Mn-Cr isotope systematics of the D'Orbigny angrite. *Meteorit Planet Sci* 39:693–700
- Glavin DP, Alexander CMO, Aponte ACM, Dworkin JP, Elsila JE, Yabuta H (2018) The origin and evolution of organic matter in carbonaceous chondrites and links to their parent bodies. In: *Primitive meteorites and asteroids*. Elsevier, Amsterdam, pp 205–271
- Göbel R, Begemann F, Ott U (1982) On neutron-induced and other noble gases in Allende inclusions. *Geochim Cosmochim Acta* 46:1777–1792
- Grady MM, Wright IP, Carr RH, Poths J, Pillinger CT (1988) Differences in isotopic composition of carbonaceous components in enstatite chondrites. *Earth Planet Sci Lett* 87:293–302
- Grady MM, Wright IP, Pillinger CT (1989) A preliminary investigation into the nature of carbonaceous material in ordinary chondrites. *Meteoritics* 24:147–154
- Grant H, Tartèse R, Jones R, Piani L, Marrocchi Y, King A, Rigaudier T (2023) Bulk mineralogy, water abundance, and hydrogen isotope composition of unequilibrated ordinary chondrites. *Meteorit Planet Sci* 58:1365–1381
- Greenwood RC, Franchi IA (2004) Alteration and metamorphism of CO3 chondrites: evidence from oxygen and carbon isotopes. *Meteorit Planet Sci* 39:1823–1838
- Greenwood RC, Franchi IA, Kearsley AT, Alard O (2010) The relationship between CK and CV chondrites. *Geochim Cosmochim Acta* 74:1684–1705
- Greshake A (1997) The primitive matrix components of the unique carbonaceous chondrite Acfer 094: a TEM study. *Geochim Cosmochim Acta* 61:437–452
- Grimm RE, McSween HY Jr (1989) Water and the thermal evolution of carbonaceous chondrite parent bodies. *Icarus* 82:244–280
- Grossman JN, Brearley AJ (2005) The onset of metamorphism in ordinary and carbonaceous chondrites. *Meteorit Planet Sci* 61:437–452
- Grossman JN, Alexander CMO, Wang J, Brearley AJ (2000) Bleached chondrules: evidence for widespread aqueous processes on the parent asteroids of ordinary chondrites. *Meteorit Planet Sci* 35:467–486
- Haenecour P, Floss C, Zega TJ, Croat TK, Wang A, Jolliff BL, Carpenter P (2018) Presolar silicates in the matrix and fine-grained rims around chondrules in primitive CO3.0 chondrites: evidence for pre-accretionary aqueous alteration of the rims in the solar nebula. *Geochim Cosmochim Acta* 221:379–405
- Hahn JH, Zenobi R, Bada JL, Zare RN (1988) Application of two-step laser mass spectrometry to cosmochemistry: direct analysis of meteorites. *Science* 239:1523–1525

- Han J, Nagashima K, Park C, Krot AN, Keller LP (2024) Grossite-bearing refractory inclusions from reduced CV chondrites: mineralogical and oxygen isotopic constraints on the parent body alteration history. *Geochim Cosmochim Acta* 385:100–117. <https://doi.org/10.1016/j.gca.2024.09.001>
- Hashimoto A, Grossman L (1987) Alteration of Al-rich inclusions inside amoeboid olivine aggregates in the Allende meteorite. *Geochim Cosmochim Acta* 51:1685–1704
- Hashimoto A, Nakano Y (2023) Sulfuric acid as a cryofluid and oxygen isotope reservoir of planetesimals. *Icarus* 398:115535
- Hevey PJ, Sanders IS (2006) A model for planetesimal meltdown by ^{26}Al and its implication for meteorite parent body. *Meteorit Planet Sci* 41:95–106
- Hohenberg CM, Pravdivtseva OV (2004) I–Xe dating: from adolescence to maturity. *Chem Erde* 68:339–351
- Hohenberg CM, Pravdivtseva OV (2008) I–Xe dating: from adolescence to maturity. *Chem Erde* 68:339–351
- Hohenberg CM, Pravdivtseva OV, Meshik AP (2004) Trapped Xe and I–Xe ages in aqueously altered CV3 meteorites. *Geochim Cosmochim Acta* 68:4745–4763
- Hohenberg CM, Pravdivtseva OV, Meshik AP (2004) Trapped Xe and I–Xe ages in aqueously altered CV3 meteorites. *Geochim Cosmochim Acta* 68:4745–4763
- Hong Y, Fegley B Jr (1998) Experimental studies of magnetite formation in the solar nebula. *Meteorit Planet Sci* 33:1101–1112
- Hoppe P, Leitner J, Kodolányi J (2015) New constraints on the abundances of silicate and oxide stardust from supernovae in the Acfer 094 meteorite. *Astrophys J Lett* 808:L9
- Hsu W, Guan Y, Leshin L, Ushikubo T, Wasserburg GJ (2006) A let episode of irradiation in the early Solar System: evidence from extinct ^{36}Cl and ^{26}Al in meteorites. *Astrophys J* 640:525–529
- Hua X, Huss GR, Tachibana S, Sharp TG (2005) Oxygen, silicon, and Mn–Cr isotopes of fayalite in the Kaba oxidized CV3 chondrite: constraints for its formation history. *Geochim Cosmochim Acta* 69:1333–1348
- Huss GR (1990) Ubiquitous interstellar diamond and SiC in primitive chondrites – abundances reflect metamorphism. *Nature* 347:159–162
- Huss GR, Lewis RS (1995) Presolar diamond, SiC, and graphite in primitive chondrites: abundances as a function of meteorite class and petrologic type. *Geochim Cosmochim Acta* 59:115–160
- Huss GR, Meshik AP, Smith JB, Hohenberg CM (2003) Presolar diamond, silicon carbide, and graphite in carbonaceous chondrites: implications for thermal processing in the solar nebula. *Geochim Cosmochim Acta* 67:4823–4848
- Hutcheon ID, Krot AN, Keil K, Phinney DL, Scott ERD (1998) ^{53}Mn – ^{53}Cr dating of fayalite formation in the CV3 chondrite Mokoia: evidence for asteroidal alteration. *Science* 282:1865–1867
- Hutchison R, Alexander CMO, Barber DJ (1987) The Semarkona meteorite: first recorded occurrence of smectite in an ordinary chondrite, and its implications. *Geochim Cosmochim Acta* 51:1875–1882
- Ichimura S, Seto Y, Tomeoka K (2017) Nepheline formation in chondrite parent bodies: verification through experiments. *Geochim Cosmochim Acta* 210:114–131
- Ireland TR, Avila J, Greenwood RC, Hicks LJ, Bridges JC (2020) Oxygen isotopes and sampling of the Solar System. *Space Sci Rev* 216:25
- Ishizaki L, Tachibana S, Okamoto T, Yamamoto D, Ida S (2023) Effective reaction temperatures of irreversible dust chemical reactions in a protoplanetary disk. *Astrophys J* 957:47
- Ito M, Messenger S (2010) Thermal metamorphic history of a Ca, Al-rich inclusion constrained by high spatial resolution Mg isotopic measurements with NanoSIMS 50L. *Meteorit Planet Sci* 45:583–595
- Ito M, Nagasawa H, Yurimoto H (2004) Oxygen isotopic SIMS analysis in Allende CAI: details of the very early thermal history of the Solar System. *Geochim Cosmochim Acta* 68:2905–2923
- Itoh D, Tomeoka K (1998) Na-bearing Ca–Al-rich inclusions in four CO3 chondrites, Kainsaz, Ornans, Lance, and Warrenton. In: 23rd Symposium on Antarctic Meteorites. NIPR, Tokyo, pp 42–44
- Itoh S, Yurimoto H (2003) Contemporaneous formation of chondrules and refractory inclusions in the early Solar System. *Nature* 423:728–731
- Itoh S, Kojima H, Yurimoto H (2004) Petrography and oxygen isotopic compositions in refractory inclusions from CO chondrites. *Geochim Cosmochim Acta* 68:183–194
- Itoh S, Russel SS, Yurimoto H (2007) Oxygen and magnesium compositions of amoeboid olivine aggregates from Semarkona LL3.0 chondrite. *Meteorit Planet Sci* 42:1241–1247
- Jacobsen B, Desch SJ (2023) The timing of ^{36}Cl production in the early Solar System and implications for gas dissipation in the protoplanetary disk. *Ann Meteorit Soc Meet* 86:6312
- Jacobsen B, Yin Q-Z, Moynier F, Amelin Y, Krot AN, Nagashima K, Hutcheon ID, Palme H (2008) ^{26}Al – ^{26}Mg and ^{207}Pb – ^{206}Pb systematics of Allende CAIs: canonical solar initial $^{26}\text{Al}/^{27}\text{Al}$ ratio reinstated. *Earth Planet Sci Lett* 272:353–364
- Jacobsen B, Matzel J, Hutcheon ID, Krot AN, Nagashima K, Ishii HA, Ramon E, Meyer BS, Davis AM, Ciesla FJ, Yin Q-Z (2011) Formation of short-lived radionuclides during epoch of late-stage irradiation in the protoplanetary disk. *Astrophys J* 731:L28–L31

- Jacquet E, Robert F (2013) Water transport in protoplanetary disks and the hydrogen isotopic composition of chondrites. *Icarus* 223:722–732
- Jacquet E, Pignatale FC, Chaussidon M, Charnoz S (2019) Fingerprints of the protosolar cloud collapse in the Solar System. II. Nucleosynthetic anomalies in meteorites. *Astrophys J* 884:32
- Jogo K, Nakamura T, Noguchi T, Zolotov MY (2009) Fayalite in the Vigarano CV3 carbonaceous chondrite: occurrences, formation age and conditions. *Earth Planet Sci Lett* 287:320–328
- Jogo K, Nakamura T, Ito M, Wakita S, Zolotov MY, Messenger SR (2017) Mn–Cr ages and formation conditions of fayalite in CV3 carbonaceous chondrites: constraints on the accretion ages of chondritic asteroids. *Geochim Cosmochim Acta* 199:58–74
- Johnson CA, Prinz M, Weisberg MK, Clayton RN, Mayeda TK (1990) Dark inclusions in Allende, Leoville, and Vigarano: evidence for nebular oxidation of CV3 constituents. *Geochim Cosmochim Acta* 54:819–830
- Jones CL, Brearley AJ (2006) Experimental aqueous alteration of the Allende meteorite under oxidizing conditions: constraints on asteroidal alteration. *Geochim Cosmochim Acta* 70:1040–1058
- Kanawati RB, Hertkorn N, Yin Q-Z, Moritz F, Harir M, Lucio M, Michalke B, Wimpenny J, Shilobreeva S, Bronsky B, Saraykin V, Gabelica Z, Gougeon RD, Quirico E, Ralew S, Jakubowski T, Haack H, Gonsior M, Jenniskens P, Hinman NW, Schmitt-Kopplin P (2017) Previously unknown class of metalorganic compounds revealed in meteorites. *Proc Natl Acad Sci USA* 114:2819–2824
- Kawasaki N, Sakamoto N, Yurimoto H (2012) Oxygen isotopic and chemical zoning of melilite crystals in a type A Ca–Al-rich inclusion of Efremovka CV3 chondrite. *Earth Planet Sci Lett* 47:2084–2093
- Kawasaki N, Kato C, Itoh S, Wakaki S, Ito M, Yurimoto H (2015) ^{26}Al – ^{26}Mg chronology and oxygen isotope distributions of multiple melting for a type C CAI from Allende. *Geochim Cosmochim Acta* 169:99–114
- Kawasaki N, Simon SB, Grossman L, Sakamoto N, Yurimoto H (2018) Crystal growth and disequilibrium distribution of oxygen isotopes in an igneous Ca–Al-rich inclusion from the Allende carbonaceous chondrite. *Geochim Cosmochim Acta* 221:318–341
- Keil K, Zucolotto ME, Krot AN, et al (2015) The Vicência meteorite fall: a new unshocked (S1) weakly metamorphosed (3.2) LL chondrite. *Meteorit Planet Sci* 50:1089–1111
- Keller LP (1998) A transmission electron microscope study of iron-nickel carbides in matrix of the Semarkona unequilibrium ordinary chondrite. *Meteorit Planet Sci* 33:913–919
- Keller LP, Buseck PR (1990) Aqueous alteration in the Kaba CV3 carbonaceous chondrite. *Geochim Cosmochim Acta* 54:2113–2120
- Keller LP, Buseck PR (1991) Calcic micas in the Allende meteorite: evidence for hydration reactions in the early solar nebula. *Science* 252:946–949
- Kerridge JF (1985) Carbon, hydrogen and nitrogen in carbonaceous chondrites: abundances and isotopic compositions in bulk samples. *Geochim Cosmochim Acta* 49:1707–1714
- Kimura M, Grossman JN, Weisberg MK (2007) Fe–Ni metal in primitive chondrites: indicators of classification and metamorphic conditions for ordinary and CO chondrites. *Meteorit Planet Sci* 43:1161–1177
- Kirschbaum C (1988) Carrier phases for iodine in the Allende meteorite and their associated $^{129}\text{Xe}/^{129}\text{I}$ ratios; a laser microprobe study. *Geochim Cosmochim Acta* 52:679–699
- Kita NT, Nagahara H, Tachibana S, Tomomura S, Spicuzza MJ, Fournelle JH, Valley JW (2010) High precision Sims oxygen three isotope study of chondrules in LL3 chondrites: role of ambient gas during chondrule formation. *Geochim Cosmochim Acta* 74:6610–6635
- Kleine T, Budde G, Burkhardt C, Kruijjer TS, Worsham EA, Morbidelli A, Nimmo F (2020) The non-carbonaceous – carbonaceous meteorite dichotomy. *Space Sci Rev* 216:55
- Kojima T, Tomeoka K (1999) Experimental hydrothermal alteration of the Allende CV3 chondrite under acidic and neutral conditions. *Meteorit Planet Sci* 34:A67
- Kojima T, Tomeoka K (2000) Transmission electron microscopy of phyllosilicates in experimentally altered Allende: comparison to naturally altered CV3 chondrites. *Meteorit Planet Sci* 35:A90
- Kojima T, Yada S, Tomeoka K (1995) Ca–Al-rich inclusions in three Antarctic CO3 chondrites, Yamato-81020 Yamato-82050 and Yamato-790992: record of low temperature alteration. *Antarct Meteor Res* 8:79
- Kolodny Y, Kerridge JF, Kaplan IR (1980) Deuterium in carbonaceous chondrites. *Earth Planet Sci Lett* 46:149–158
- Kööp L, Nakashima D, Heck PR, Kita NT, Tenner TJ, Krot AN, Nagashima K, Park C, Davis AM (2018) A multielement isotopic study of refractory FUN and F CAIs: mass-dependent and mass-independent isotope effects. *Geochim Cosmochim Acta* 221:296–317
- Krämer Ruggiu L, Devouard B, Gattacceca J, Bonal L, Leroux H, Eschrig J, Borschneck D, King AJ, Beck P, Marrocchi Y, Debaille Y, Hanna RD, Grauby O (2022) Detection of incipient aqueous alteration in carbonaceous chondrites. *Geochim Cosmochim Acta* 336:308–331

- Krot AN (2019) Refractory inclusions in carbonaceous chondrites: records of early Solar System processes. *Meteorit Planet Sci* 54:1647–1692
- Krot AN, Todd CS (1998) Metal-carbide-magnetite-fayalite association in a Bali-like clast in the reduced CV3 chondrite breccia Vigarano. *Meteorit Planet Sci* 34:A88–A89
- Krot AN, Scott ERD, Zolensky ME (1995) Mineralogic and chemical variations among CV3 chondrites and their components: nebular and asteroidal processing. *Meteoritics* 30:748–775
- Krot AN, Zolensky ME, Wasson JT, Scott ERD, Keil K, Ohsumi K (1997) Carbide-magnetite-bearing type 3 ordinary chondrites. *Geochim Cosmochim Acta* 61:219–237
- Krot AN, Zolensky ME, Keil K, Scott ERD, Nakamura K (1998) Secondary Ca-Fe-rich minerals in the Bali-like and Allende-like oxidized CV3 chondrites and Allende dark inclusions. *Meteorit Planet Sci* 33:623–645
- Krot AN, Brearley AJ, Ulyanov AA, Biryukov VV, Swindle TD, Keil K, Mittlefehldt DW, Scott ERD, Clayton RN, Mayeda TK (1999) Mineralogy, petrography, bulk chemical, iodine-xenon, and oxygen-isotopic composition of dark inclusions in the reduced CV3 chondrite Efremovka. *Meteorit Planet Sci* 34:67–89
- Krot AN, Brearley AJ, Petaev MI, Kallemeyn GW, Sears DWG, Benoit PH, Hutcheon ID, Zolensky ME, Keil K (2000) Evidence for in situ growth of fayalite and hedenbergite in MacAlpine Hills 88107, ungrouped carbonaceous chondrite related to CM-CO clan. *Meteorit Planet Sci* 35:1365–1387
- Krot AN, Petaev MI, Meibom A, Keil K (2001) In situ growth of Ca-rich rims around Allende dark inclusions. *Cosmochem Iss Geochem Int* 36:351–368
- Krot AN, Yurimoto H, Hutcheon ID, MacPherson GJ (2005) Relative chronology of CAI and chondrule formation: evidence from chondrule-bearing igneous CAIs. *Nature* 434:998–1001
- Krot AN, Hutcheon ID, Brearley AJ, Pravdivtseva OV, Petaev MI, Hohenberg CM (2006) Timescales for secondary alteration of chondritic meteorites. In: Lauretta D, McSween H (eds) *Meteorites and the early Solar System II*. University of Arizona Press, Tucson, pp 525–555
- Krot AN, Nagashima K, Hutcheon ID, Ishii HA, Yin Q-Z, Davis AM, Simon SB (2010) Mineralogy, petrography, oxygen and magnesium isotopic compositions and formation age of grossular-bearing assemblages in the Allende CAIs. *Lunar Planet Sci* 41:1406
- Krot AN, Keil K, Goodrich C, Weisberg MK, Scott ERD (2014a) Classification of meteorites. In: Davis AM (ed) *Meteorites and cosmochemical processes. Treatise on geochemistry* (eds. H. D. Holland and K. K. Turekian), vol 1. Elsevier, Oxford, pp 1–63
- Krot AN, Nagashima K, Wasserburg GJ, Huss GR, Papanastassiou D, Davis AM, Hutcheon ID, Bizzarro M (2014b) Calcium-aluminum-rich inclusions with fractionation and unknown nuclear effects (FUN CAIs): I. Mineralogy, petrology, and oxygen-isotope compositions. *Geochim Cosmochim Acta* 145:206–247
- Krot AN, Nagashima K, Alexander CMO, Ciesla FJ, Fujiya W, Bonal L (2015) Sources of water and aqueous activity on the chondrite parent asteroids. In: *Asteroids IV*. University of Arizona Press, Tucson, pp 21–32
- Krot AN, Nagashima K, Fintor K, Pál-Molnár E (2018) Evidence for oxygen isotopic exchange in chondrules from Kaba (CV3.1) carbonaceous chondrite during aqueous fluid – rock interaction on the CV parent asteroid. *Acta Geogr Geol Meteorol Debr: Geol Geom Phys Geogr Ser* 13:137–149
- Krot AN, Ma C, Nagashima K, Davis AM, Beckett JR, Simon SB, Komatsu M, Fagan TJ, Brenker F, Ivanova MA, Bischoff A (2019b) Mineralogy, petrography, and oxygen isotopic compositions of ultrarefractory inclusions from carbonaceous chondrites. *Geochemistry* 79:125519
- Krot AN, Nagashima K, Fintor K, Pál-Molnár E (2019c) Evidence for oxygen-isotope exchange in refractory inclusions from Kaba (CV3.1) carbonaceous chondrite during fluid-rock interaction on the CV parent asteroid. *Geochim Cosmochim Acta* 246:419–435
- Krot AN, Nagashima K, Simon SB, Ma C, Connolly HC Jr, Huss GR, Davis AM, Bizzarro M (2019a) Mineralogy, petrography, and oxygen and aluminum-magnesium isotope systematics of grossite-bearing refractory inclusions. *Geochemistry* 79:125529
- Krot AN, Nagashima K, Lyons JR, Lee J-E, Bizzarro M (2020) Oxygen isotopic heterogeneity in the early Solar System inherited from the protosolar molecular cloud. *Sci Adv* 6:eaa2724
- Krot AN, Petaev MI, Nagashima K (2021) Infiltration metasomatism of the Allende coarse-grained calcium-aluminum-rich inclusions. *Prog Earth Planet Sci* 8:61
- Krot AN, Doyle P, Nagashima K, Dobrică E (2022a) Mineralogy, petrology and oxygen-isotope compositions of magnetite±fayalite assemblages in CO3, CV3 and LL3 chondrites. *Meteorit Planet Sci* 57:392–428
- Krot AN, Nagashima K, MacPherson GJ, Ulyanov AA (2022b) On the nature of oxygen-isotope heterogeneity of igneous calcium-aluminum-rich inclusions in CV carbonaceous chondrites. *Geochim Cosmochim Acta* 332:327–354
- Krot AN, Nagashima K, Dunn TL, Petaev MI, Ma C (2023) Mineralogy, petrography, oxygen- and aluminum-magnesium isotope systematics of igneous CAIs from CK3 chondrites. In: 86th Meteoritic Soc Meet, vol 6116

- Krot AN, Dunn TL, Petaev MI, Ma C, Nagashima K, Zipfel J (2024) Metasomatic alteration of coarse-grained igneous calcium-aluminum-rich inclusions from CK3 carbonaceous chondrites. *Meteorit Planet Sci* 59:809–835
- Kruijer TS, Burkhardt C, Budde G, Kleine T (2017) Age of Jupiter inferred from the distinct genetics and formation times of meteorites. *Proc Natl Acad Sci USA* 114:6712–6716
- Kurat G, Palme H, Brandstätter F, Huth J (1989) Allende xenolith AF: undisturbed record of condensation and aggregation of matter in the solar nebula. *Z Naturforsch* 44a:988–1004
- LaTourette T, Wasserburg GJ (1998) Mg diffusion in anorthite: implications for the formation of early Solar System planetesimals. *Earth Planet Sci Lett* 158:91–108
- Le Guillou C, Rouzaud JN, Bonal L, Quirico E, Derenne S, Remusat L (2012) High resolution TEM of chondritic carbonaceous matter: metamorphic evolution and heterogeneity. *Meteorit Planet Sci* 47:345–362
- Lee MR, Alexander CMO, Bischoff A et al (2025) Low-temperature aqueous alteration of chondrites. *Space Sci Rev* 221. <https://doi.org/10.1007/s11214-024-01132-8>
- Leitner J, Vollmer C, Hoppe P, Zipfel J (2012) Characterization of Presolar Material in the CR Chondrite Northwest Africa 852. *Astrophys J* 745:38–53
- Leitner J, Vollmer C, Floss C, Zipfel J, Hoppe P (2016) Ancient stardust in fine-grained chondrule dust rims from carbonaceous chondrites. *Earth Planet Sci Lett* 434:117–128
- Lewis AL, Jones RH (2019) Primary feldspar in the Semarkona LL3.00 chondrite: constraints on chondrule formation and secondary alteration. *Meteorit Planet Sci* 54:72–89
- Lewis RS, Ming T, Wacker JF, Anders E, Steel E (1987) Interstellar diamonds in meteorites. *Nature* 326:160–162
- Lewis AL, Jones RH, Brearley AJ (2022) Plagioclase alteration and equilibration in ordinary chondrites: metasomatism during thermal metamorphism. *Geochim Cosmochim Acta* 316:201–229
- Leya I, Masarik J, Lin Y (2018) Alteration of CAIs as recorded by $^{36}\text{S}/^{34}\text{S}$ as a function of $^{35}\text{Cl}/^{34}\text{S}$. *Meteorit Planet Sci* 53:1252–1266
- Libourel G, Krot AN, Tissandier L (2006) Role of gas-melt interaction during chondrule formation. *Earth Planet Sci Lett* 251:232–240
- Lin Y, Guan Y, Leshin LA, Ouyang Z, Wang D (2005) Short-lived chlorine-36 in a Ca- and Al-rich inclusion from the Ningqiang carbonaceous chondrite. *Proc Natl Acad Sci* 102:1306–1311
- Llorca J, Casanova I (1998) Formation of carbides and hydrocarbons in chondritic interplanetary dust particles: a laboratory study. *Meteorit Planet Sci* 33:243–251
- Lyons JR, Young ED (2005) O self-shielding as the origin of oxygen isotope anomalies in the early solar nebula. *Nature* 435:317–320
- Lyons JR, Bergin EA, Ciesla FJ, Davis AM, Desch SJ, Hashizume K, Lee J-E (2009) Timescales for the evolution of oxygen isotope compositions in the solar nebula. *Geochim Cosmochim Acta* 73:4998–5017
- MacPherson GJ (2014) Calcium-aluminum-rich inclusions in chondritic meteorites. In: Davis AM (ed) *Meteorites, comets and planets. Treatise on geochemistry* (eds. H. D. Holland and K. K. Turekian), vol 1. Elsevier, Oxford, pp 139–179
- MacPherson GJ, Davis AM, Zinner EK (1995) The distribution of ^{26}Al in the early Solar System – a reappraisal. *Meteoritics* 30:365–386
- MacPherson GJ, Kita NT, Ushikubo T, Bullock ES, Davis AM (2012) Well-resolved variations in the formation ages for Ca-Al-rich inclusions in the early Solar System. *Earth Planet Sci Lett* 331:43–54
- MacPherson GJ, Nagashima K, Krot AN, Doyle PM, Ivanova MA (2017) ^{53}Mn - ^{53}Cr chronology of Ca-Fe silicates in CV3 chondrites. *Geochim Cosmochim Acta* 201:260–274
- MacPherson GJ, Krot AN, Kita NT, Bullock ES, Nagashima K, Ushikubo T, Ivanova MA (2022) The formation of type B CAIs: evolution from type A CAIs. *Geochim Cosmochim Acta* 321:343–374
- MacPherson GJ, Nagashima K, Krot AN, Kuehner SM, Irving AJ, Ziegler K, Mallozzi L, Corrigan C, Pitt D (2023) Northwest Africa 8418: the first CV4 chondrite. *Meteorit Planet Sci* 58:135–157
- Marrocchi Y, Chaussidon M, Piani L, Libourel G (2016) Early scattering of the solar protoplanetary disk recorded in meteoritic chondrules. *Sci Adv* 2:11601001
- Marrocchi Y, Bekaert DV, Piani L (2018) Origin and abundance of water in carbonaceous asteroids. *Earth Planet Sci Lett* 482:23–32
- Marrocchi Y, Bonal L, Gattacceca J, Piani L, Beck P, Greenwood R, Eschrig J, Basque A, Nuccio PM, Martin FF (2020) The Piancaldoli meteorite: a forgotten primitive LL3.10 ordinary chondrite. *Meteorit Planet Sci* 55:1924–1935
- Matsumoto M, Tsuchiyama A, Nakato A, Matsuno J, Miyake A, Kataoka A, Ito M, Tomioka N, Kodama Y, Uesugi K, Takeuchi A, Nakano T, Vaccaro E (2019) Discovery of fossil asteroidal ice in primitive meteorite Acfer 094. *Sci Adv* 5:eaax5078
- Matsumoto M, Tsuchiyama A, Miyake A, Ito M, Matsuno J, Uesugi K, Takeuchi A, Kodama Y, Yasutake M, Vaccaro E (2022) Three-dimensional microstructure and mineralogy of a cosmic symplectite in the Acfer 094 carbonaceous chondrite: implication for its origin. *Geochim Cosmochim Acta* 323:220–241

- McGuire AV, Hashimoto A (1989) Origin of zoned fine-grained inclusions in the Allende meteorite. *Geochim Cosmochim Acta* 53:1123–1133
- McKeegan KD, Leshin LA, Russel SS, MacPherson GJ (1998) Oxygen isotopic abundances in calcium-aluminum-rich inclusion from ordinary chondrites: implications for nebular heterogeneity. *Science* 280:414–418
- McKeegan KD, Kallio APA, Heber VS, Jarzabinski G, Mao PH, Coath CD, Kunihiro T, Wiens RC, Nordholt JE, Moses RW Jr, Reisenfeld DB, Jurewicz AJG, Burnett DS (2011) The oxygen isotopic composition of the Sun inferred from captured solar wind. *Science* 332:1528–1532
- McKibbin SJ, Ireland TR, Amelin Y, Holden P (2015) Mn–Cr dating of Fe- and Ca-rich olivine from ‘quenched’ and ‘plutonic’ angrite meteorites using secondary ion mass spectrometry. *Geochim Cosmochim Acta* 157:13–27
- McNaughton NJ, Borthwick J, Fallick AE, Pillinger CT (1981) Deuterium/hydrogen ratios in unequilibrated ordinary chondrites. *Nature* 294:639–641
- McNaughton NJ, Hinton RW, Pillinger CT, Fallick AE (1982) D/H ratios of some ordinary and carbonaceous chondrites. *Meteoritics* 17:252
- Mendybaev RA, Richter FM, Georg RB, Janney PE, Spicuzza MJ, Davis AM, Valley JW (2013) Experimental evaporation of Mg- and Si-rich melts: implications for the origin and evolution of FUN CAIs. *Geochim Cosmochim Acta* 123:368–384
- Mendybaev RA, Williams CD, Spicuzza MJ, Richter FM, Valley JW, Fedkin AY, Wadhwa M (2017) Thermal and chemical evolution of early Solar System solids as seen by Allende FUN CAI CMS-1: part II – laboratory evaporation of potential CMS-1 precursor. *Geochim Cosmochim Acta* 201:49–64
- Michel-Levy MC, Lautie A (1981) Microanalysis by Raman spectroscopy of carbon in the Tieschitz chondrite. *Nature* 292:321–322
- Morbidelli A, Bitsch B, Crida A, Gounelle M, Guillot T, Jacobson S, Johansen A, Lambrechts N, Lega E (2016) Fossilized condensation lines in the Solar System protoplanetary disk. *Icaris* 267:368–376
- Murty SVS, Goswami JN, Shukolyukov YA (1997) Excess ^{36}Ar in the Efremovka meteorite: a strong hint for the presence of ^{36}Cl in the early Solar System. *Astrophys J* 475:L65–L68
- Nagashima K, Krot AN, Yurimoto H (2004) Stardust from primitive meteorites. *Nature* 428:921–924
- Nagashima K, Huss GR, Krot AN, Yurimoto H (2011) Disturbance of magnesium isotopes in anorthite from an Allende CAI inferred from magnesium isotope mapping with isotope microscope. *Lunar Planet Sci* 42:2447
- Nagashima K, Krot AN, Komatsu M (2017) ^{26}Al - ^{26}Mg systematics in chondrules from Kaba and Yamato 980145 CV3 chondrites. *Geochim Cosmochim Acta* 201:303–319
- Nagashima K, Kita NT, Luu T-H (2018) ^{26}Al - ^{26}Mg systematics of chondrules. In: Russell SS, Connolly HC, Krot AN (eds) *Chondrules: records of protoplanetary disk processes*. Cambridge University Press, Cambridge, pp 247–275
- Nakashima D, Ott U, Hoppe P, El Goresy A (2008) Search for extinct ^{36}Cl : vigarano CAIs, the Pink Angel from Allende, and a Ningqiang chondrule. *Geochim Cosmochim Acta* 72:6141–6153
- Nakashima D, Ott U, Hoppe P (2010) Search for extinct chlorine-36: a halite grain from the Zag meteorite. *Ann Meteorit Soc Meet* 73:5289
- Nakasyo E, Maruoka T, Matsumoto T, Matsuda J-I (2000) A laboratory experiment on the influence of aqueous alteration on noble gas compositions in the Allende meteorite. *Antarct Meteor Res* 13:135
- Newton J, Bischoff A, Arden JW, Franchi IA, Geiger T, Pillinger CT (1995) Acfer 094, a uniquely primitive carbonaceous chondrite from the Sahara. *Meteoritics* 30:47–56
- Nguyen AN, Stadermann FJ, Zinner E, Stroud RM, Alexander CMO, Nittler LR (2007) Characterization of presolar silicate and oxide grains in primitive carbonaceous chondrites. *Astrophys J* 656:1223–1240
- Nguyen AN, Nittler LR, Stadermann FJ, Stroud RM, Alexander CMO (2010) Coordinated analyses of presolar grains in the Allan Hills 77307 and Queen Elizabeth Range 99177 meteorites. *Astrophys J* 719:166–189
- Nittler LR, Ciesla FJ (2016) Astrophysics and extraterrestrial materials. *Annu Rev Astron Astrophys* 54:53–93
- Nittler LR, Alexander CMO, Gao X, Walker RM, Zinner E (1997) Stellar sapphires: the properties and origins of presolar Al_2O_3 in meteorites. *Astrophys J* 483:479–495
- Nittler LR, Alexander CMO, Gallino R, Hoppe P, Nguyen AN, Stadermann FJ, Zinner EK (2008) Aluminum-, calcium- and titanium-rich oxide stardust in ordinary chondrite meteorites. *Astrophys J* 682:1450–1478
- Nittler LR, Alexander CMO, Davidson J, Riebe MEI, Stroud RM, Wang J (2018) High abundances of presolar grains and ^{15}N -rich organic matter in CO3.0 chondrite dominion range 08006. *Geochim Cosmochim Acta* 226:107–131
- Nittler LR, Alexander CMO, Patzer A, Verdier-Paoletti MJ (2021) Presolar stardust in highly pristine CM chondrites Asuka 12169 and Asuka 12236. *Meteorit Planet Sci* 56:260–276

- Nomura K, Miyamoto M (1998) Hydrothermal experiments on alteration of Ca–Al-rich inclusions (CAIs) in carbonaceous chondrites: implication for aqueous alteration in parent asteroids. *Geochim Cosmochim Acta* 62:3575–3588
- Oba Y, Naraoka H (2009) Elemental and isotope behavior of macromolecular organic matter from CM chondrites during hydrous pyrolysis. *Meteorit Planet Sci* 44:943–953
- Ohnishi I, Tomeoka K (2007) Hydrothermal alteration experiments of enstatite: implications for aqueous alteration of carbonaceous chondrites. *Meteorit Planet Sci* 42:49–61
- Okumura F, Mimura K (2011) Gradual and stepwise pyrolyses of insoluble organic matter from the Murchison meteorite revealing chemical structure and isotopic distribution. *Geochim Cosmochim Acta* 75:7063–7080
- Petaev MI, Mironenko MV (1997) Thermodynamic modeling of aqueous alteration in CV chondrites. In: Zolensky ME, Krot AN, Scott ERD (eds) Workshop on parent-body and nebular modification of chondritic materials. LPI Technical Report 97-02, 49–50
- Piani L, Marrocchi Y (2018) Hydrogen isotopic composition of water in CV-type carbonaceous chondrites. *Earth Planet Sci Lett* 504:64–71
- Piani L, Robert F, Remusat L (2015) Micron-scale D/H heterogeneity in chondrite matrices: a signature of the pristine Solar System water? *Earth Planet Sci Lett* 415:154–164
- Piani L, Marrocchi Y, Vacher LG, Yurimoto H, Bizzarro M (2021) Origin of hydrogen isotopic variations in chondritic water and organics. *Earth Planet Sci Lett* 567:117008
- Piralla M, Villeneuve J, Schnuriger N, Bekaert DV, Marrocchi Y (2023) A unified chronology of dust formation in the early Solar System. *Icarus* 394:115427
- Plage M, Ott U, Hoppe P (2006) Search for extinct ^{36}Cl in an Allende CAI. *Lunar Planet Sci* 37:1287
- Pravdivtseva OV, Amelin Y, Hohenberg CM, Meshik AP (2002) I–Xe and Pb–Pb ages of Richardton chondrules. *Geochim Cosmochim Acta* 66:A614
- Pravdivtseva OV, Krot AN, Hohenberg CM, Meshik AP, Weisberg MK, Keil K (2003) The I–Xe record of alteration in the Allende CV chondrite. *Geochim Cosmochim Acta* 67:5011–5026
- Pravdivtseva OV, Amelin Y, Meshik AP, Hohenberg CM (2004) I–Xe and Pb–Pb ages of individual Elenovka (L5) chondrules. *Geochim Cosmochim Acta* 68:A760
- Pravdivtseva O, Meshik A, Hohenberg CM, Petaev MI (2009) Interpreting the I–Xe system in individual silicate grains from Toluca IAB. *Meteorit Planet Sci* 44:1787–1796
- Pravdivtseva O, Meshik A, Hohenberg CM, Kurat G (2013) I–Xe ages of Campo del Cielo silicates as a record of the complex early history of the IAB parent body. *Meteorit Planet Sci* 48:2480–2490
- Pravdivtseva OV, Krot AN, Hohenberg CM (2017b) I–Xe dating of aqueous alteration in the CI chondrite Orgueil: I. Magnetite and ferromagnetic separates. *Geochim Cosmochim Acta* 227:38–47
- Pravdivtseva OV, Meshik AP, Hohenberg CM, Krot AN (2017a) I–Xe systematics of the impact plume produced chondrules from the CB carbonaceous chondrites: implications for the half-life value of ^{129}I and absolute age normalization of ^{129}I – ^{129}Xe chronometer. *Geochim Cosmochim Acta* 201:320–330
- Quirico E, Raynal PI, Bourot-Denise M (2003) Metamorphic grade of organic matter in six unequilibrated ordinary chondrites. *Meteorit Planet Sci* 38:795–811
- Quirico E, Montagnac G, Rouzaud JN, Bonal L, Bourot-Denise M, Duber S, Reynard B (2009) Precursor and metamorphic condition effects on Raman spectra of poorly ordered carbonaceous matter in chondrites and coals. *Earth Planet Sci Lett* 287:185–193
- Quirico E, Orthous-Daunay FR, Beck P, Bonal L, Brunetto R, Dartois E, Pino T, Montagnac G, Rouzaud J-N, Engrand C, Duprat J (2014) Origin of insoluble organic matter in type 1 and 2 chondrites: new clues, new questions. *Geochim Cosmochim Acta* 136:80–99
- Rai VK, Murty SVS, Ott U (2003) Noble gases in ureilites: cosmogenic, radiogenic, and trapped components. *Geochim Cosmochim Acta* 67:4435–4456
- Remusat L, Palhol F, Robert F, Derenne S, France-Lanord C (2006) Enrichment of deuterium in insoluble organic matter from primitive meteorites: a Solar System origin? *Earth Planet Sci Lett* 243:15–25
- Remusat L, Le Guillou C, Rouzaud JN, Binet L, Derenne S, Robert F (2008) Molecular study of insoluble organic matter in Kainsaz CO3 carbonaceous chondrite: comparison with CI and CM IOM. *Meteorit Planet Sci* 43:1099–1111
- Remusat L, Piani L, Bernard S (2016) Thermal recalcitrance of the organic D-rich component of ordinary chondrites. *Earth Planet Sci Lett* 435:36–44
- Remusat L, Bonnet J-Y, Bernard S, Buch A, Quirico E (2019) Molecular and isotopic behavior of insoluble organic matter of the Orgueil meteorite upon heating. *Geochim Cosmochim Acta* 263:235–249
- Riebe MEI, Foustoukos DI, Alexander CMO, Steele A, Cody GD, Mysen BO, Nittler LR (2020) The effects of atmospheric entry heating on organic matter in interplanetary dust particles and micrometeorites. *Earth Planet Sci Lett* 540:116266
- Riebe MEI, Busemann H, Alexander CMO, Herd CDK, Maden C, Wieler R (2016) Effects of aqueous alteration on primordial noble gas in Tagish Lake (C2-ungr.). *Meteorit Planet Sci* 51:6211


- Rietmeijer FJM, MacKinnon IDR (1985) Poorly graphitized carbon as a new cosmo-thermometer for primitive extraterrestrial materials. *Nature* 315:733–736
- Righter K, Neff KE (2007) Temperature and oxygen fugacity constraints on CK and R chondrites and implications for water and oxidation in the early Solar System. *Polar Sci* 1:25–44
- Robert F, Epstein S (1982) The concentration and isotopic composition of hydrogen, carbon and nitrogen in carbonaceous meteorites. *Geochim Cosmochim Acta* 46:81–95
- Robert F, Merlivat L, Javoy M (1979) Deuterium concentration in the early Solar System: hydrogen and oxygen isotope study. *Nature* 282:785–789
- Robert F, Javoy M, Halbout J, Dimon B, Merlivat L (1987) Hydrogen isotope abundances in the Solar System. Part I: unequilibrated chondrites. *Geochim Cosmochim Acta* 51:1787–1805
- Rouzaud J-N, Oberlin A (1990) The characterization of coals and cokes by transmission electron microscopy. In: Charcosset H, Nickel-Pepin-Donat B (eds) *Advanced methodologies in coal characterization*. Elsevier, Amsterdam, pp 311–355
- Rubin AE (1998) Correlated petrologic and geochemical characteristics of CO₃ chondrites. *Meteorit Planet Sci* 33:385–391
- Ruf A, Kanawati B, Hertkorn N, Yin Q-Z, Moritz F, Harir M, Lucio M, Michalke B, Wimpenny J, Shilobreeva S, Bronsky B, Saraykin V, Gabelica Z, Gougeon RD, Quirico E, Ralew S, Jakubowski T, Haack H, Gonsior M, Jenniskens P, Hinman NW, Schmitt-Kopplin P (2017) Previously unknown class of metalorganic compounds revealed in meteorites. *Proc Natl Acad Sci USA* 114:2819–2824
- Russell SS, Ott U, Alexander CMO, Zinner EK, Arden JW, Pillinger CT (1997) Presolar silicon carbide from the Indarch (EH4) meteorite: comparison with silicon carbide populations from other meteorite classes. *Meteorit Planet Sci* 32:719–732
- Russell SS, Huss GR, Fahey AJ, Greenwood RC, Hutchison R, Wasserburg GJ (1998) An isotopic and petrologic study of calcium–aluminum-rich inclusions from CO₃ meteorites. *Geochim Cosmochim Acta* 62:689–714
- Ryerson FJ, McKeegan KD (1994) Determination of oxygen self-diffusion in åkermanite, anorthite, diopside, and spinel: implications for oxygen isotopic anomalies and the thermal histories of Ca–Al-rich inclusions. *Geochim Cosmochim Acta* 58:3713–3734
- Sackett WM (1978) Carbon and hydrogen isotope effects during the thermocatalytic production of hydrocarbons in laboratory simulation experiments. *Geochim Cosmochim Acta* 42:571–580
- Sakamoto N, Seto Y, Itoh S, Kuramoto K, Fujino K, Nagashima K, Krot AN, Yurimoto H (2007) Oxygen isotope evidence for remnants of the early Solar System primordial water. *Science* 317:231–233
- Sakurai R, Yamamoto D, Takigawa A, Tachibana S (2023) Crystallization kinetics of amorphous ferromagnesian silicate with olivine-like composition. *Lunar Planet Sci* 54:2011
- Schmitt-Kopplin P, Harir M, Kanawati B, Tziozis N, Hertkorn N, Gabelica Z (2012) Chemical footprint of the solvent soluble extraterrestrial organic matter occluded in Softmany ordinary chondrite. *Meteorites* 2:79–92
- Shibita Y (1996) Opaque minerals in Antarctic CO₃ carbonaceous chondrites Yamato-74153, -790992, -791717, -81020, -81025, and Allan Hills-77307. *Proc NIPR Symp Antarc Meteorit* 9:79–96
- Shollenberger QR, Borg LE, Render J, Ebert S, Bischoff A, Russell SS, Brennecka GA (2018) Isotopic coherence of refractory inclusions from CV and CK meteorites: evidence from multiple isotope systems. *Geochim Cosmochim Acta* 228:62–80
- Simon JI, Young ED, Russell SS, Tonui EK, Dyl KA, Manning CE (2005) A short timescale for changing oxygen fugacity in the solar nebula revealed by high-resolution ²⁶Al–²⁶Mg dating of CAI rims. *Earth Planet Sci Lett* 238:272–283
- Simon JI, Hutcheon ID, Simon SB, et al (2011) Oxygen isotope variations at the margin of a CAI records circulation within the solar nebula. *Science* 331:1175–1178
- Simon JI, Matzel JEP, Simon SB, Hutcheon ID, Ross DK, Weber PK, Grossman L (2016) Oxygen isotopic variations in the outer margins and Wark-Lovering rims of refractory inclusions. *Geochim Cosmochim Acta* 186:242–276
- Simon SB, Krot AN, Nagashima K (2019) Oxygen and Al–Mg isotopic compositions of grossite-bearing refractory inclusions from CO₃ chondrites. *Meteorit Planet Sci* 54:1362–1378
- Siron G, Fukuda K, Kimura M, Kita NT (2021) New constraints from ²⁶Al–²⁶Mg chronology of anorthite bearing chondrules in unequilibrated ordinary chondrites. *Geochim Cosmochim Acta* 293:103–126
- Smith PPK, Buseck PR (1981) Graphitic carbon in the Allende meteorite: a microstructural study. *Science* 212:322–324
- Smith JW, Kaplan IR (1970) Endogenous carbon in carbonaceous meteorites. *Science* 167:1367–1370
- Smith LR, Haenecour P, Barnes J, Dominik K, Neuman M, Wang K, Oglione R, Koefoed P (2023) Abundance of presolar grains in the C3.00-ungrouped chondrite Chwichiya 002. *Lunar Planet Sci* 54:2425
- Stolper E (1982) Crystallization sequences of Ca–Al-rich inclusions from Allende: an experimental study. *Geochim Cosmochim Acta* 46:2159–2180

- Sutton S, Alexander CMO, Bryant A, Lanzirotti A, Newville M, Cloutis EA (2017) The bulk valence state of Fe and the origin of water in chondrites. *Geochim Cosmochim Acta* 211:115–132
- Swindle TD, Caffee MW, Hohenberg CM, Lindstrom MM (1983) I-Xe studies of individual Allende chondrules. *Geochim Cosmochim Acta* 47:2157–2177
- Swindle TD, Caffee MW, Hohenberg CM (1988) I-Xe studies of Allende inclusions: EGGs and the Pink Angel. *Geochim Cosmochim Acta* 52:2215–2229
- Tachibana S, Huss GR (2005) Sulfur isotope composition of putative primary troilite in chondrules from Bishunpur and Semarkona. *Geochim Cosmochim Acta* 69:3075–3097
- Tang M, Anders E (1988) Isotopic anomalies of Ne, Xe, and C in meteorites. II. Interstellar diamond and SiC: carriers of exotic noble gases. *Geochim Cosmochim Acta* 52:1235–1244
- Tang H, Liu M-C, McKeegan KD, Tissot FLH, Dauphas N (2017) In situ isotopic studies of the U-depleted Allende CAI Curious Marie: pre-accretionary alteration and the co-existence of ^{26}Al and ^{36}Cl in the early solar nebula. *Geochim Cosmochim Acta* 207:1–18
- Taylor GJ, Okada A, Scott ERD, Rubin AE, Huss GR, Keil K (1981) The occurrence and implications of carbide-magnetite assemblages in unequilibrated ordinary chondrites. In: *Proc. Lunar Planet. Sci. Conf.*, vol 12, pp 1076–1078
- Tenner TJ, Ushikubo T, Nakashima D, Schrader DL, Weisberg MK, Kimura M, Kita N (2018) Oxygen isotope characteristics of chondrules from recent studies by secondary ion mass spectrometry. In: Russel SS, Connolly HC Jr, Krot AN (eds) *Chondrules: records of the protoplanetary disk processes*. Cambridge University Press, Cambridge, pp 196–247
- Tenner TJ, Nakashima D, Ushikubo T, Tomioka N, Kimura M, Weisberg MK, Kita NT (2019) Extended chondrule formation intervals in distinct physicochemical environments: evidence from Al-Mg isotope systematics of CR chondrites chondrules with unaltered plagioclase. *Geochim Cosmochim Acta* 260:133–160
- Thiemens MH (2006) History and applications of mass-independent isotope effects. *Annu Rev Earth Planet Sci* 34:217–262
- Tomeoka K, Buseck PR (1990) Phyllosilicates in the Mokoia CV carbonaceous chondrite: evidence for aqueous alteration in an oxidizing environment. *Geochim Cosmochim Acta* 54:1745–1754
- Tomeoka K, Itoh D (2004) Sodium-metasomatism in chondrules in CO3 chondrites: relationship to parent body thermal metamorphism. *Meteorit Planet Sci* 39:1359–1373
- Tomeoka K, Nomura K, Takeda H (1992) Na-bearing Ca-Al-rich inclusions in the Yamato-791717 CO carbonaceous chondrite. *Meteoritics* 27:136–143
- Turner G, Crowther SA, Burgess R, Gilmour JD, Kelley SP, Wasserburg GJ (2013) Short lived ^{36}Cl and its decay products ^{36}Ar and ^{36}S in the early solar system. *Geochim Cosmochim Acta* 123:358–367
- Ushikubo T, Guan Y, Hiyagon H, Sugiura N, Leshin LA (2007a) ^{36}Cl , ^{26}Al , and O isotopes in an Allende type B2 CAI: implications for multiple secondary alteration events in the early Solar System. *Meteorit Planet Sci* 42:1267–1279
- Ushikubo T, Guan Y, Hiyagon H, Sugiura N, Leshin LA (2007b) ^{36}Cl , ^{26}Al , and O isotopes in an Allende type B2 CAI: implications for multiple secondary alteration events in the early Solar System. *Meteorit Planet Sci* 42:1267–1279
- Ushikubo T, Kimura M, Kita NT, Valley JW (2012) Primordial oxygen isotope reservoirs of the solar nebula recorded in chondrules in Acfer 094 carbonaceous chondrite. *Geochim Cosmochim Acta* 90:242–264
- Ushikubo T, Tenner TJ, Hiyagon H, Kita NT (2017) A long duration of the ^{16}O -rich reservoir in the solar nebula, as recorded in fine-grained refractory inclusions from the least metamorphosed carbonaceous chondrites. *Geochim Cosmochim Acta* 201:103–122
- Vacher LG, Piani L, Rigaudier T, Thomassin D, Florin G, Piralla M, Marrocchi Y (2020) Hydrogen in chondrites: influence of parent body alteration and atmospheric contamination on primordial components. *Geochim Cosmochim Acta* 281:53–66
- Vacher LG, Oglione RC, Jones C, Liu N, Fike DA (2021) Cosmic symplectite recorded irradiation by nearby massive stars in the Solar System's parent molecular cloud. *Geochim Cosmochim Acta* 309:135–150
- Van Orman JA, Cherniak DJ, Kita NT (2014) Magnesium diffusion in plagioclase: dependence on composition, and implications for thermal resetting of the ^{26}Al – ^{26}Mg early Solar System chronometer. *Earth Planet Sci Lett* 385:79–88
- Vandenbroucke M, Largeau C (2007) Kerogen origin, evolution and structure. *Org Geochem* 38:719–833
- Villa IM, Huneke JC, Papanastassiou DA, Wasserburg GJ (1981) The Allende pink angel: chronological constraints from Xe, Ar, and Mg. In: *Proc. Lunar sci. conf.*, vol 12, pp 1115–1117
- Visser R, John T, Patzek M, Bischoff A, Whitehouse MJ (2019) Sulfur isotope study of sulfides in CI, CM, C2ung chondrites and volatile-rich clasts—evidence for different generations and reservoirs of sulfide formation. *Geochim Cosmochim Acta* 261:210–223
- Vollmer C, Hoppe P, Stadermann FJ, Floss C, Brenker FE (2009) NanoSIMS analysis and Auger electron spectroscopy of silicate and oxide stardust from the carbonaceous chondrite Acfer 094. *Geochim Cosmochim Acta* 73:7127–7149

- Wark DA, Lovering JF (1976) Marker events in the early evolution of the Solar System: evidence from rims on Ca-Al-rich inclusions in carbonaceous chondrites meteorites. In: Proc. Lunar sci. conf., vol 8, pp 95–112
- Warren PH (2011) Stable isotopic anomalies and the accretionary assemblage of the Earth and Mars: a subordinate role for carbonaceous chondrites. *Earth Planet Sci Lett* 311:93–100
- Wasserburg GJ, Hutcheon ID, Aléon J, Ramon EC, Krot AN, Nagashima K, Brearley AJ (2011) Extremely Na- and Cl-rich chondrule from the CV3 carbonaceous chondrite Allende. *Geochim Cosmochim Acta* 75:4752–4770
- Weisberg MK, McCoy TJ, Krot AN (2006) Systematics and evaluation of meteorite classification. In: Lauretta DS, McSween HY Jr (eds) *Meteorites and the early Solar System II*, pp 19–52
- Wick MJ, Jones RH (2012) Formation conditions of plagioclase-bearing type I chondrules in CO chondrites: a study of natural samples and experimental analogs. *Geochim Cosmochim Acta* 98:140–159
- Wieler R, Anders E, Baur H, Lewis RS, Signer P (1992) Characterisation of Q-gases and other noble gas components in the Murchison meteorite. *Geochim Cosmochim Acta* 56:2907–2921
- Yamamoto D, Kawasaki N, Tachibana S, Ishizaki L, Sakurai R, Yurimoto H (2024) An experimental simulation of oxygen isotope exchange reaction between amorphous silicate dust and carbon monoxide gas in the early Solar System. *Geochim Cosmochim Acta* 374:93–105
- Yang J, Epstein S (1983) Interstellar organic matter in meteorites. *Geochim Cosmochim Acta* 47:2199–2216
- Yang L, Ciesla FJ, Alexander CMO (2013) The D/H ratio of water in the solar nebula during its formation and evolution. *Icarus* 226:256–267
- Yesiltas M, Young J, Glotch TD (2021) Thermal metamorphic history of Antarctic CV3 and CO3 chondrites inferred from the first- and second-order Raman peaks of polyaromatic organic carbon. *Amer Mineralogist: J Earth Planet Mater* 106:506–517
- Yurimoto H, Kuramoto K (2004) Molecular cloud origin for the oxygen–isotope heterogeneity in the Solar System. *Science* 305:1763–1766
- Yurimoto H, Morioka M, Nagasawa H (1989) Diffusion in single crystals of melilite. I. Oxygen *Geochim Cosmochim Acta* 53:2387–2394
- Yurimoto H, Ito M, Nagasawa H (1998) Oxygen isotope exchange between refractory inclusion in Allende and solar nebula gas. *Science* 282:1874–1877
- Yurimoto H, Krot AN, Choi B-G, Aléon J, Kunihiro T, Brearley AJ (2008) Oxygen isotopes of chondritic components. In: MacPherson GJ (ed) *Oxygen in the Solar System*. *Rev. Mineral. Geochem.*, vol 68, pp 141–187
- Zanetta P-M, Le Guillou C, Leroux H, Zanda B, Hewins R, Bellino G (2022) Processes and temperatures of FGR formation in chondrites. *Geochim Cosmochim Acta* 319:94–117
- Zheng Y-F (1991) Calculation of oxygen isotope fractionation in metal oxides. *Geochim Cosmochim Acta* 55:2299–2307
- Zheng Y-F (1993) Calculation of oxygen isotope fractionation in anhydrous silicate minerals. *Geochim Cosmochim Acta* 57:1079–1091
- Zheng Y-F (2011) On the theoretical calculations of O isotope fractionation factors for carbonate-water systems. *Geochem J* 45:341–354
- Zinner E (2014) Presolar grains. In: Davis AM (ed) *Meteorites and cosmochemical processes*, 2nd edn. *Treatise on geochemistry*, vol 1. Elsevier, Amsterdam, pp 181–213
- Zinner E, Nittler LR, Hoppe P, Gallino R, Straniero O, Alexander CMO (2005) Oxygen, magnesium and chromium isotopic ratios of presolar spinel grains. *Geochim Cosmochim Acta* 69:4149–4165
- Zolotov MY, Mironenko MV (2007) Hydrogen chloride as a source of acid fluids in parent bodies of chondrites. *Lunar Planet Sci* 38:2340
- Zolotov MY, Mironenko MV, Shock EL (2006) Thermodynamic constraints on fayalite formation on parent bodies of chondrites. *Meteorit Planet Sci* 41:1775–1796

Publisher's Note Springer Nature remains neutral with regard to jurisdictional claims in published maps and institutional affiliations.

Authors and Affiliations

A.N. Krot¹  · M.I. Petaev² · L. Piani³ · Y. Marrocchi³ · W. Fujiya⁴ · O.V. Pravdivtseva⁵ · E. Dobricá¹ · L.G. Vacher⁶ · A.J. King⁷ · M. Lee⁸ · E. Van Kooten⁹ · B. Jacobsen¹⁰ · C.M.O'D. Alexander¹¹ · A. Bischoff¹² · A.J. Brearley¹³ · C. Le Guillou¹⁴ · L. Remusat¹⁵ · J. Leitner^{16,17} · G.R. Huss¹

✉ J. Leitner
jan.leitner@mpic.de

A.N. Krot
sasha@higp.hawaii.edu

L. Piani
laurette.piani@univ-lorraine.fr

- 1 Hawai'i Institute of Geophysics & Planetology, School of Ocean & Earth Science & Technology, University of Hawai'i at Mānoa, Honolulu, HI, 96822, USA
- 2 Department of Earth & Planetary Sciences, Harvard University, Cambridge, MA, 02138, USA
- 3 CRPG, UMR 7358 CNRS, Université de Lorraine, 54500, Vandoeuvre-lès-Nancy, France
- 4 Faculty of Science, Ibaraki University, 2-1-1 Bunkyo, Mito, Ibaraki, 310-8512, Japan
- 5 Physics Department, Washington University, St. Louis, MO, 63130, USA
- 6 University of Grenoble Alpes, CNRS, IPAG, 38000, Grenoble, France
- 7 Planetary Materials Group, Department of Earth Sciences, Natural History Museum, Cromwell Road, London, SW7 5BD, UK
- 8 School of Geographical & Earth Sciences, University of Glasgow, Gregory Building, Lilybank Gardens, Glasgow, G12 8QQ, UK
- 9 Centre for Star & Planet Formation & Natural History Museum of Denmark, University of Copenhagen, DK-1350, Copenhagen, Denmark
- 10 Lawrence Livermore National Laboratory, 7000 East Ave, Livermore, CA, 94550, USA
- 11 Earth & Planets Laboratory, Carnegie Institution of Washington, 5241 Broad Branch Road, NW, Washington, DC, 20015, USA
- 12 Institut für Planetologie, Wilhelm-Klemm-Str. 10, Münster, 48149, Germany
- 13 University of New Mexico, Albuquerque, NM, 87131-0001, USA
- 14 CNRS, INRAE, Centrale Lille, UMR 8207 - UMET - Unité Matériaux et Transformations, University of Lille, F-59000, Lille, France
- 15 IMPMC, UMR CNRS 7590, Sorbonne Université, MNHN, CP52 57 rue Cuvier, 75231, Paris Cedex 05, France
- 16 Geo- & Cosmochemistry Group, Institute of Earth Sciences, Heidelberg University, Im Neuenheimer Feld 234-236, D-69120, Heidelberg, Germany
- 17 Max Planck Institute for Chemistry, Particle Chemistry Department, Hahn-Meitner-Weg 1, 55128, Mainz, Germany